12-14-2014

Structural Studies and Reactions of Rhenium and Rhenium-Gold Metal Carbonyl Complexes

Yuen Onn Wong
University of South Carolina - Columbia

STRUCTURAL STUDIES AND REACTIONS OF RHENIUM AND RHENIUM-GOLD METAL CARBONYL COMPLEXES

by

Yuen Onn Wong

Bachelor of Science
University of Montana, 2008

Submitted in Partial Fulfillment of the Requirements

For the Degree of Doctor of Philosophy in

Chemistry

College of Arts and Sciences

University of South Carolina

2014

Accepted by:

Richard D. Adams, Major Professor

Donna A. Chen, Committee Member

Krishna C. Mandal, Committee Member

Daniel L. Reger, Chairperson, Examining Committee

Lacy Ford, Vice Provost and Dean of Graduate Studies

ACKNOWLEDGEMENTS

The first person I like to thank is my mentor, Professor Adams. I am grateful to be able to benefit from his extensive knowledge of chemistry. Thanks to his guidance and mentorship, I was able to grow as a synthetic chemist.

I would also like to extend my gratitude towards my Ph.D. committee members, Dr. Reger, Dr. Chen and Dr. Mandal for their time and contributions throughout my graduate career. Dr. Mark Smith has been extremely helpful in assisting me on problems I encountered during crystal structure solving. Besides providing extensive NMR support, Dr. Perry Pellechia has offered many interesting conversations on life in general and the NFL.

To my former lab mates: Dr. William Pearl, Dr. Qiang Zhang and Dr. Yuwei Kan, I appreciate all your help in starting my graduate career. To my current lab mates: Gaya, Joseph, Jonathan, Zhongwen and Poonam, I wish you all luck in your research career. The time I spent with my former and current lab mates has been a pleasure.

Both of my families have been a constant source of support and inspiration throughout my life and graduate career. To my father, Min Wong, who has always encouraged me to work hard and focus on my studies, I thank you greatly. Despite being far away, my siblings: Yuen Shein, Chen Mey and Kit Mey has always been on my mind. Lastly, I would also like to thank my mother, Vicki for welcoming me to the family. You have been supportive of me for a long time

no matter how difficult I was. Not to forget Donnie, Brandon, Michal, Nicholas and Donnetta, all of you have treated me as family

ABSTRACT

CHAPTER 2

The six-membered heavy atom heterocycles $[Re_2(CO)_8(\mu\text{-}H)(\mu\text{-}SbPh_2)]_2$, **2.1** and $Pd[Re_2(CO)_8(\mu\text{-}H)(\mu\text{-}SbPh_2)]_2$, **2.3**, have been prepared by the palladium-catalyzed ring-opening cyclo-dimerization of the three-membered heterocycle $Re_2(CO)_8(\mu\text{-}H)(\mu\text{-}SbPh_2)$. The palladium atom that lies in the center of the heterocycle **2.3** was removed to yield **2.1**. The palladium removal was found to be partially reversible leading to an unusual example of host-guest behavior. A related dipalladium complex $Pd_2Re_4(\mu\text{-}Ph)(CO)_{16}(\mu_4\text{-}SbPh)(\mu_3\text{-}SbPh_2)(\mu\text{-}H)_2$, **2.2**, was also formed in these reactions of palladium with $Re_2(CO)_8(\mu\text{-}H)(\mu\text{-}SbPh_2)$. Thermolysis of **2.1** at 85 °C yielded $Re_3(CO)_{12}(\mu\text{-}SbPh_2)(\mu\text{-}H)_2$, **2.4** (2.9% yield), $Re_3(CO)_{12}(\mu\text{-}SbPh_2)_2(\mu\text{-}H)$, **2.5** (25.1% yield), and $Re_3(CO)_{13}(\mu\text{-}SbPh)(\mu\text{-}H)$, **2.6** (14.6% yield). The electronic structure of **2.1** and **2.3** were also investigated by DFT computational analyses.

CHAPTER 3

The compounds $Re_2(CO)_8(\mu\text{-}AuPPh_3)_2$, **3.1**, a dimer of $Re(CO)_4(\mu\text{-}AuPPh_3)$ and $Re_2(CO)_8(PPh_3)_2$ were obtained from UV-Vis induced decarbonylation of the compound $Re(CO)_5[Au(PPh_3)]$. Compound **3.1** contains two rhenium atoms bridged by two $AuPPh_3$ groups. It is formally unsaturated, 32 valence electrons, and exhibits a short Re – Re interaction, Re – Re = 2.9070(3)

Å, in the solid state. The nature of the metal – metal bonding in **3.1** was established by DFT computational analyses which provided evidence not only for σ-bonding but also for some complementary π-bonding directly between the two rhenium atoms. The electronic structure of $Re_2(CO)_8(\mu\text{-}H)_2$, **3.2** was similarly analyzed and is compared with **3.1**. Compound **3.1** is intensely colored due to metal-based low energy allowed electronic transitions between the HOMO and HOMO-2 and the LUMO. Compound **3.1** reacts with I_2 to yield $Re_2(CO)_8(\mu\text{-}AuPPh_3)(\mu\text{-}I)$, **3.3** and the known compound $Re_2(CO)_8(\mu\text{-}I)_2$, **3.4** by substitution of the bridging $AuPPh_3$ groups with bridging iodide ligands. Compound **3.3** is electronically saturated, 34 valence electrons, and contains a formal Re – Re single bond, Re – Re = 3.2067(5) Å. The bonding in compounds **3.3**, **3.4** and $Re_2(CO)_{10}$ were also analyzed computationally and was compared with **3.1** and **3.2**.

CHAPTER 4

The electronically unsaturated dirhenium complex $Re_2(CO)_8(\mu\text{-}AuPPh_3)(\mu\text{-}Ph)$, **4.1** was obtained from the reaction of $Re_2(CO)_8[\mu\text{-}\eta^2\text{-}C(H)=C(H)Bu^n](\mu\text{-}H)$ with $Au(PPh_3)Ph$. The bridging $AuPPh_3$ group was replaced by a bridging hydrido ligand to yield the unsaturated dirhenium complex $Re_2(CO)_8(\mu\text{-}H)(\mu\text{-}Ph)$, **4.2** by reaction of **4.1** with $HSnPh_3$. Compound **4.2** reductively eliminates benzene upon addition of NCMe at 25 °C. The electronic structure of **4.2** and the mechanism of the reductive elimination of the benzene molecule in its reaction with NCMe were investigated by DFT computational analyses. Reacting compound **4.2** with N,N-Diethylaniline formed another unsaturated dirhenium complex $Re_2(CO)_8(\mu\text{-}H)[\mu\text{-}$

$(C_2H_5)_2NC_6H_4]$, **4.3**. This reaction showed a C-H bond activation at the phenyl ring of **4.3**.

CHAPTER 5

Compound **5.1** was first isolated from the reaction of **4.1** with Ph_3SnH. In this chapter, an improved synthesis of **5.1** was reported. Interestingly enough, compound **5.1** is the first example of an X-ray crystallographic characterization of a gold-tin cluster complex having phenyl substituents.

CHAPTER 6

Reaction of HgI_2 with **4.1** yielded an interesting product $[Re_2(CO)_8(\mu\text{-}HgI)(\mu\text{-}\eta^1\text{-}C_6H_5)]_2$, **6.1**. In the solid state, compound **6.1** consists of a centrosymmetric dimer of empirical formula unit $Re_2(CO)_8(\mu\text{-}HgI)(\mu\text{-}\eta^1\text{-}C_6H_5)$. The dimer is being held together by two bridging iodide ligands between the two mercury atoms. The reaction of $Re_2(CO)_8[\mu\text{-}\eta^2\text{-}C(H)=C(H)Bu^n](\mu\text{-}H)$ with $HgPh_2$ produced another new rhenium mercury complex, $\{Re_2(CO)_8[\mu\text{-}\eta^2\text{-}C(H)=C(H)Bu^n]\}_2(\mu_4\text{-}Hg)$, **6.2** which consists of a spiro, μ_4 mercury atom bridging two hexenyl-bridged $Re_2(CO)_8[\mu\text{-}\eta^2\text{-}C(H)=C(H)Bu^n]$ groupings.

TABLE OF CONTENTS

LIST OF TABLES

LIST OF FIGURES

LIST OF SCHEMES

CHAPTER 1

INTRODUCTION

Dirheniumdecacarbonyl is one of the key starting material in the chemistry of rhenium carbonyl metal.[1] Dirheniumdecacarbonyl was first discovered by Hieber and Fuchs who heated Re_2O_7 and $KReO_4$ with carbon monoxide at 250-270 °C and 200-250 atm (eq. 1).[2] An X-ray crystal structure determination of $Re_2(CO)_{10}$ show a rhenium-rhenium bond joining two $[Re(CO)_5]$ units whose radial carbonyl groups lie in a staggered conformation (Figure 1.1). Hence an approximate D_{4d} symmetry is observed in $Re_2(CO)_{10}$. Specifically for rhenium a rich polynuclear chemistry has been reported. Examples include $H_2Re_2(CO)_8$[3], $H_3Re_3(CO)_{12}$[4], $H_6Re_4(CO)_{12}$[5] (Scheme 1.1). One prominent feature observed in the above mentioned rhenium polynuclear carbonyl hydride complexes is the absence of bridging carbonyl ligands.

$$Re_2O_7 + 17CO \longrightarrow [Re_2(CO)_{10}] + 7CO_2 \quad \text{(eq. 1)}$$

The photochemistry of $Re_2(CO)_{10}$ has been studied extensively, mainly with regards to substitution by phosphine ligands[6] and to a lesser extent with nitrogen bases[7]. However, it was the photolysis of $Re_2(CO)_{10}$ in the presence of a terminal olefin, 1-hexene that yielded the reactive compound, $Re_2(CO)_8[(\mu\text{–}H)(\mu\text{–}\eta^2\text{–}C(H)=C(H)nBu]$ that serves as a valuable reagent[8]. For example, reaction of $Re_2(CO)_8[(\mu\text{–}H)(\mu\text{–}\eta^2\text{–}C(H)=C(H)nBu]$ with Ph_3SnH gave a new dirhenium-diti

complex $Re_2(CO)_8(\mu–SnPh_2)_2$ (eq.2)[9]. The Re–Re bond distance in $Re_2(CO)_8(\mu–SnPh_2)_2$ is 3.1971(4) Å which is slightly longer than the Re–Re bond distance in $Re_2(CO)_{10}$ which is [3.042(1) Å]. Addition of $Pd(PBu^t_3)_2$ to $Re_2(CO)_8(\mu–SnPh_2)_2$ yielded the adduct $Pd_2Re_2(CO)_8(\mu–SnPh_2)_2(PBu^t_3)_2$ (eq. 3),[9] in which $Pd(PBu^t_3)$ groups have been added to the Re–Sn bonds. As a result, the Re–Re bond lengthens to 3.262(1) Å.

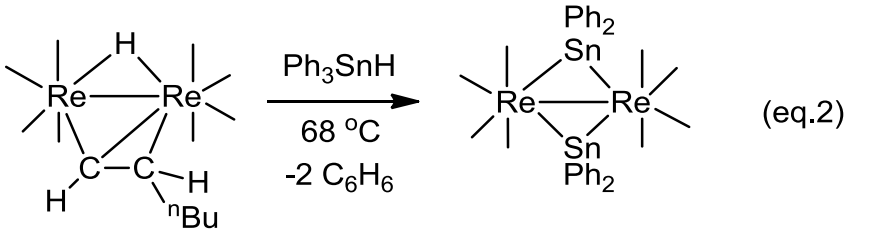

(eq.2)

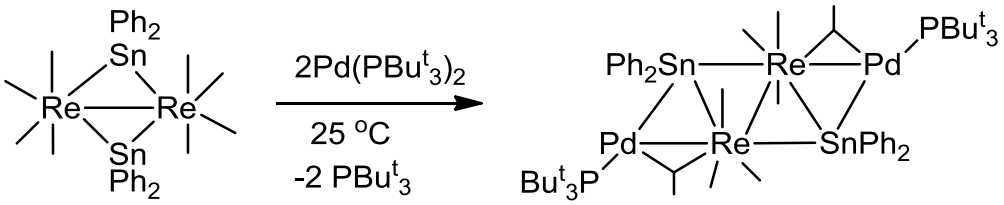

(eq. 3)

Reaction of $Re_2(CO)_8[(\mu–H)(\mu–\eta^2–C(H)=C(H)nBu]$ with group 15 ligands also yielded complexes with the general structure, $Re_2(CO)_8(\mu–EPh_2)_2$ where E=Sb,Bi[10,11] (eq. 4). The large Re–Re distance, 4.483(1)Å, in these molecules indicates the absence of any significant direct Re–Re bonding interactions.

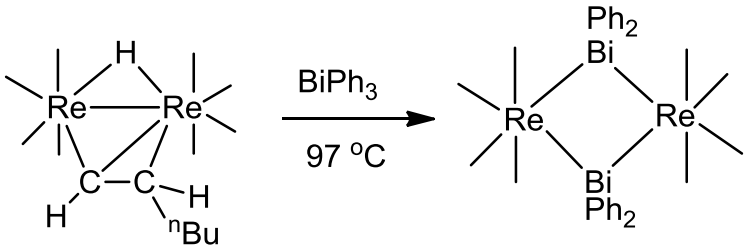

(eq. 4)

Recently, gold nanoparticles have been shown to exhibit significant catalytic activity for the oxidation of CO and certain olefins.[12] By mixing gold with transition metals, interesting new bimetallic catalysts for the oxidation of hydrocarbons have been discovered that exhibit even better catalytic activity.[13] Reacting $[NEt_4][Ir_4(CO)_{11}(Ph)]$ with $[Au(PPh_3)]NO_3$ yielded the compound $Ir_4(CO)_{11}(Ph)(\mu\text{-}AuPPh_3)$ (eq. 5).[14] An $AuPPh_3$ group was added to one of the Ir–Ir bonds which causes a bond lengthening effect to 2.9143(4) Å.

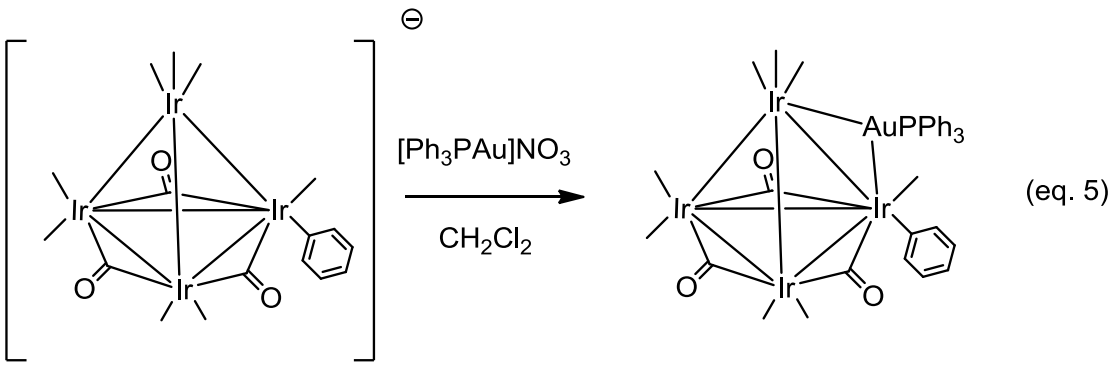

(eq. 5)

Similarly, the reaction of $Os_3(CO)_{10}(NCMe)_2$ with $C_6H_5AuPPh_3$ yielded the metal complex, $Os_3(CO)_{10}(\mu\text{-}C_6H_5)(\mu\text{-}AuPPh_3)$ (eq.6).[15] The molecule contains a triangular cluster of three osmium atoms with an η^1-bridging phenyl ligand and a bridging $AuPPh_3$ group across an Os–Os bond.[15]

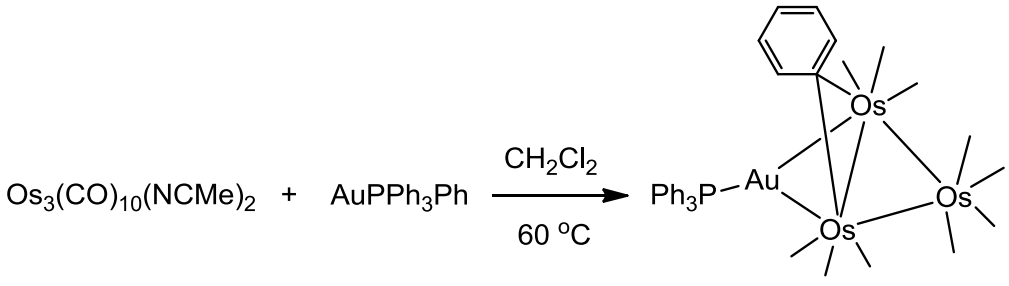

(eq. 6)

Saturated hydrocarbons are the major components of natural gas and petroleum even though there are only a few practical processes for converting them directly to more valuable products.[16] Hence developing the ability to selectively functionalize C–H bonds could potentially establish the most broadly applicable and powerful class of transformations in organic synthesis.[17] Activation of C–H bonds by transition metal-based systems has been around for a number of years.[17]

The first reported example of “C–H activation” by a transition metal complex can be traced to Chatt and Davidson.[18] It was shown that Ru(0)(dmpe)2, where dmpe=1,2-Bis(dimethylphosphino)ethane can react with naphthalene to give [Ru(H)(Ar)(dmpe)2] (eq. 7). The dmpe ligand has limited back-bonding capability so low-valent [Ru(dmpe)$_2$] has a very high tendency to display oxidative addition.

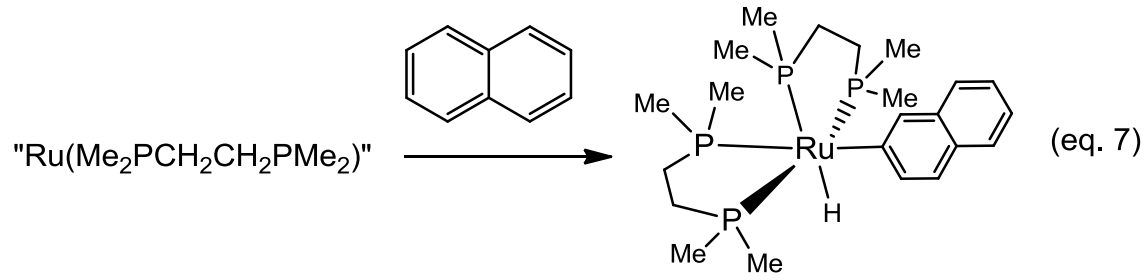

(eq. 7)

Shilov showed that the addition of Pt(IV) to the aqueous reaction of $PtCl_4^{2-}$ with methane led to the production of the selectively oxidized species, methanol and methyl chloride (eq. 8).[19] The “Shilov” system demonstrated selective alkane

functionalization under mild conditions although using platinum as a stoichiometric oxidant is not economically viable.[17]

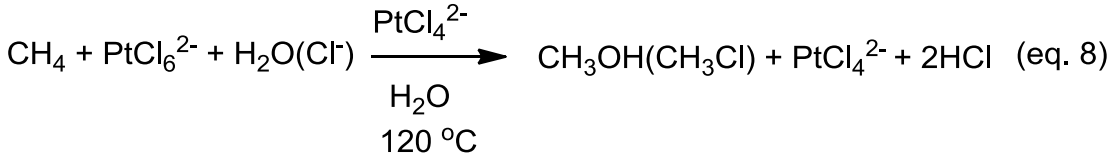

(eq. 8)

Recently, a successful hydroarylation of α-Methylstyrene with N,N-Diethylaniline was reported.[20] The reaction proceeded in the presence of a diaminocarbene gold chloride catalyst, pyrNHC-AuCl and $KB(C_6F_5)_4$.

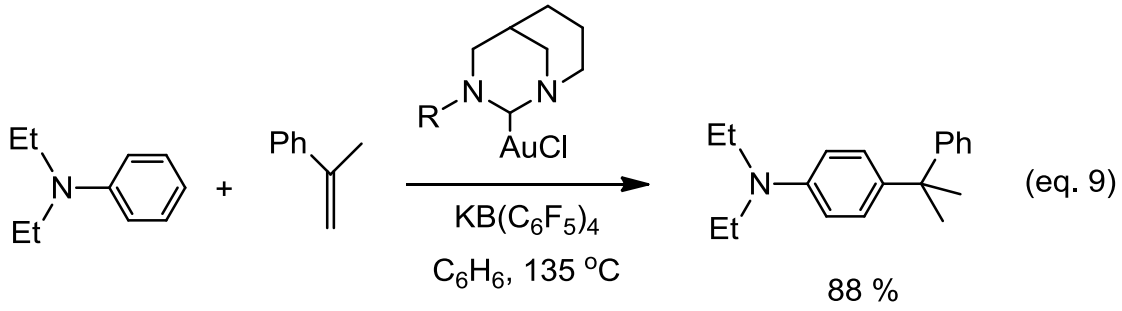

(eq. 9)

At elevated temperatures,TpRu(CO)(NCMe)(Ph),(Tp= hydridotris(pyrazolyl) borate) acts as a catalyst for the addition of arene C-H bonds across the C=C bond for olefins.[21] For instance, under 25 psi of ethylene pressure, 0.1 mol% of TpRu(CO)(NCMe)(Ph) in benzene (90 °C) catalyzes the formation of ethylbenzene with 51 turnovers after 4h (eq.10).[21]

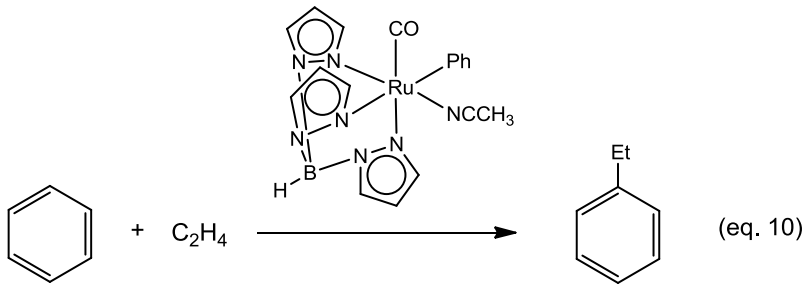

(eq. 10)

The design of new metal cluster complexes containing late third-row transition metals that can activate C-H bonds should further the understanding of C-H bond transformations on metal surfaces and by heterogeneous metal catalysts. The mechanisms of such reactions can also be investigated and evaluated by the methods of density functional theory (DFT) analyses.

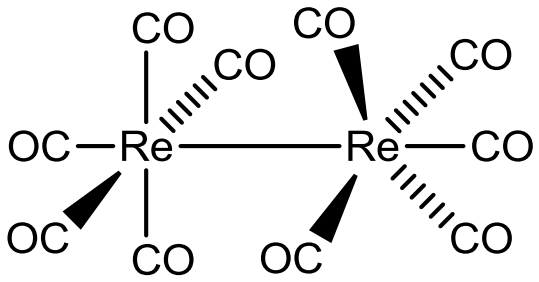

Figure 1.1. Molecular structure of $Re_2(CO)_{10}$

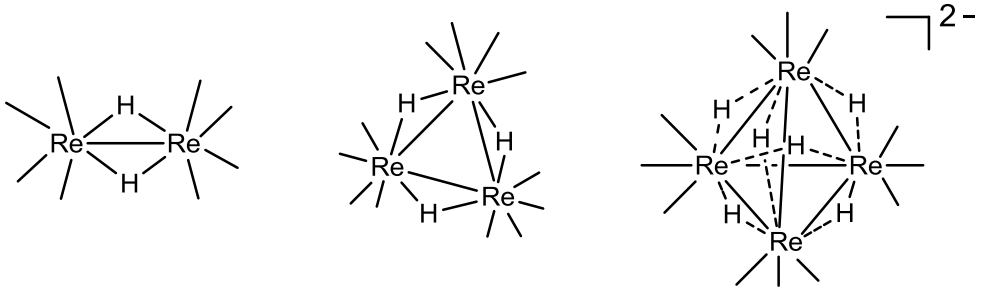

A **B** **C**

Scheme 1.1. Examples of polynuclear rhenium carbonyl hydride complexes. **A**, $H_2Re_2(CO)_8$ **B**, $H_3Re_3(CO)_{12}$, **C**, $H_6Re_4(CO)_{12}^{2-}$

REFERENCES

1) (a)Abel, E.W.;Stone, F.G.A., *Quart. Rev.*, **1970**, *24*, 498. (b) Abel, E.W. and Tyfield, S.P., *Adv. Organomet. Chem.*, **1970**, *8*, 117.

2) (a) Hieber, W.; Schuh, S.;Fuchs, H., *Z.Anorg.Allg.Chem*. **1941**, *248*, 243 (b) *Organometallic Syntheses*, ed. Eisch, J.J.; King, R.B., Academic Press, **1965**, Vol.1.

3) Bennett,M.J.;Graham,W.A.G.;Hoyano,J.K.;Hutcheon,W.L. *J.Am.Chem.Soc.*, **1972**, *94*, 6232

4) Johnson, J.R.; Kaesz, H.D. *Inorg. Synth.* **1978**, *18*, 60.

5) Kaesz, H. D.; B. Fontal; R. Bau; S. W. Kirtley; M. R. Churchill, J. Am. Chem. Soc., **1969**, *91*, 1021.

6) (a) Wrighton, M.S.; Ginley, D.S. *J.Am.Chem.Soc.* **1975**, 97, 2065. (b) Morse, D. L.; Wrighton, M. S. *Ibid* **1976**, *98*, 3931. (c) Byers, B. H.; Brown, T. L. *Ibid* **1975**, *97*, 947. (d) Kidd, D. R.; Brown, T. L. *Ibid*, **1978**, *100*, 4095.

7) (a) McCullen, S.B.; Brown, T.L. *Inorg. Chem.* **1981**, *20*, 3528. (b) Ziegler, M. L.; Hass, H.; Sheline, R. K. *Chem. Ber.* **1965**, *98*, 2454. (c) Allen, D.M.; Cox, A.; Kemp, T. J.; Sultana, Q.; Pitts, R. B. *J. Chem. Soc., Dalton Trans.* **1976**, 1189. (d) Gard, D. R.; Brown, T. L. *Organometallics* **1982**, *1*, 1143.

8) Nubel, P. O.; Brown,T.L. *J. Am. Chem. Soc.* **1984**, *106*, 644 – 652.

9) Adams, R. D.; Captain, B.; Johansson, M.; Smith, J. L. Jr *J.Am.Chem.Soc*, **2005**, *127*, 488-489.

10) Adams, R. D.;Pearl, W. C. *Inorg. Chem.* **2009**, *48*, 9519-9525.

11) Adams, R. D.; Captain, B.; Pearl, W. C. Jr. *J. Organomet. Chem.* **2008**, *693*, 1636-1644.

12)(a) Haruta, M. *Catal. Today* **1997**, *36*, 153-166. (b) Haruta, M.; Date, M. *Appl. Catal., A* **2001**, *222*, 427-437. (c) Hashmi, A. S. K.; Hutchings, G. J. *Angew. Chem., Int. Ed.* **2006**, *45*, 7896-7936.(d) Della Pina, C.; Falletta, E.; Prati, L.; Rossi, M. *Chem. Soc. Rev.***2008**, *37*, 2077-2095.

13)(a) Hutchings, G. J. *Chem. Commun.* **2008**, 1148-1164. (b) Lopez-Sanchez, J. A.; Dimitratos, N.; Glanvilla, N; Kesavan, L.; Hammond, C.; Edwards, J. K.; Carley, A. F.; Kiely, C. J.; Hutchings, G. J. *Catal. Today* **2011**, *391*, 400-406. (c) Enache, D. I.; Edwards, J. K.; Landon, P.; Solsona-Espriu, B.; Carley, A. F.; Herzing, A. A.; Watanabe, M.; Kiely, C. J.; Knight, D. W.; Hutchings, G. J. *Science* **2006**, *311*, 362-365. (d) Ortiz-Soto, L. B.; Alexeev, O. S.; Amiridis, M. D. *Langmuir* **2006**, *22*, 3112-3117. (e) Evans, J.; Gao, J. *J. Chem. Soc., Chem. Commun.* **1985**, 39-40. (f) Li, Y.; Pan, W.-X.; Wong, W.-T. *J. Cluster Sci.* **2002**, *13*, 223-233.

14) Adams, R. D.; Chen, M.; Yang, X. *Organometallics*, **2012**, *31*, 3588-3598.

15) Adams, R. D.; Rassolov, V.; Zhang, Q. *Organometallics*, **2012** *31*, 2961-2964.

16) Labinger, J. A.; Bercaw, J. E. *Nature*, **2002**, *417*, 507.

17) Goldman, A. S.; Goldberg, K. I. eds, ACS Symposium Series 885, Activation and Functionalization of C–H Bonds, **2004**, Chapter 1, 1-43.

18) Chatt, J.; Davidson, J. M. *J. Chem. Soc.* **1965**, 843

19) Shilov, A. E.; Shul'pin, G. B. Activation and Catalytic Reactions of Saturated Hydrocarbons in the presence of metal complexes, Kluwer, **2002**.

20) Hu, X.; Martin, D.; Melaimi, M.; Bertrand, G. *J. Am. Chem. Soc.* **2014**, *136*(39), 13594-13597.

21) Foley, N.A.; Lee, J.P.; Ke,Z.; Gunnoe,T.B.; Cundari,T.R. *Acc.Chem.Res.*,**2009**, *42*, 585-597.

CHAPTER 2

SYNTHESIS AND PROPERTIES OF A RHENIUM–ANTIMONY METALLA-HETEROCYCLE

INTRODUCTION

Antimony is considered to be a vital component of metal oxide catalysts used in the oxidation of hydrocarbons.[1] Rhenium-antimony and rhenium-bismuth complexes have shown to be precursors to effective heterogeneous nanoscale catalysts under unusually mild conditions for the ammoxidation of 3-picoline to 3-cyanopyridine, a precursor to Niacin or vitamin B3, eq. (1).[2]

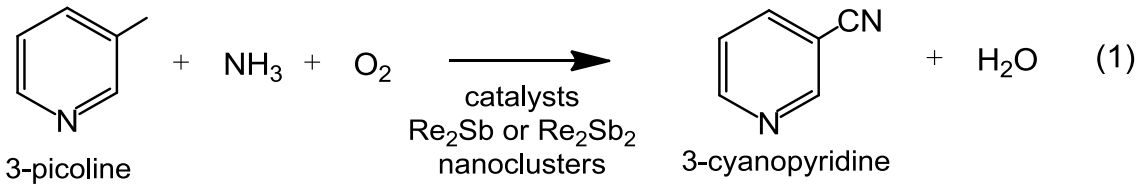

Using heavy atom ligands, such as diphenylantimony and diphenylbismuth to bond with heavy transition metals, unusual new metallaheterocycles like $HPtRe_2(CO)_8(\mu\text{-}SbPh_2)_2(P\text{-}t\text{-}Bu_3)$ [3], $[Re(CO)_4(\mu\text{-}BiPh_2)]_3$ [4a] and $[Os_3(\mu\text{-}H)(\mu\text{-}SbPh_2)(CO)_{10}]_2$ [4b] have been synthesized (Scheme 2.1). Heterocycles with binding sites are well known to serve effectively as ligands. In this work we have demonstrated that our new heavy atom heterocycles can also

serve as ligands. The 3-membered heterocyclic complex $Re_2(CO)_8(\mu\text{-}SbPh_2)(\mu\text{-}H)$ [5] containing a bridging diphenylantimony ligand was previously shown to react with $Pt(P\text{-}t\text{-}Bu_3)_2$,[6] by insertion of the Pt atom into one of the Re–Sb bonds to yield the bridging diphenylantimony ligand was previously shown to react with $Pt(P\text{-}t\text{-}Bu_3)_2$,[6] by insertion of the Pt atom into one of the Re–Sb bonds to yield the compound $Re_2[Pt(P\text{-}t\text{-}Bu_3)](\mu\text{-}SbPh_2)(CO)_8(\mu\text{-}H)$ (Scheme 2.2). Interestingly, at 125°C, the $Pt(P\text{-}t\text{-}Bu_3)$ group was eliminated to regenerate the original heterocyclic complex. This demonstrated the reversible addition and elimination of $Pt(P\text{-}t\text{-}Bu_3)$ (Scheme 2.2). By replacing $Pt(P\text{-}t\text{-}Bu_3)_2$ with $Pd(P\text{-}t\text{-}Bu_3)_2$, studies were undertaken to examine the reaction of $Pd(P\text{-}t\text{-}Bu_3)_2$ with $Re_2(CO)_8(\mu\text{-}SbPh_2)$. It was found that the heterocycle $Re_2(CO)_8(\mu\text{-}SbPh_2)(\mu\text{-}H)$ opens, dimerizes to from a six-membered heterocycle and simultaneously inserts a single uncharged palladium atom into the center of the ring. Interestingly, the palladium atom can be removed from the ring by treatment with $P\text{-}t\text{-}Bu_3$. The results of these studies are described in this chapter.

Experimental Details

General Data. Reagent grade solvents were dried by the standard procedures and were freshly distilled prior to use. Infrared spectra were recorded on a Thermo Nicolet Avatar 360 FT-IR spectrophotometer. ^1H NMR spectra were recorded on a Varian Mercury 300 spectrometer operating at 300.1 MHz. Mass spectrometric (MS) measurements performed by a direct-inlet probe by using electron impact ionization (EI) were made on a VG 70S instrument. $Pd(P\text{-}t\text{-}Bu_3)_2$,

$Pd(dba)_2$, dba = $(C_6H_5CH=CHCOCH=CHC_6H_5)_2$, $SbPh_3$ and $Re_2(CO)_{10}$ were purchased from STREM and were used without further purification. $Re_2(CO)_8(\mu\text{-}H)(\mu\text{-}SbPh_2)$, was prepared according to a previously reported procedure.[5] Product separations were performed by TLC in air on Analtech 0.25 and 0.5 mm silica gel 60 Å F_{254} glass plates.

Reaction of $Re_2(CO)_8(\mu\text{-}H)(\mu\text{-}SbPh_2)$ with $Pd(P\text{-}t\text{-}Bu_3)_2$.

40.0 mg (0.0457 mmol) of $Re_2(CO)_8(\mu\text{-}H)(\mu\text{-}SbPh_2)$ was added to 5.8 mg (0.0114 mmol) of $Pd(P\text{-}t\text{-}Bu_3)_2$ and dissolved in 0.2 mL of benzene and sealed under vacuum in a test tube. The reaction was heated for 3h at 50 °C. Yellow crystals formed. The solvent was decanted, washed with 2 mL of benzene followed by a 2 mL of 1:1 benzene/hexane solvent mixture. 11.9 mg (29% yield) of yellow $[Re_2(CO)_8(\mu\text{-}H)(\mu\text{-}SbPh_2)]_2$, **2.1** was obtained from crystallization in air. The washes were combined and then separated by TLC in air by using a 3:1 hexane/methylene chloride solvent mixture to yield 1.7 mg (4% yield) of red $Pd_2Re_4(\mu\text{-}Ph)(CO)_{16}(\mu_4\text{-}SbPh)(\mu_3\text{-}SbPh_2)(\mu\text{-}H)_2$, **2.2**. Spectral data for **2.1**: IR ν_{CO} (cm^{-1} in methylene chloride): 2093(s), 2021(vs), 1999(m), 1983(s), 1956(m). ^1H NMR (CD_2Cl_2, in ppm) δ = 7.39-7.61 (m, 20H, Ph), -14.94 (s, 2H, hydride). Mass Spec. EI/MS *m*/*z*. 1746. The isotope distribution pattern is consistent with the presence of four rhenium atoms and two antimony atoms. Spectral data for **2.2**. IR ν_{CO} (cm^{-1} in hexane): 2098(m), 2076(s), 2015(vs), 2008(s), 2002(s), 1996(s), 1984(s), 1966(m), 1959(m), 1936(w). ^1H NMR (CD_2Cl_2, in ppm) δ = 7.05-7.71 (m, 20H, Ph), -11.97 (d, 1H, J= 4.3 Hz, Re-H-Pd), -15.11 (d, 1H, J= 4.3 Hz, Pd-H-

Pd). Mass Spec. EI/MS *m*/*z*. 1960. The isotope distribution pattern is consistent with the presence of four rhenium atoms, two antimony atoms and two palladium atoms.

Reaction of $Re_2(CO)_8(\mu\text{-}H)(\mu\text{-}SbPh_2)$ with $Pd(dba)_2$.

30.0 mg (0.0343 mmol) of $Re_2(CO)_8(\mu\text{-}H)(\mu\text{-}SbPh_2)$ was added to 11.8 mg (0.0206 mmol) of $Pd(dba)_2$ in 0.4 mL of benzene and sealed *under vacuo* in a test tube. The reaction was heated for 3h at 50 °C. Orange-red crystals consisting of a mixture of $Pd[Re_2(CO)_8(\mu\text{-}H)(\mu\text{-}SbPh_2)]_2$, **2.3** and **2.1** cocrystallized from the reaction solution. The reaction solution was decanted and the crystals were washed three times with benzene. These samples of **2.3** are always contaminated with some **2.1**, and compound **2.3** is very difficult to separate in a pure form. Combined yield of **2.1** and **2.3** was 11.1 mg (33%). 1.2 mg of **2.2** (6% yield) was also obtained in this reaction. Since we have been able to obtain **2.1** in a pure form, see above, it is easy to identify the spectral features of **2.3** in mixtures that contain **2.1**. Spectral data for **2.3**: IR ν_{CO} (cm^{-1} in methylene chloride): 2082(s), 2016(vs), 1994(m), 1981(s), 1952(m). ^1H NMR ($CD_3C_6D_5$, in ppm) δ = 7.10 (m, 20H, Ph), -17.89 (s, 2H, hydride).

Removal of Pd from 2.3 to yield 2.1.

2.0 mg (0.0011 mmol) of **2.3** and 1.5 mg (0.0053 mmol) of $P(C_6H_{11})_3$ were dissolved in CD_2Cl_2. At t=0 hr, the solution contained 12% of **2.3** and 88% of **2.1**.

At t=3 hrs, most of the Pd was removed from **2.3** and the solution contained 5% of **2.3** and 95% of **2.1**.

Addition of Pd to 2.1 to yield 2.3

2.0 mg (0.0011 mmol) of **2.1**, 3.3 mg (0.0057 mmol) of $Pd(dba)_2$ and 3.8 mg (0.0051 mmol) of $H_4Ru_4(CO)_{12}$ (added for use as an internal standard) were dissolved in CD_2Cl_2. The NMR tube then further cooled to -21°C. At t=0 hr, the solution contained 96% of **2.1** and 4% of **2.3**. At t=24 hrs, the solution contained 57% of **2.1** and 43% of **2.3**.

Thermolysis of 2.1 at 85°C.

A 35.0 mg portion of **2.1** was dissolved in 5 mL of freshly distilled toluene and was heated to reflux for 24 h. After cooling, the solvent was removed in vacuo, and the residue was then extracted in methylene chloride and separated by TLC by using a 4:1 hexane/methylene chloride (v/v) solvent mixture. The products listed in order of elution include: a colorless band of unreacted $Re_2(CO)_8(\mu\text{-}SbPh_2)(\mu\text{-}H)$[5], 1.4 mg (4.0% yield), a colorless band of $Re_3(CO)_{12}(\mu\text{-}SbPh_2)(\mu\text{-}H)_2$, **2.4**, 0.9 mg (2.9% yield), a colorless band of $Re_2(CO)_8(\mu\text{-}SbPh_2)_2$ [2], 0.8 mg (1.7% yield), a colorless band of $Re_3(CO)_{12}(\mu\text{-}SbPh_2)_2(\mu\text{-}H)$, **2.5**, 9.7 mg (25.1% yield), a yellow band of $Re_3(CO)_{13}(\mu\text{-}SbPh)(\mu\text{-}H)$, **2.6**, 4.4 mg (14.6% yield). Spectral data for **2.4**: IR (ν_{CO} cm^{-1} in hexane): 2114(w), 2084(s), 2022(vs), 2006(m), 1987(m), 1973(m). ^1H NMR (CD_2Cl_2, in ppm) δ = 7.5-7.3 (m, 10H, Ph), -19.2 (s, 2H, hydride). Mass Spec. EI/MS: 1172(M^+), 1144(M^+-CO), 1116(M^+-

2CO), 1088(M^+-3CO) *m/z*. The isotope pattern is consistent with the presence of three rhenium and one antimony atoms. Spectral data for **2.5**: IR (ν_{CO} cm^{-1} in hexane): 2101(w), 2076(s), 2013(vs), 1995(s), 1984(m), 1979(m), 1970(m), 1964(w). ^1H NMR (CD_2Cl_2, in ppm) δ = 7.5-7.2 (m, 10H, Ph), -12.7 (s, 1H, hydride). Mass Spec. EI/MS: 1448(M^+) *m/z*. The isotope pattern is consistent with the presence of three rhenium and two antimony atoms. Spectral data for **2.6**: IR (ν_{CO} cm^{-1} in hexane): 2132(w), 2093(m), 2073(m), 2038(vs), 2032(s), 2011(m), 2005(s), 1990(vs), 1960(s). ^1H NMR (300 MHz, $CDCl_3$, rt, TMS, in ppm) δ = 7.9-7.2 (m, 5H, Ph), -15.8 (s, 1H, hydride). Mass Spec. EI/MS: 1122(M^+), 1066 (M^+-2CO), 1038(M^+-3CO), 1010(M^+-4CO) *m/z*. The isotope pattern is consistent with the presence of three rhenium and one antimony atoms.

Crystallographic Analyses: Colorless single crystals of **2.1** suitable for x-ray diffraction analyses were obtained from the reaction solution when it was cooled to room temperature. Red single crystals of **2.2** suitable for x-ray diffraction analyses were obtained by slow evaporation of solvent from hexane at room temperature. Orange-red single crystals of **2.3** suitable for x-ray diffraction analyses were obtained from the reaction solution when it was cooled to room temperature. Colorless single crystals of **2.4**, **2.5, and 2.6** suitable for x-ray diffraction analyses were obtained by slow evaporation of solvent from a hexane/methylene chloride solvent mixture at -25 °C. Each data crystal was glued onto the end of a thin glass fiber. X-ray intensity data were measured by using a Bruker SMART APEX CCD-based diffractometer by using Mo Kα

radiation (λ = 0.71073 Å). The raw data frames were integrated with the SAINT+ program by using a narrow-frame integration algorithm.[7] Corrections for Lorentz and polarization effects were also applied with SAINT+. An empirical absorption correction based on the multiple measurement of equivalent reflections was applied using the program SADABS. All structures were solved by a combination of direct methods and difference Fourier syntheses, and refined by full-matrix least-squares on F^2, using the SHELXTL software package.[8] All non-hydrogen atoms were refined with anisotropic displacement parameters. Hydrogen atoms on the phenyl groups were placed in geometrically idealized positions and included as standard riding atoms during the least-squares refinements. Compound **2.1** crystallized in the monoclinic crystal system. The systematic absences in the data were consistent with the space groups Cc and C2/c. The latter was initially selected and was confirmed by the successful solution and refinement of the structure. The hydride ligands in **2.1** were refined on their positional parameters with a fixed thermal parameter. Compound **2.2** crystallized in the triclinic crystal system. The centrosymmetric space group $P\bar{1}$ was selected and was confirmed by the successful solution and refinement of the structure. The hydride ligands in **2.2** were refined as follows: H1 was refined with the Re - H and Pd - H distances fixed at 1.75 Å. H2 was refined without any restraints. Compound **2.3** crystallized in the orthorhombic crystal system. The space group Fdd2 was uniquely identified by the pattern of systematic absences observed in the data. The hydride ligands in the crystal of **2.3** were located and fully refined in the analysis with an isotropic thermal parameter. This crystal was found to be a

cocrystallized mixture of **2.1** and **2.3**. In the final stages of refinement the occupancy factor of the palladium atom was refined. It converged to a value of 0.51. Compound **2.4** crystallized in the triclinic space group. The hydrides were refined as follows: H1 was refined with the Re1 – H1 and Re2 – H1 bond distances fixed at 1.75 Å. Compound **2.5** also crystallized in the triclinic system. The hydride ligand was located along the Re – Re bond and refined on its positional parameter with a fixed isotropic thermal parameter. Compound **2.6** crystallized in the monoclinic crystal system. Based on the systematic absences in the intensity data for **2.6**, the space group $P2_1/m$ was uniquely identified. Crystal data, data collection parameters, and results of the analyses are listed in Tables 2.1 and 2.2.

Computational Details.

Density functional theory (DFT) calculations were performed with the Amsterdam Density Functional (ADF) suite of programs [9] by using the PBEsol functional [10] with Zero Order Relativistic Approximation (ZORA). Valence quadruple-ζ + 4 polarization, relativistically optimized (QZ4P) basis sets were used for palladium, rhenium, antimony, oxygen, carbon and hydrogen atoms with no frozen cores. The molecular orbitals for **2.1** and **2.3** and their energies were obtained by geometry optimized calculations that were initiated on their respective structures based on their structures obtained from single crystal X-Ray diffraction analyses. The fragment analysis for compound **2.3** was also performed with the ADF programs by using the meta-Generalized Gradient Approximation (meta-GGA)

level non-empirical Tao-Perdew-Staroverov-Scuseria(TPSS) functional [11]. The above mentioned basis sets were used.

Results and Discussion

When $Re_2(CO)_8(\mu\text{-}SbPh_2)(\mu\text{-}H)$ was heated to 45 °C in the presence of $Pd(P\text{–}t\text{–}Bu_3)_2$, it was transformed into the new six–membered tetrarhena-heterocycle $Re_4(CO)_{16}(\mu\text{–}SbPh_2)_2(\mu\text{–}H)_2$, **2.1** in 29% yield by ring-opening cyclo-dimerization process. Compound **2.1** was characterized by single–crystal x-ray diffraction analysis and an ORTEP diagram of its molecular structure is shown in Figure 2.1.

The structure of compound **2.1** consists of a puckered 6-membered Re_2SbRe_2Sb ring having a chair–like conformation. The $SbPh_2$ ligands lie at opposite sides of the ring. The molecule contains two–fold rotational symmetry in the solid state. Compound **2.1** contains two equivalent hydrido ligands that bridge the Re—Re bonds, Re1–Re2= 3.2607(4) Å, between the two $Re_2(CO)_8$ groupings, ^1H NMR δ = –14.94. Interestingly, the hydrido ligands lie inside the ring. There was no spectroscopic evidence for formation of **2.1** even by heating $Re_2(CO)_8(\mu\text{-}SbPh_2)(\mu\text{-}H)$ to 100 °C for 2h in the absence of a source of palladium.

To better understand the bonding nature of the structure of compound **2.1**, a geometry optimized DFT calculation was performed (Figure 2.7). The HOMO

orbital of **2.1** showed a bonding interaction between the p_x orbitals on the two antimony atoms and the $d_{x^2-y^2}$ orbital on rhenium atoms. HOMO-30 and HOMO-31 show the bonding hydride ligands to the rhenium atoms. The bonding is a combination of the 1s orbital of H with the d_{xz} orbitals of the rhenium atoms. This molecular orbital consists of two three-center two-electron Re–H–Re bonds. HOMO-39 orbital is an interesting molecular orbital that shows the nature of the Re – Sb bonding across the entire six membered ring. This molecular orbital looks like a doughnut and includes the 1s orbital from each H ligand, the two antimony p_z orbitals and the d_{xz} orbitals from the four rhenium atoms. This highly-delocalized orbital lies a low energy (-9.80 eV) and greatly stabilizes the structure of the ring.

There was a second product, $Pd_2Re_4(CO)_{16}(\mu_4\text{–}SbPh)(\mu_3\text{–}SbPh_2)(\mu\text{–}Ph)(\mu\text{–}H)_2$, **2.2** obtained in only 4% yield that contains two mutually–bonded palladium atoms, see Figure 2.2. Formally, compound **2.2** contains two ring–opened equivalents of $Re_2(CO)_8(\mu\text{-}SbPh_2)(\mu\text{-}H)$, but they are separated by the two Pd atoms and a phenyl ring was cleaved from one of the original $SbPh_2$ ligands. This phenyl ring serves as a bridging ligand across the Re(2)–Pd(2) bond.

When a concentrated solution of compound $Re_2(CO)_8(\mu\text{-}SbPh_2)(\mu\text{-}H)$ was treated with $Pd(dba)_2$, dba=dibenzylideneacetone at 45°C, compound **2.1** together with a second product, $Pd[Re_2(CO)_8(\mu\text{–}SbPh_2)(\mu\text{–}H)]_2$, **2.3** was

obtained. Because of their structural similarities, the two compounds cocrystallize from the reaction mixture. The ratio of the two compounds in the crystalline form varies from reaction to reaction and crystal to crystal depending on the original concentrations of $Re_2(CO)_8(\mu\text{-}SbPh_2)(\mu\text{-}H)$ and $Pd(dba)_2$ in the reaction solution. It is possible to find samples that contain as much as 96% of **2.3**.[12] Compound **2.3** was characterized crystallographically and an ORTEP diagram of its molecular structure is shown in Figure 2.3.

Compound **2.3** contains a slightly puckered 6–membered Re_4Sb_2 ring similar to that of **2.1**, but it also contains a palladium atom in the center of the ring. This particular crystal contained only 51% Pd (determined by occupancy refinement) in the center of the Re_4Sb_2 ring. The palladium atom is bonded to all four Re atoms, Pd(1)–Re(1)=2.9348(18) Å, Pd(1)–Re(2)=2.9455(19) Å, Pd(1)–Re(3)=2.9820(18) Å, Pd(1)–Re(4)=2.9823(19) Å. The Re—Re bond distances in **2.3** have increased relative to those in **2.1**, Re(1)–Re(2)=3.4235(7) Å, Re(3)–Re(4)=3.3592(6) Å as a result of the insertion of the Pd atom into the ring.[13] Although these Re – Re distances seem long, they are not unprecedented. The hydride-bridged Re – Re interactions are 3.439(24) Å[14] in $Re_4(CO)_{16}(\mu\text{–}H)_4$ and 3.2742(4) Å in $HPtRe_2(CO)_8(P\text{-}t\text{–}Bu_3)(\mu\text{–}SbPh_2)_2(\mu\text{–}H)$.[3] The observed Pd–Sb distances, Pd(1)–Sb(1)=2.6306(18) Å, Pd(1)–Sb(2)=2.6351(18) Å, in **2.3** are short enough to imply significant bonding interactions between these atoms. The Pd–Sb bond distances in the compounds $Pd(SbPh_3)_2(Ph)X$, X=Cl and Br, are 2.5568(5) Å and 2.5421(5) Å, respectively.[15] The two equivalent hydrido ligands

H1 and H2, ^{1}H NMR δ = –17.89, were located and refined in this low temperature structural analysis and they serve as triply bridging ligands across the two oppositely positioned Re_2Pd triangles, Pd(1)–H(1)=1.90(10) Å, Pd(1)–H(2)=1.76(10) Å.

The nature of the bonding between the palladium atom and the heterocycle was investigated by geometry–optimized DFT molecular orbital calculations.[16] The bonding between the d_{xy} orbital on the palladium atom and the p–orbitals on the Sb atoms are shown in the orbital HOMO–29, (Figure 2.8). Interactions between the palladium atom and the two hydride ligands are shown in HOMO–40 and HOMO-52. These bonding interactions stabilize the molecule to a surprisingly large degree as the neutral Pd atom's binding energy is 40 kcal mol^{-1}.

In order to understand the nature of the coordination of palladium to the 6-membered Re_4Sb_2 ring further, a computational fragment analysis of compound **2.3** was also performed. The fragment molecular orbitals were created by using an isolated palladium atom (shown on the left side) and the 6-membered Re_4Sb_2 ring (shown on the right side) in the combined MO energy level diagram (Figure 2.9). The HOMO–41 of **2.3** is another important molecular orbital showing the nature of the bonding of palladium to the Re_4Sb_2 ring. The bonding is a combination of the $d_{x^2-y^2}$ orbital of palladium and HOMO–31 of the Re_4Sb_2 ring fragment. HOMO-41 shows bonding between the hydride ligands and also a Sb–

Pd–Sb, three-center two-electron interaction. An antisymmetric combination of HOMO-31 is represented by the fragment orbital HOMO–30 which interacts with an empty p_x orbital on the palladium atom to form the HOMO–40 of the molecule. The HOMO-29 is formed by a strong interaction between the d_{xy} orbital on the palladium atom and the HOMO of ring fragment orbital. The HOMO of **2.3** is formed by an asymmetric combination of these two fragment orbitals which is slightly antibonding between the ring and the palladium atom. The Pd–Re_4Sb_2 ring interactions in HOMO–40 and HOMO–52 are created by combinations of the HOMO–30, HOMO–31 Re_4Sb_2 ring fragment molecular orbital and d-orbitals on the palladium atom.

There is a remarkable relationship between **2.1**/**2.3** that resembles a host/guest type of behavior. For example, when a solution of a **2.1**/**2.3** mixture (12%/88%) was treated with PCy_3, Cy=C_6H_{11} (cyclohexyl), the palladium atom was removed from **2.3** with complete conversion to **2.1** in 3 h at 25°C. No **2.3** remained as determined by ^{1}H NMR spectroscopy. Interestingly, the palladium atom could be partially reintroduced into the ring of **2.1** although as yet we have not been able to drive this conversion back to **2.3** to completion. The Pd readdition will, of course, depend on the nature of the Pd reagent and the ligands that are bonded to it. For example, when a solution of **2.3**/**2.1** (4%/96%) in CD_2Cl_2 solvent in an NMR tube was treated with $Pd(dba)_2$ at –20°C, the **2.3**/**2.1** ratio increased to 43%/57% over a period of 24 h as determined by the increase

in the hydride resonance of **2.3** at δ = –17.89 relative to that of **2.1** at δ = –14.94.[17]

The mechanism of the palladium-catalyzed cyclo-dimerization of $Re_2(CO)_8(\mu\text{-}SbPh_2)(\mu\text{-}H)$ to **2.1**, the addition of Pd to **2.1** and its removal from **2.3** have not yet been fully established. However, it seems most likely that the cyclo-dimerization begins with the insertion of a Pd–containing grouping into one of the Re—Sb bonds in $Re_2(CO)_8(\mu\text{-}SbPh_2)(\mu\text{-}H)$ as was observed in the reaction of $Re_2(CO)_8(\mu\text{-}SbPh_2)(\mu\text{-}H)$ with $Pt(P\text{–}t\text{–}Bu_3)_2$, Scheme 2.2.[6] This process may even involve **2.3** as an intermediate. More interestingly, however, is the observation that the palladium atom can not only be removed from **2.3** but can also be reinserted back into the metallacycle **2.1**. The heterocycle **2.1** can thus be viewed as a host for the complexation of a single, uncharged palladium atom, see Scheme 2.3.

After synthesizing compound **2.1**, its thermal stability was investigated. Upon heating compound **2.1** in toluene at 85 °C, several new compounds were formed and subsequently characterized. Compounds **2.4**, **2.5** and **2.6** were characterized crystallographically. ORTEP diagrams of the molecular structures of **2.4**, **2.5** and **2.6** are shown in Figures 2.4, 2.5 and 2.6, respectively. Since thermolysis is not specific in bond breaking, the result is fragmentation of compound **2.1**. One of the thermolysis product is $Re_2(CO)_8(\mu\text{-}SbPh_2)(\mu\text{-}H)$, the original reagent for synthesizing **2.1**. In the presence of heat, two oppositely-

positioned Re-Sb bonds are cleaved. This results in the nucleophilic attack by the lone pair of electrons of antimony on a rhenium atom. (Scheme 2.4.).

Another possible pathway for the fragmentation involves the loss of a "$HRe(CO)_4$" fragment followed by cleavage of the Re-Sb bond. With the loss of a "$HRe(CO)_4$" fragment, the lone pair of electrons on antimony can then perform a nucleophilic attack on a rhenium atom. A five-membered ring compound, $Re_3(CO)_{12}(\mu\text{-}SbPh_2)_2(\mu\text{-}H)$, **2.5** is then formed (Scheme 2.5). Compound **2.5** was structurally characterized by X-ray diffraction analysis. The compound crystallized with two independent molecules in the asymmetric unit. Each molecule contains three $Re(CO)_4$ groups. A $SbPh_2$ ligand bridges the Re(1) and Re(2) atoms and the Re(1) and Re(3) atoms. Since the Re(1)···Re(2) bond distance is 4.82 Å and the Re(1) ···Re(3) bond distance is 4.79 Å, there are no significant Re-Re bonding interactions between these pairs of rhenium atoms which are bridged by $SbPh_2$ ligands (Figure 2.5). The Re(2)-Re(3) bond distance is long, 3.2665(7) Å, which reflects the presence of a bridging hydride ligand.

One other possible fragmentation pathway involves the breaking of three bonds: Re-Sb, Re-H and Re-Re. A "$Ph_2SbRe(CO)_4$" fragment is eliminated from the six-membered dimer and the stable molecule $Re_3(CO)_{12}(\mu\text{-}SbPh_2)(\mu\text{-}H)_2$, **2.4** is formed. Two "$Ph_2SbRe(CO)_4$" fragments then dimerize to form the four-membered ring compound, $[Re(CO)_4(\mu\text{-}SbPh_2)]_2$ [2](Scheme 2.6). The crystal of compound **2.4** contains three crystallographically independent molecules in the

asymmetric crystal unit. The Re(1)-Sb(1) and Re(3)-Sb(1) bond lengths are 2.7525(8) and 2.7527(8) Å, respectively (Figure 1.4). Lengthening of the Re—Re bonds (Re(1)-Re(2)=3.4545(6)Å, Re(2)-Re(3)=3.4387(6) Å) was also observed due to the presence of the bridging hydrido ligands.

In the presence of the "$HRe(CO)_4$" fragment, an insertion into the Sb-Ph bond forms a proposed intermediate, "$Re_2(CO)_8(\mu\text{-}H)(\mu_3\text{-}SbPh)Re(CO)_4(\sigma\text{-}H)(\sigma\text{-}Ph)$". The reductive elimination of benzene from this intermediate followed by a CO addition could yield the observed product $Re_3(CO)_{13}(\mu_3\text{-}SbPh)(\mu\text{-}H)$, **2.6** (scheme 2.7). The crystal of compound **2.6** contains two crystallographically-independent molecules in the asymmetric crystal unit. Compound **2.6** consists of two mutually-bonded rhenium atoms that are bridged by a '$SbPhRe(CO)_5$' group and a hydrido ligand (Figure 2.6). The Re(1)-Re(1*) bond distance is 3.2284(7)Å.

Summary

In the presence of $Pd(P\text{-}t\text{-}Bu_3)_2$, $Re_2(CO)_8(\mu\text{-}SbPh_2)(\mu\text{-}H)$ undergoes a remarkable ring-opening cyclo-dimerization to form the new six-membered tetrarhena-heterocycle, $Re_4(CO)_{16}(\mu\text{-}SbPh_2)_2(\mu\text{-}H)_2$, **2.1**. Similarly, the reaction of $Pd(dba)_2$ and $Re_2(CO)_8(\mu\text{-}SbPh_2)(\mu\text{-}H)$ yielded the same six-membered tetrarhenadiantimony-heterocycle but a palladium was inserted into the middle of the ring, $Pd[Re_2(CO)_8(\mu\text{-}SbPh_2)(\mu\text{-}H)]_2$, **2.3**. Complexes **2.1** and **2.3** exhibit a host/guest behavior. Host-guest phenomena have been one of the most exciting methods for gaining control over the reactivity of ions, molecules, metal

complexes and nanomaterials in recent years.[18–22] Crown ethers, cryptands, metallacycles, cavitands and capsules are well known for their ability to complex ions and molecules in solutions.[18–22] The compound may prove to be a potential new family of hosts, heavy atom metallaheterocycles, that could add a new direction to this important field, namely, the ability to complex and sustain uncharged metal atoms.

Thermolysis of **2.1** yielded three new compounds. The first compound is the doubly $SbPh_2$-bridged trirhenium complex, **2.4**, followed by a five membered ring **2.5** containing two doubly bridging $SbPh_2$ ligands and a bridging hydride ligand. Also included was **2.6**, a trirhenium complex with a bridging hydride and pendant $SbPhRe(CO)_5$ grouping.

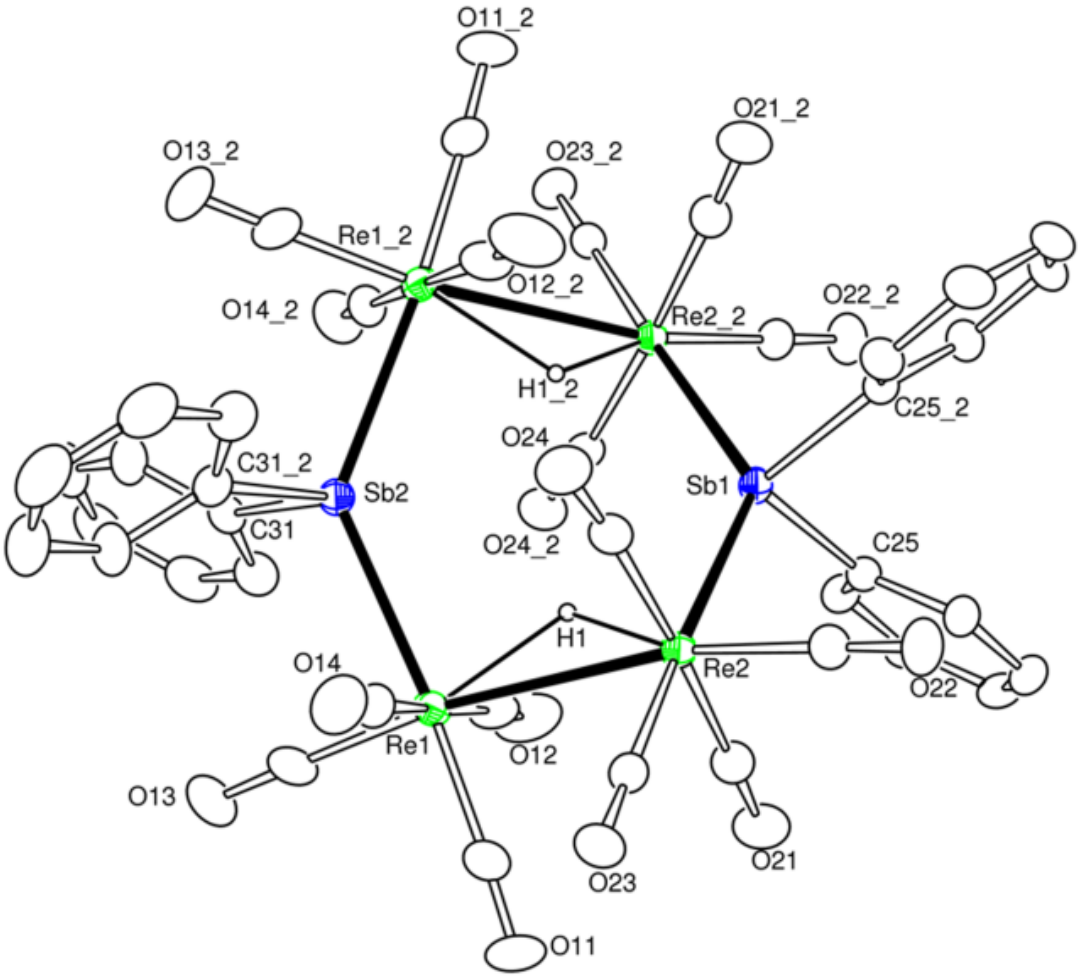

Figure 2.1. An ORTEP diagram of the molecular structure of $[Re_2(CO)_8(\mu–SbPh_2)(\mu–H)]_2$, **2.1**, showing 30% thermal ellipsoid probability.

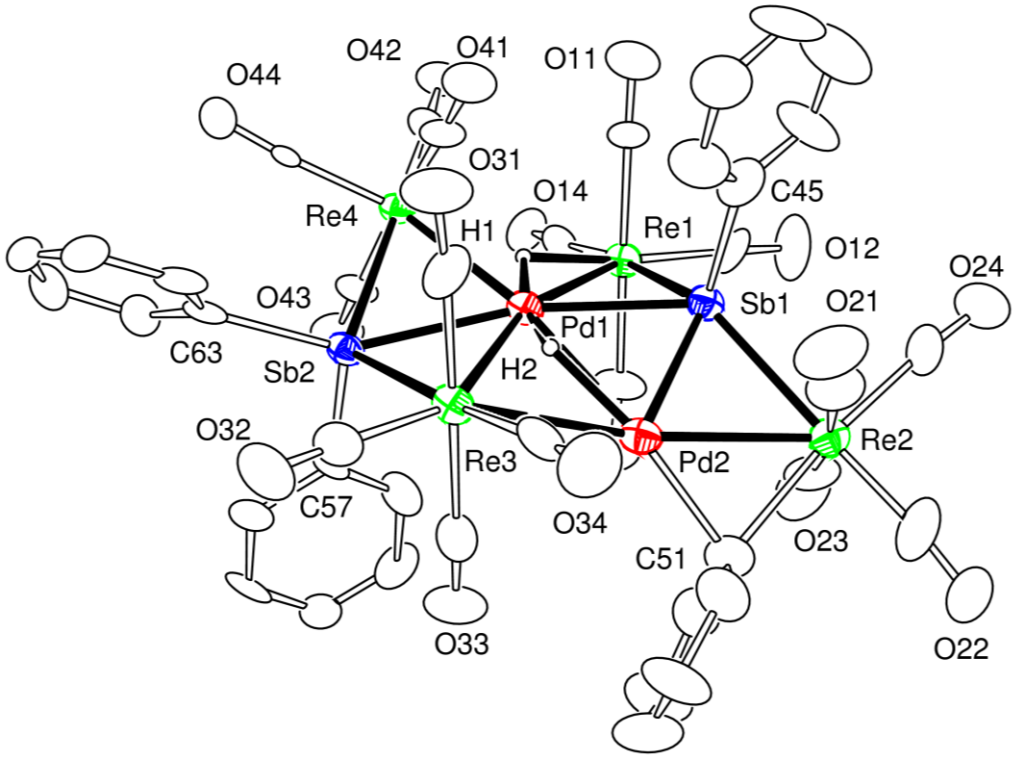

Figure 2.2. An ORTEP diagram of the molecular structure of $Pd_2Re_4(CO)_{16}(\mu_4\text{–}SbPh)(\mu_3\text{–}SbPh_2)(\mu\text{–}Ph)(\mu\text{–}H)_2$, **2.2**, showing 30% thermal ellipsoid probability.

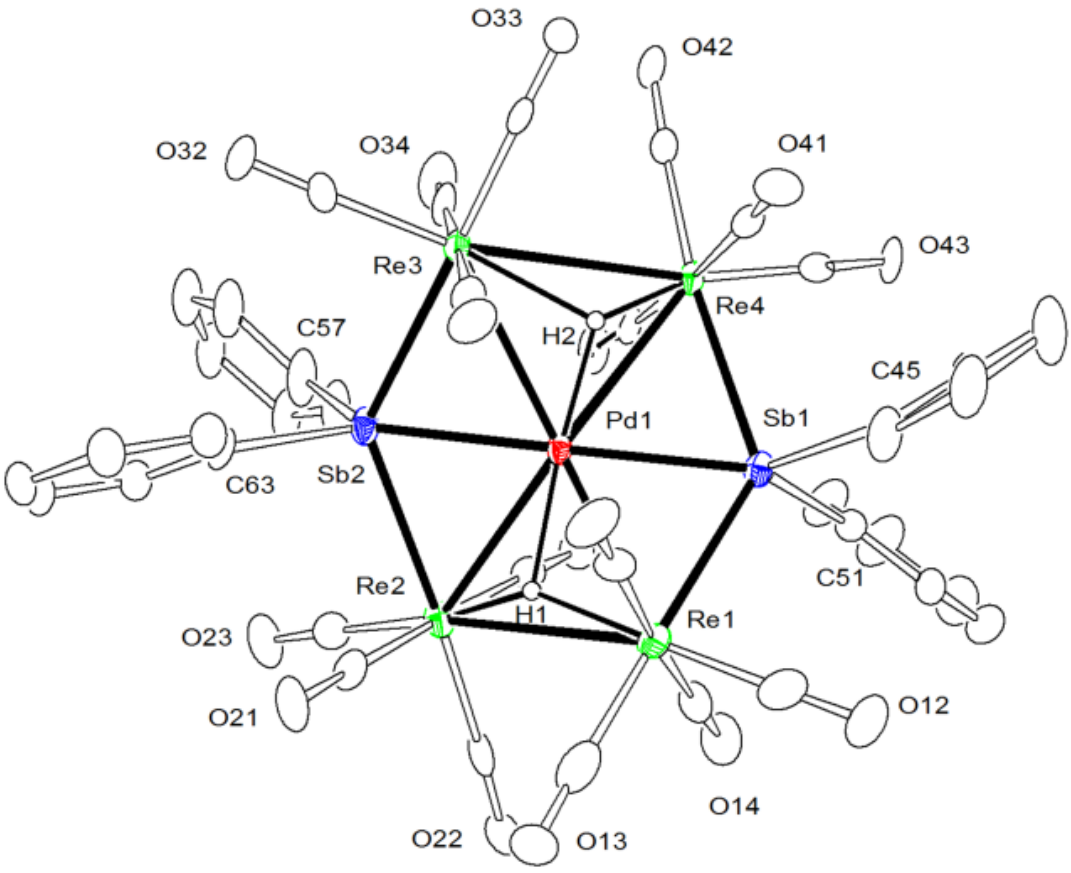

Figure 2.3. An ORTEP diagram of the molecular structure of $Pd[Re_2(CO)_8(\mu–SbPh_2)(\mu–H)]_2$, **2.3**, showing 30% thermal ellipsoid probability.

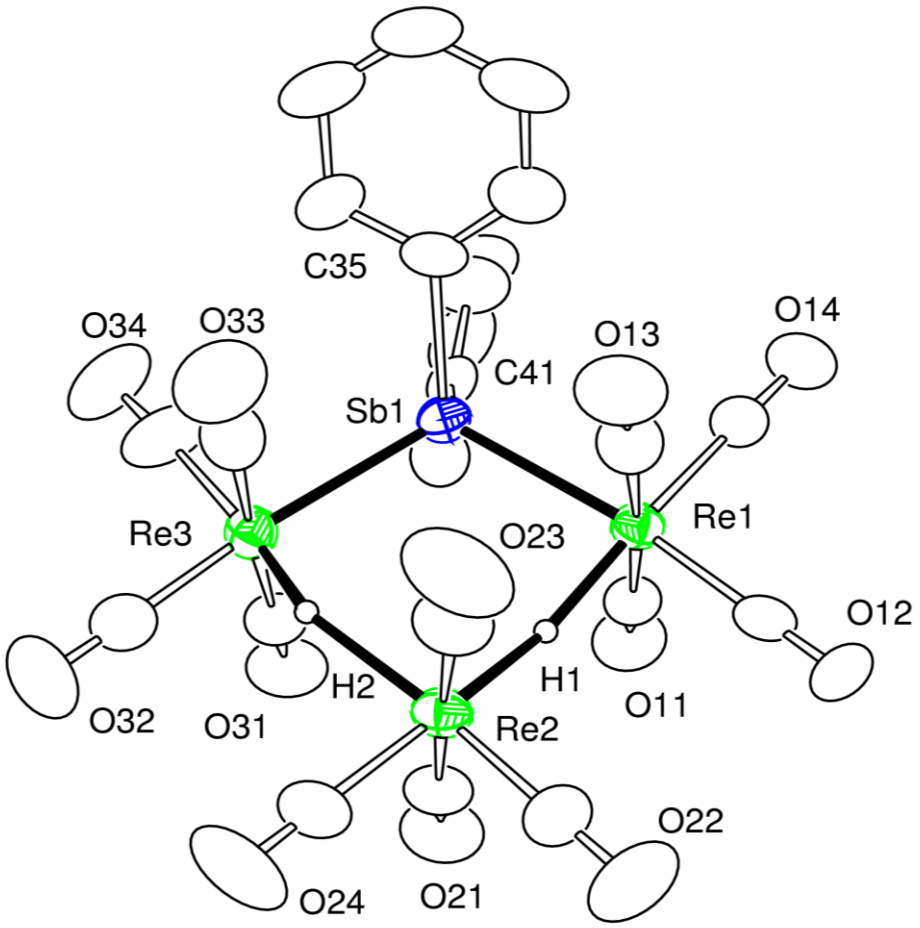

Figure 2.4. An ORTEP diagram of the molecular structure of $Re_3(CO)_{12}(\mu\text{-}SbPh_2)(\mu\text{-}H)_2$, **2.4** showing 30% thermal ellipsoid probability.

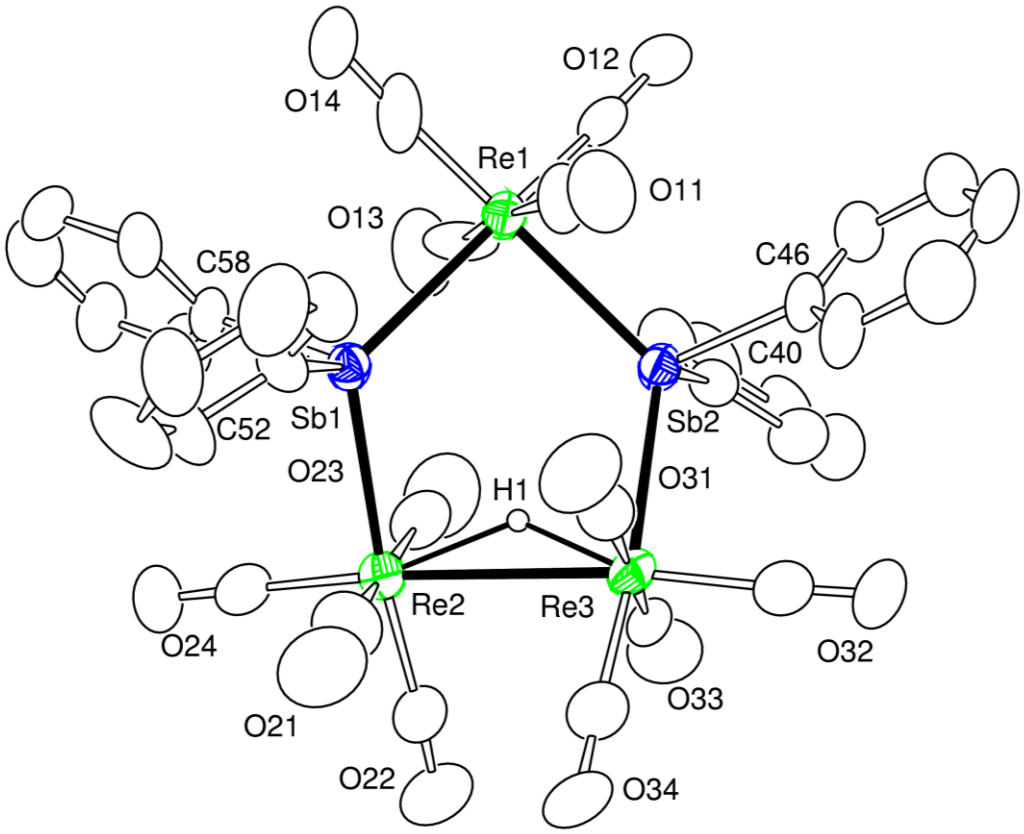

Figure 2.5. An ORTEP diagram of the molecular structure of $Re_3(CO)_{12}(\mu\text{-}SbPh_2)_2(\mu\text{-}H)$, **2.5** showing 30% thermal ellipsoid probability.

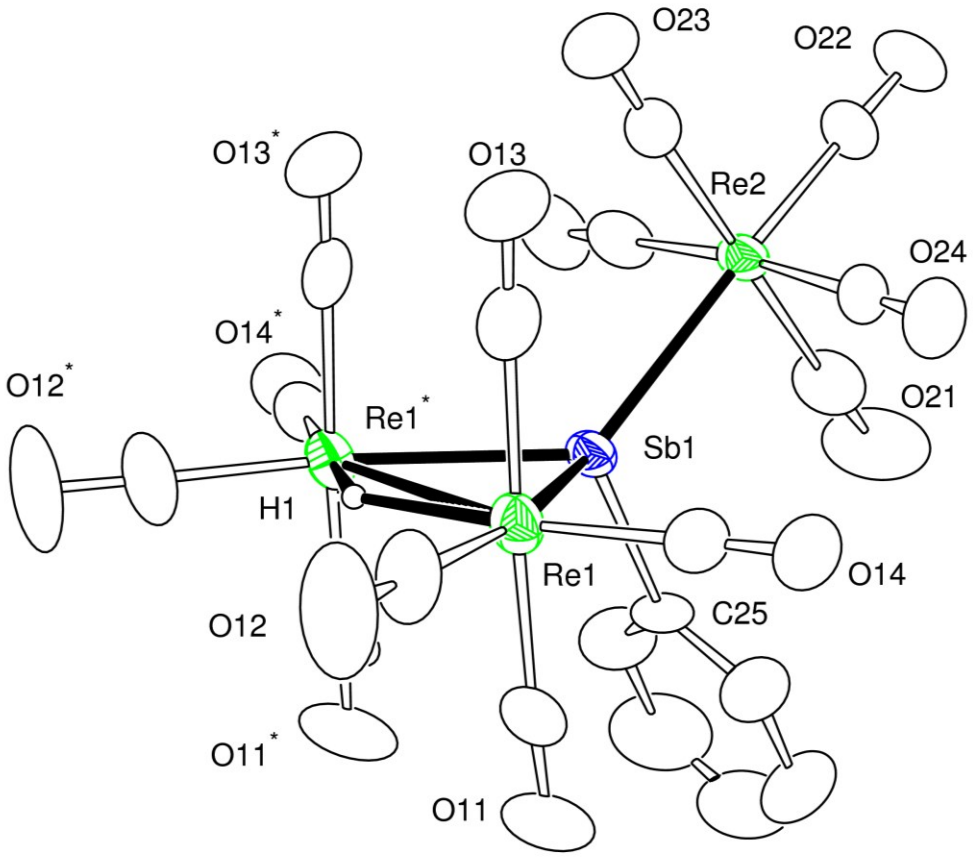

Figure 2.6. An ORTEP diagram of the molecular structure of $Re_3(CO)_{13}(\mu_3$-SbPh)(μ-H), **2.6** showing 30% thermal ellipsoid probability.

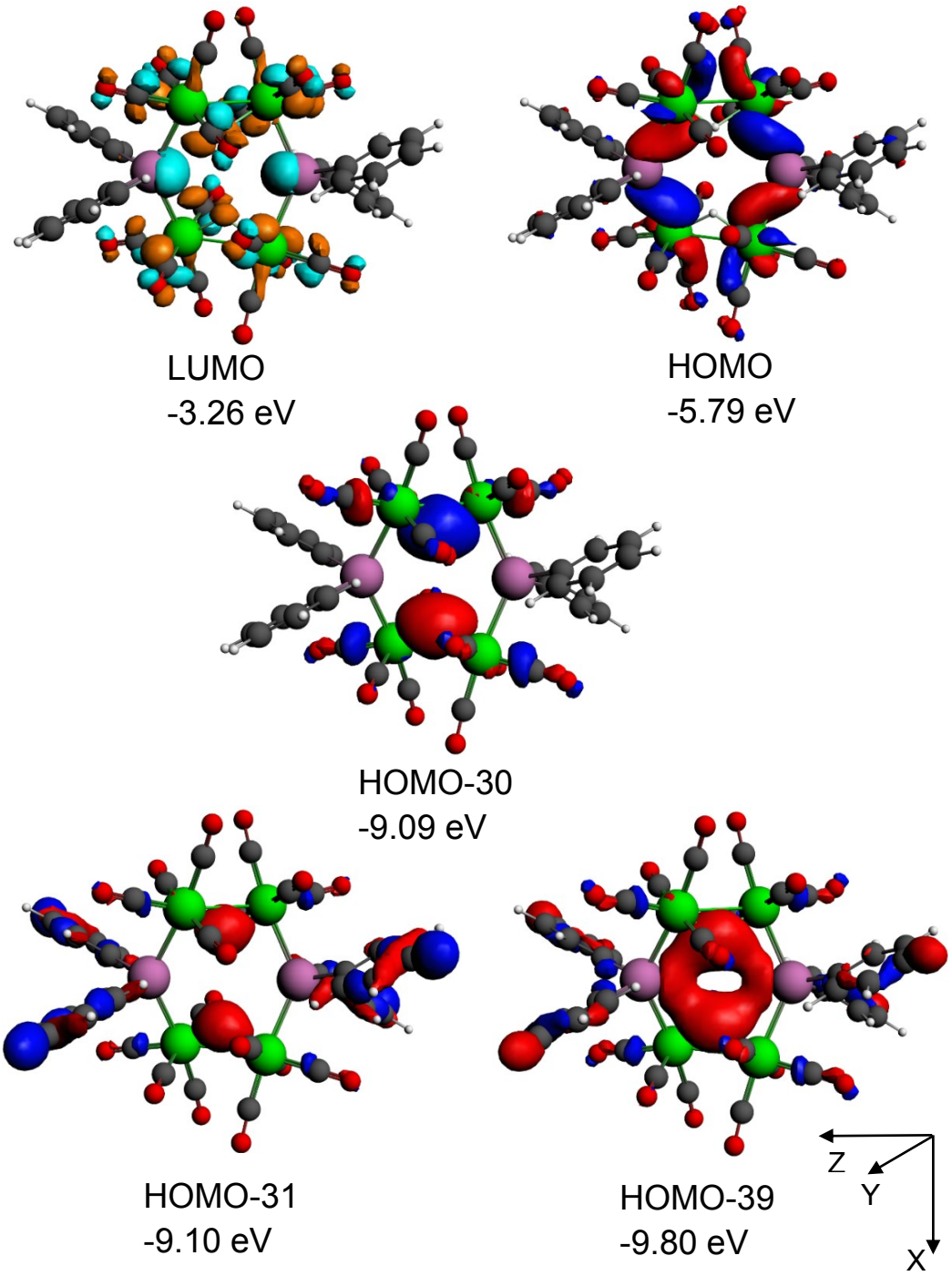

Figure 2.7. Selected molecular orbitals showing bond interactions in **2.1** and their respective calculated energy level.

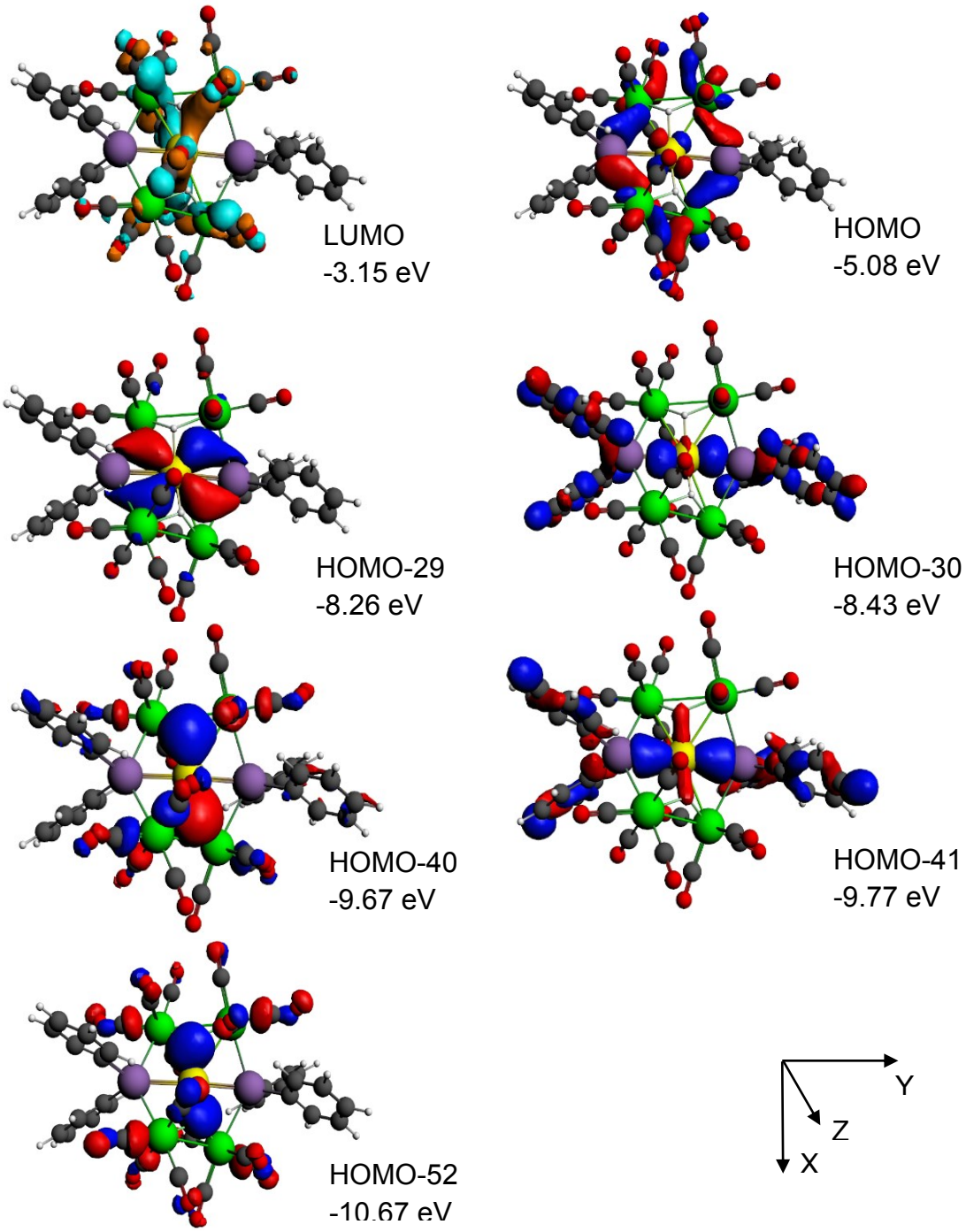

Figure 2.8. MOs with Calculated Energies for the LUMO, HOMO, HOMO-29, HOMO-30, HOMO-40, HOMO-41 and HOMO-52 of **2.3**.

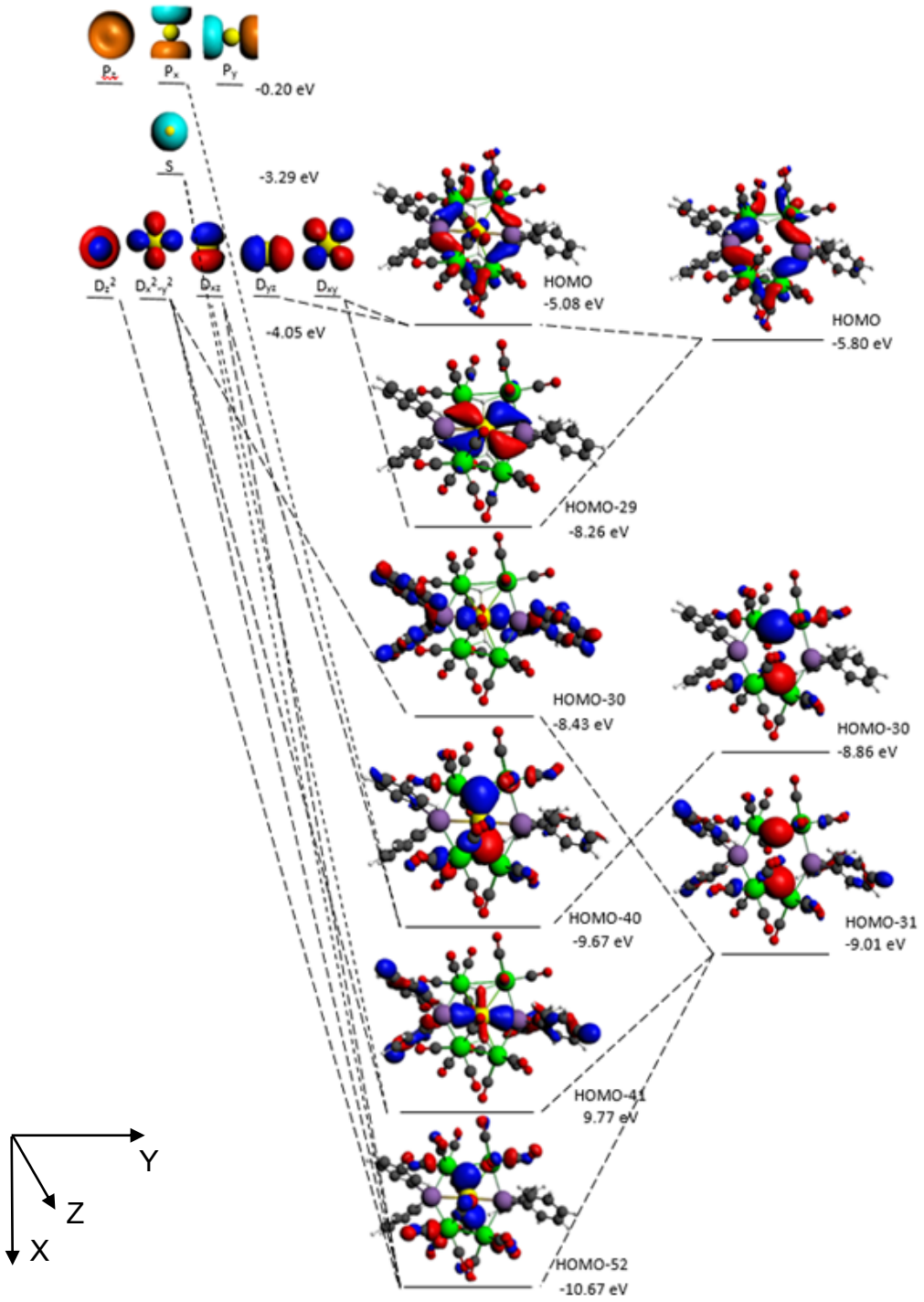

Pd Compound 2.3 Re_4Sb_2 ring

Figure 2.9. Energy level diagram of molecular orbitals with calculated energies from the fragment analysis of compound **2.3**.

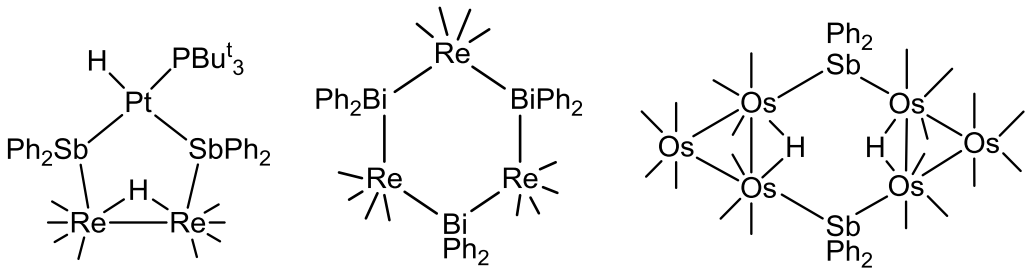

Scheme 2.1. Metallaheterocycles, $HPtRe_2(CO)_8(P\text{-}t\text{-}Bu_3)$, $[Re(CO)_4(\mu\text{-}BiPh_2)]_3$ and $[Os_3(\mu\text{-}H)(\mu\text{-}SbPh_2)(CO)_{10}]_2$

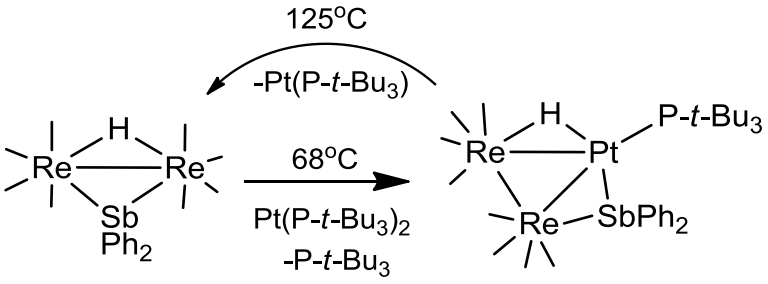

Scheme 2.2. Reversible addition and elimination of $Pt(P\text{-}t\text{-}Bu_3)$ to $Re_2(CO)_8(\mu\text{–}SbPh_2)(\mu\text{–}H)$

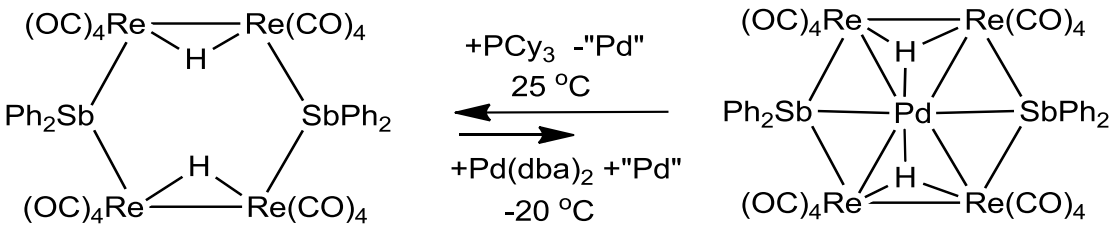

2.1 **2.3**

Scheme 2.3. Reversible addition and removal of palladium to the metallacycle

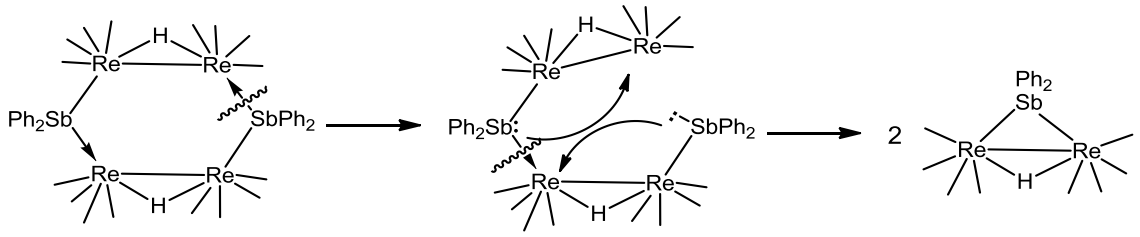

Scheme 2.4. Fragmentation of **2.1** to form $Re_2(CO)_8(\mu–SbPh_2)(\mu–H)$

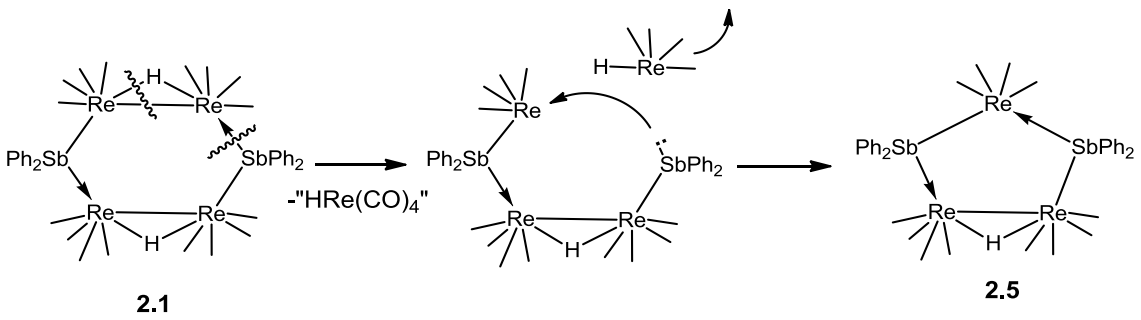

Scheme 2.5. Fragmentation of **2.1** to form **2.5**

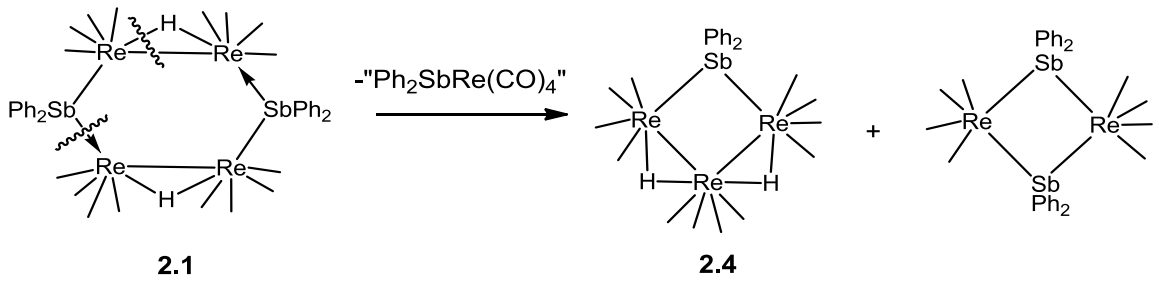

2.1 **2.4**

Scheme 2.6 Fragmentation of **2.1** to form **2.4** and $Re_2(CO)_8(\mu\text{-}SbPh_2)_2$

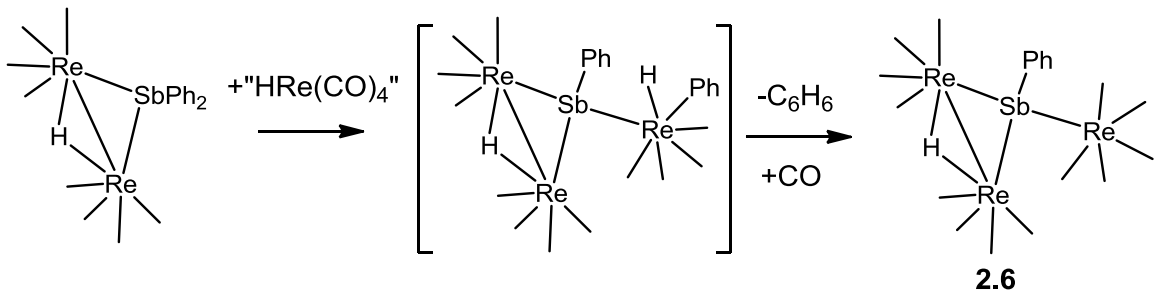

Scheme 2.7. Fragmentation of **2.1** to form **2.6**

Table 2.1. Crystallographic data for **2.1**, **2.2** and **2.3**[a]

Compound	**2.1**	**2.2**	**2.3**
Empirical formula	$Re_4Sb_2O_{16}C_{40}H_{22}$	$Re_4Sb_2Pd_2O_{16}C_{40}H_{22}$	$Re_4Sb_2Pd_{0.5}O_{16}C_{40}H_{22}$
Formula weight	1746.88	1959.6	1839.13
Crystal system	Monoclinic	Triclinic	Orthorhombic
Lattice parameters			
a (Å)	19.9667(18)	10.8973(15)	35.2421(15)
b (Å)	13.5280(12)	11.0822(15)	52.7954(19)
c (Å)	19.2161(17)	22.043(3)	10.2274(4)
α (deg)	90.00	94.339(2)	90.00
β (deg)	118.476(2)	91.570(3)	90.00
γ (deg)	90.00	114.493(2)	90.00
V ($Å^3$)	4562.5(7)	2410.5(6)	19029.3(13)
Space group	C2/c	$P\bar{1}$ (#2)	Fdd2
Z value	4	2	16
ρ_{calc} (g/cm^3)	2.543	2.700	2.568
μ (Mo Kα) (mm^{-1})	11.804	11.894	11.506
Temperature (K)	294(2)	294(2)	100(2)
$2\theta_{max}(^\circ)$	56.12	50.70	50.06
No. Obs. (I>2σ(I))	4030	4771	7447
No. Parameters	284	584	566
Goodness of fit (GOF)	1.044	0.965	1.037
Max. shift in cycle	0.001	0.001	0.001
Residuals*: R1; wR2	0.0247; 0.0465	0.0667;0.1372	0.0356; 0.0692
Absorption Correction, Max/min	Multi-scan 1.000/0.741	Multi-scan 1.000 / 0.097	Multi-scan 1.000/0.853
Largest peak in Final Diff. Map ($e^-/ Å^3$)	0.898	2.874	1.028

[a] $R = \Sigma_{hkl}(||F_{obs}| - |F_{calc}||)/\Sigma_{hkl}|F_{obs}|$; $R_w = [\Sigma_{hkl}w(|F_{obs}| - |F_{calc}|)^2/\Sigma_{hkl}wF^2_{obs}]^{1/2}$; $w = 1/\sigma^2(F_{obs})$; GOF = $[\Sigma_{hkl}w(|F_{obs}| - |F_{calc}|)^2/(n_{data} - n_{vari})]^{1/2}$.

Table 2.2. Crystallographic data for **2.4**, **2.5** and **2.6**[a]

Compound	**2.4**	**2.5**	**2.6**
Empirical formula	$Re_3SbO_{12}C_{24}H_{12}$	$Re_3Sb_2O_{12}C_{36}H_{21}$	$Re_3SbO_{13}C_{19}H_6$
Formula weight	1172.69	1447.63	1122.59
Crystal system	Triclinic	Triclinic	Monoclinic
Lattice parameters			
a (Å)	13.6204(8)	16.0769(7)	10.3134(5)
b (Å)	19.0089(12)	17.2298(7)	14.3792(7)
c (Å)	20.2437(13)	18.7642(8)	18.3407(9)
α (deg)	99.8700(10)	100.1100(10)	90
β (deg)	106.9340(10)	107.7140(10)	90.5710(10)
γ (deg)	109.9330(10)	117.6320(10)	90
V ($Å^3$)	4495.0(5)	4066.1(3)	2719.8(2)
Space group	$P\bar{1}$	$P\bar{1}$	$P2_{1/m}$
Z value	6	4	4
ρ_{calc} (g/cm^3)	2.599	2.635	2.742
μ (Mo Kα) (mm^{-1})	13.027	10.266	14.349
Temperature (K)	294(2)	294(2)	294(2)
$2\theta_{max}(°)$	52.74	52.04	56.60
No. Obs. (I>2σ(I))	12944	10944	7010
No. Parameters	1105	963	355
Goodness of fit (GOF)	1.047	1.015	1.213
Max. shift in cycle	0.001	0.002	0.001
Residuals*: R1; wR2	0.0407; 0.0952	0.0483; 0.0795	0.0400; 0.0933
Absorption Correction, Max/min	Multi-Scan 1.000/0.468	Multi-Scan 1.000/0.657	Multi-Scan 1.000/0.223
Largest peak in Final Diff. Map ($e^-/ Å^3$)	2.321	1.864	1.489

[a] $R = \Sigma_{hkl}(||F_{obs}| - |F_{calc}||)/\Sigma_{hkl}|F_{obs}|$; $R_w = [\Sigma_{hkl}w(|F_{obs}| - |F_{calc}|)^2/\Sigma_{hkl}wF^2_{obs}]^{1/2}$; $w = 1/\sigma^2(F_{obs})$; GOF = $[\Sigma_{hkl}w(|F_{obs}| - |F_{calc}|)^2/(n_{data} - n_{vari})]^{1/2}$

Table 2.3. Selected intramolecular angles and bond distances for **2.1**[a]

Atom	Atom	Distance(Å)	Atom	Atom	Atom	Angle(°)
Re1	Re2	3.2607(4)	Re1	Sb2	Re1_2	133.10(2)
Re1	Sb2	2.8002(4)	Sb2	Re1	Re2	102.018(12)
Re2	Sb1	2.7959(3)				
Re1	H1	2.02(5)				
Re2	H1	1.65(5)				

[a] Estimated standard deviations in the least significant figure are given in parentheses.

Table 2.4. Selected intramolecular angles and bond distances for **2.2**[a]

Atom	Atom	Distance(Å)	Atom	Atom	Atom	Angle(°)
Re1	Sb1	2.7439(17)	Sb1	Re1	Pd1	55.91(5)
Re1	Pd1	2.9317(18)	Sb1	Re1	H1	87.6(15)
Re2	Sb1	2.7434(18)	Sb1	Re2	Pd2	54.89(5)
Pd1	Pd2	2.848(2)	Sb2	Re3	Pd2	105.15(5)
Re2	Pd2	2.839(2)				
Re3	Pd2	2.961(2)				
Re3	Pd1	3.0949(19)				
Re4	Pd1	2.7895(19)				
Re4	Sb2	2.8527(17)				
Pd1	Sb1	2.666(2)				
Pd1	Sb2	2.736(2)				
Pd2	Sb1	2.574(2)				
Pd1	H1	1.75(10)				
Re1	H1	1.75(10)				
Pd1	H2	1.37(14)				
Pd2	H2	1.83(14)				

[a] Estimated standard deviations in the least significant figure are given in parentheses.

Table 2.5. Selected intramolecular angles and bond distances for **2.3**[a]

Atom	Atom	Distance(Å)	Atom	Atom	Atom	Angle(°)
Re1	Re2	3.4235(7)	Sb1	Pd1	Sb2	171.36(8)
Re3	Re4	3.3592(6)	Re1	Sb1	Re4	131.74(3)
Pd1	Re1	2.9348(18)	Re2	Re1	Sb1	100.23(2)
Pd1	Re2	2.9455(19)				
Pd1	Re3	2.9820(18)				
Pd1	Re4	2.9823(19)				
Re1	Sb1	2.7825(10)				
Re2	Sb2	2.8007910)				
Pd1	Sb1	2.6306(18)				
Pd1	Sb2	2.6351(18)				
Pd1	H1	1.90(10)				
Pd1	H2	1.76(10)				
Re1	H1	1.92(10)				
Re2	H1	1.67(10)				
Re3	H2	2.05(9)				
Re4	H2	1.75(10)				

[a] Estimated standard deviations in the least significant figure are given in parentheses.

Table 2.6. Selected intramolecular angles and bond distances for **2.4**[a]

Atom	Atom	Distance(Å)	Atom	Atom	Atom	Angle(°)
Re1	Sb1	2.7525(8)	Re1	Sb1	Re3	111.82(3)
Re1	Re2	3.4545(6)				
Re1	H1	1.74(9)				
Re2	H1	1.75(9)				
Re2	H2	2.05(12)				
Re3	H2	1.49(12)				

[a] Estimated standard deviations in the least significant figure are given in parentheses.

Table 2.7. Selected intramolecular angles and bond distances for **2.5**[a]

Atom	Atom	Distance(Å)	Atom	Atom	Atom	Angle(°)
Re1	Sb1	2.7821(8)	Sb2	Re1	Sb1	92.31(2)
Re2	Re3	3.2665(7)				
Re2	H1	1.747(10)				

[a] Estimated standard deviations in the least significant figure are given in parentheses.

Table 2.8. Selected intramolecular angles and bond distances for **2.6**[a]

Atom	Atom	Distance(Å)	Atom	Atom	Atom	Angle(°)
Re1	Re1*	3.2284(7)	Re1*	Sb1	Re1	72.38(2)
Re2	Sb1	2.7854(8)				
Re1	Sb1	2.7337(6)				
Re1	H1	1.81(4)				

[a] Estimated standard deviations in the least significant figure are given in parentheses.

Table 2.9. Cartesian coordinates for geometry optimization of **2.1**

Atom	x	y	z	Atom	x	y	z
Re	0.2582	2.4214	4.5498	O	0.8773	3.3286	1.6142
Re	0.0055	-0.4692	3.1161	O	1.5048	-1.3857	5.7129
Sb	-2.2905	-1.6258	4.2228	O	0.3830	-3.1669	1.6837
Sb	-2.2905	3.5475	4.2228	O	2.6630	0.3586	1.7932
H	-0.7621	0.9459	4.0492	O	-1.5032	0.8128	0.7021
C	2.0947	1.8624	4.7289	Re	-4.8392	2.4214	3.8958
C	-0.0711	1.7377	6.3730	Re	-4.5866	-0.4692	5.3295
C	0.7311	4.1646	5.2038	H	-3.8189	0.9459	4.3965
C	0.6141	2.9966	2.6819	C	-6.6757	1.8624	3.7167
C	0.9443	-1.0724	4.7604	C	-4.5099	1.7377	2.0726
C	0.2235	-2.1630	2.2337	C	-5.3121	4.1646	3.2418
C	1.6674	0.0993	2.3187	C	-5.1951	2.9966	5.7637
C	-0.9783	0.3127	1.5978	C	-5.5254	-1.0724	3.6853
C	-1.5390	-3.0208	5.6681	C	-4.8045	-2.1630	6.2119
C	-0.9232	-4.2014	5.2418	C	-6.2485	0.0993	6.1269
H	-0.8689	-4.4459	4.1749	C	-3.6028	0.3127	6.8478
C	-0.3882	-5.0863	6.1756	C	-3.0420	-3.0208	2.7775
H	0.0836	-6.0116	5.8342	C	-3.6578	-4.2014	3.2038
C	-0.4528	-4.7936	7.5364	H	-3.7122	-4.4459	4.2708
H	-0.0324	-5.4894	8.2673	C	-4.1928	-5.0863	2.2700
C	-1.0550	-3.6134	7.9631	H	-4.6646	-6.0116	2.6115
H	-1.1083	-3.3759	9.0287	C	-4.1283	-4.7936	0.9092
C	-1.5974	-2.7303	7.0312	H	-4.5486	-5.4894	0.1783
H	-2.0741	-1.8099	7.3845	C	-3.5260	-3.6134	0.4825
C	-2.5532	4.9476	5.8283	H	-3.4727	-3.3759	-0.5831
C	-2.0926	4.6455	7.1099	C	-2.9836	-2.7303	1.4145
H	-1.5393	3.7198	7.2990	H	-2.5070	-1.8099	1.0612
C	-2.3308	5.5204	8.1686	C	-2.0278	4.9476	2.6173
H	-1.9652	5.2725	9.1684	C	-2.4885	4.6455	1.3358
C	-3.0296	6.7043	7.9501	H	-3.0417	3.7198	1.1466
H	-3.2132	7.3930	8.7790	C	-2.2502	5.5204	0.2771
C	-3.4924	7.0103	6.6721	H	-2.6158	5.2725	-0.7228
H	-4.0409	7.9393	6.4937	C	-1.5514	6.7043	0.4955
C	-3.2616	6.1338	5.6136	H	-1.3678	7.3930	-0.3334
H	-3.6300	6.3886	4.6135	C	-1.0886	7.0103	1.7736
O	3.2128	1.6054	4.8636	H	-0.5402	7.9393	1.9520
O	-0.1703	1.3186	7.4413	C	-1.3194	6.1338	2.8320
O	1.0398	5.2148	5.5749	H	-0.9510	6.3886	3.8321

O	-7.7939	1.6054	3.5821	O	-6.0859	-1.3857	2.7327
O	-4.4108	1.3186	1.0043	O	-4.9640	-3.1669	6.7620
O	-5.6208	5.2148	2.8708	O	-7.2440	0.3586	6.6524
O	-5.4584	3.3286	6.8314	O	-3.0779	0.8128	7.7436

Table 2.10. Cartesian coordinates for geometry optimization of **2.3**

Atom	x	y	z	Atom	x	y	z
Pd	3.645	8.284	9.236	C	2.856	10.637	13.094
Re	5.955	7.237	7.651	C	4.969	4.196	10.215
Re	4.53	10.445	7.257	C	4.402	2.922	10.421
Re	1.531	6.26	10.139	H	3.502	2.624	9.881
Re	2.494	9.198	11.842	C	4.997	2.023	11.318
Sb	3.975	5.559	8.869	H	4.554	1.037	11.467
Sb	3.663	10.968	9.913	C	6.154	2.391	12.022
O	4.565	6.466	4.904	H	6.614	1.692	12.721
O	7.711	4.674	7.686	C	6.717	3.659	11.824
O	7.215	8.283	10.366	H	7.616	3.952	12.368
O	8.232	8.689	6.085	C	6.129	4.559	10.921
O	1.578	9.836	6.274	H	6.579	5.542	10.778
O	5.563	9.968	4.347	C	3.514	4.151	7.291
O	7.441	11.105	8.339	C	4.438	3.13	6.989
O	4.113	13.464	6.657	H	5.354	3.023	7.571
O	0.283	7.338	7.432	C	4.18	2.234	5.941
O	0.509	3.401	9.478	H	4.899	1.443	5.72
O	2.865	5.122	12.787	C	3.007	2.354	5.181
O	-1.15	6.921	11.602	H	2.809	1.657	4.366
O	-0.283	10.435	10.93	C	2.088	3.372	5.474
O	1.046	7.654	14.137	H	1.174	3.472	4.888
O	5.189	7.709	12.601	C	2.339	4.265	6.527
O	3.063	11.501	13.849	H	1.613	5.05	6.741
C	5.069	6.721	5.914	C	2.229	12.587	9.828
C	7.051	5.634	7.679	C	2.171	13.511	10.891
C	6.716	7.889	9.395	H	2.868	13.437	11.727
C	7.356	8.194	6.672	C	1.219	14.542	10.877
C	2.653	10.038	6.661	H	1.187	15.255	11.702
C	5.188	10.108	5.439	C	0.314	14.654	9.811
C	6.382	10.839	7.955	H	-0.425	15.456	9.804
C	4.265	12.332	6.89	C	0.364	13.734	8.755
C	0.768	6.962	8.417	H	-0.335	13.814	7.922
C	0.9	4.472	9.72	C	1.32	12.706	8.761
C	2.392	5.561	11.825	H	1.345	12	7.931
C	-0.137	6.709	11.07	C	5.279	12.039	10.86
C	0.74	10.009	11.262	C	5.572	13.344	10.416
C	1.58	8.186	13.25	H	4.968	13.811	9.636
C	4.222	8.268	12.284	C	6.64	14.057	10.98

H	6.856	15.069	10.633	C	6.07	11.456	11.865
C	7.428	13.471	11.982	H	5.862	10.447	12.218
H	8.259	14.026	12.418	H	4.517	8.533	7.65
C	7.143	12.171	12.422	H	2.159	8.101	10.283
H	7.752	11.708	13.201				

REFERENCES

1) Zhang, C.; Catlow, C.R.A. *J. Catal.* **2008**, *259*, 17-25. (b) Shaikh, S.; Bethke, Mamedov, E. *Topics in Catal.* **2006**, *38*, 241-249. (c) Allen, M. D.; Poulston, S.; Bithell, E. G.; Goringe, M. J.; Bowker, M. *J. Catal.* **1996**, *163*, 204-214. (d) Grasselli, R. K. *Catal. Today* **1999**, *49*, 141-153. (e) Bowker, M.; Bicknell, C. R.; Kerwin, P. *Appl. Catal. A: Gen*. **1996**, *136*, 205-229. (f) Nilsson, R.; Lindblad, T.; Andersson, A. *J. Catal.* **1994**, *148*, 501-513. (g) Guerrero-Perez, M.O.; Fierro, J.L.G.; Vicente, M.A. *J. Catal.* **2002**, *206*, 339-348. (h) Guerrerro-Perez, M.O.; Chang, J.S.;Hong, D.Y.; Lee. J.M.; Banares, M.A. *Catal. Lett.* **2008**, *125*, 192-196.

2) Raja, R.; Adams, R.D.; Blom, D.A.; Pearl, W.C.; Gianotti, E.; Thomas, J.M. *Langmuir*, **2009**, *25*, 7200.

3) Adams, R. D.; Pearl, W. C., Jr. *Organometallics* **2010**, *29*, 3887–3895.

4) (a) Adams, R. D.; Pearl, W. C., Jr. *Organometallics* **2009**, *48*, 9519–9525.(b) Leong, W. K.; Chen, G. *J.Chem.Soc.Dalton Trans.* **2000**, 4442-4445.

5) Adams, R. D.; Captain, B.; Pearl, W. C., Jr. *J. Organomet. Chem.* **2008**, *693*, 1636–1644.

6) Adams, R. D.; Hall, M. B.; Pearl, W. C., Jr.; Yang, X. *Inorg. Chem*. **2009**, *48*, 652–662.

7) SAINT+, version 6.2a, Bruker Analytical X-ray Systems, Inc., Madison, WI, 2001.

8) G. M. Sheldrick, SHELXTL, version 6.1, Bruker Analytical X-ray Systems, Inc., Madison, WI, 1997.

9) *ADF, SCM, Theoretical Chemistry*; Vrije Universiteit: Amsterdam, The Netherlands. http://www.scm.com.

10) Perdew, J. P.; Ruzsinszky, A.; Csonka, G.I.; Vydrove, O. A.; Scuseria, G.E. *Phys. Rev. Lett.* **2008**, *100*, 136406.

11) Tao, J.; Perdew, J. P.; Staroverov, V. N.; Scuseria, G. E. *Phys. Rev. Lett.* **2003**, *91*, 146401

12) The amount of **2.3** in any particular crystal can only be determined by a complete single-crystal X-ray diffraction analysis and an occupancy refinement of the site of the palladium atom. The ratio of **2.1**:**2.3** in samples containing enough material for a ^{1}H NMR spectroscopic analysis is easily determined by the intensity ratio of their hydride resonances, d = -14.94 for **2.1** and -17.89 for **2.3**. Compound **2.2** is also formed in this reaction.

13) The numbers given in the Figure 1.3 caption are the observed numbers from the crystallographic analysis. Since this crystal contains 51% of **2.3** and 49% of **2.1**, the observed numbers are really an average of the distances in **2.1** and **2.3**. One can obtain a better estimate of the true distances in **2.3** by recalculating using an expression that accounts for the partial occupancy, e.g. (0.49x + 0.51y = z), where x =the bond distance observed in **2.1**, z = bond distance observed in this mixed crystal of **2.1** and **2.3**, and y is the unknown and would be the bond distance expected for **2.3** in a crystal that contains 100% of **2.3**. By using this calculation, the estimated interatomic distances in **2.3** would be: Re(1)-Re(2) = 3.5789(7), Re(3)-Re(4) = 3.4538(6), Pd(1)-Re(1) = 2.9348(18), Pd(1)-Re(2) = 2.9455(19), Pd(1)-Re(3) = 2.9820(18), Pd(1)-Re(4) = 2.9823(19),Re(1)-Sb(1) = 2.7696(10), Re(2)-Sb(2) = 2.8012(10), Pd(1)-Sb(1) = 2.6306(18), Pd(1)-Sb(2) = 2.6351(18), Pd(1)-H(1) = 1.90(10),Pd(1)-H(2) = 1.76(10), Re(1)-H(1) = 1.82(10), Re(2)-H(1) = 1.68(10), Re(3)-H(2) = 2.07(9), Re(4)-H(2) = 1.84(10).

14) Masciocchi, N.; Sironi, A.; D'Alfonso, G. *J. Am. Chem. Soc.* **1990**, *112*, 9395–9397.

15) Mentes, A.; Kemmit, R. D. W.; Fawcett, J.; Russell, D. R. *J. Organomet. Chem.* **1997**, *528*, 59–63.

16) Gaussian 09, Revision A.02, M. J. Frisch, G. W. Trucks, H. B. Schlegel, G. E. Scuseria, M. A. Robb, J. R. Cheeseman, G. Scalmani, V. Barone, B. Mennucci, G. A. Petersson, H. Nakatsuji, M. Caricato, X. Li, H. P. Hratchian, A. F. Izmaylov, J. Bloino, G. Zheng, J. L. Sonnenberg, M. Hada, M. Ehara, K. Toyota, R. Fukuda, J. Hasegawa, M. Ishida, T. Nakajima, Y. Honda, O. Kitao, H. Nakai, T. Vreven, J. A. Montgomery, Jr., J. E. Peralta, F. Ogliaro, M. Bearpark, J. J. Heyd, E. Brothers, K. N. Kudin, V. N. Staroverov, R. Kobayashi, J. Normand, K. Raghavachari, A. Rendell, J. C. Burant, S. S. Iyengar, J. Tomasi, M. Cossi, N. Rega, J. M. Millam, M. Klene, J. E. Knox, J. B. Cross, V. Bakken, C. Adamo, J. Jaramillo, R. Gomperts, R. E. Stratmann, O. Yazyev, A. J. Austin, R. Cammi, C. Pomelli, J. W. Ochterski, R. L. Martin, K. Morokuma, V. G. Zakrzewski, G. A. Voth, P. Salvador, J. J. Dannenberg, S. Dapprich, A. D. Daniels, O. Farkas, J. B. Foresman, J. V. Ortiz, J. Cioslowski, and D. J. Fox, Gaussian, Inc., Wallingford CT, 2009.

17) Compounds **2.1** and **2.3** are unstable in solution over extended periods, and therefore it was not possible to increase the conversion of **2.1** to **2.3** further by extending the reaction period of **2.1** with $Pd(dba)_2$.

18) (a) Cram, D. J.; Cram, J. M. *Science* **1974**, *183*, 803–809. (b) Gokel, G. W.; Leevy, W. M.; Weber, M. E. *Chem. Rev.* **2004**, *104*, 2723–2750. (c) Schneider, H. J. *Angew. Chem., Int. Ed. Engl.* **1991**, *30*, 1417–1436. (d) Lagona, J.; Mukhopadhyay, P.; Chakrabarti, S.; Isaacs, L. *Angew. Chem., Int. Ed.* **2005**, *44*, 4844–4870. (e) Lee, J. W.; Samal, S.; Selvapalam, N.; Kim, H..J.; Kim, K. *Acc. Chem. Res.* **2003**,*36*, 621–630.

19) Crooks, R. M.; Zhao, M. Q.; Sun, L.; Chechik, V.; Yeung, L. K. *Acc. Chem. Res.* **2001**, *34*, 181–190.

20) (a) Leininger, S.; Olenyuk; Stang, P. J. *Chem. Rev.* **2000**,*100*, 853–908. (b) Pluth, M. D.; Bergman, R. G.; Raymond, K. N. *Acc. Chem. Res.* **2009**, *42*, 1650–1659. (c) Fiedler, D.; Leung, D. H.; Bergman,R. G.; Raymond, K. N. *Acc. Res.* **2005**, *38*, 351–360. (d) McKinlay, R. M.; Cave, G. W. V.; Atwood, J. L. *Proc. Natl. Acad. Sci. U.S.A*. **2005**, *102*, 5944–5948. (e) Fujita., M.; Umemoto, K.; Yoshizawa, M.; Fujita, N.; Kusukawa, T.; Biradha, K. *Chem. Commun.* **2001**, 509–518. (f) Koblenz, T. S.; Wassenaar, J.; Reek, J. N. H. *Chem. Soc. Rev.* **2008**, *37*, 247–262. (g) Andrikopoulos, P. C.; Armstrong, D. R; Clegg, W.; Gilfillan, C. J.; Hevia, E.; Kennedy, A. R.; Mulvey, R. E.; O'Hara, C. T.; Parkinson, J. A.; Tooke, D. M. *J. Am. Chem. Soc.* **2004**, *126*, 11612–11620. (h) Kennedy, A. R.; Klett, J.; Mulvey, R. E.; Newton, S.; Wright, D. S. *Chem. Commun.* **2008**, 308–310.

21) (a) Conn, M. M.; Rebek, J. *Chem. Rev.* **1997**, *97*, 1647–1668. (b)Atwood, J. L.; Barbour, L. J.; Jerga, A. *Proc. Natl. Acad. Sci. U.S.A.* **2002**, *99*, 4837–4841.

22) (a) Houk, K. N.; Leach, A. G.; Kim, S. P.; Zhang, X. *Angew. Chem., Int. Ed.* **2003**, *42*, 4872–4897. (b) Hill, D. J.; Mio, M. J.; Prince, R. B.; Hughes, T. S.; Moore, J. S. *Chem. Rev.* **2001**, *101*, 3893–4012.

CHAPTER 3

STUDIES OF THE STRUCTURES AND BONDING OF GOLD-BRIDGED DIRHENIUM CARBONYL CLUSTER COMPLEXES*

Introduction

The similarities between the hydrogen atom and the $Au(PPh_3)$ group are well known.[1] The two species are effectively isolobal and both contain only one valence electron. H and the $Au(PPh_3)$ group are well known to bridge metal – metal bonds effectively in polynuclear metal complexes.[2,3] There are a number of hydride-bridged metal carbonyl cluster complexes such as $Re_2(CO)_8(\mu\text{-}H)_2$,[4] $Os_3(CO)_{10}(\mu\text{–}H)_2$,[5] $Re_4(CO)_{12}(\mu\text{–}H)_4$,[6] (Scheme 2.1) and higher nuclear cluster complexes such as $Pt_2Re_3(CO)_9(P\text{-}t\text{-}Bu_3)_3(\mu\text{–}H)_6$,[7] and $[Ru_3(CO)_8(\mu_3\text{–}CMe)(\mu\text{–}H)_2(\mu_3\text{–}H)]_2$[8] that have attracted interest because they are formally electronically unsaturated. Unsaturated metal cluster complexes are of interest because they exhibit higher reactivity than their electronically-saturated counterparts.[7 - 10]

A few unsaturated triosmium cluster complexes containing the bridging $Au(PR_3)$ group(s) have also been prepared, e.g. $Os_3(CO)_{10}(\mu\text{-}AuPEt_3)_2$,[11] $Os_3(CO)_{10}(\mu\text{-}AuPPh_3)(\mu\text{-}H)$[12] and $Os_3(CO)_{10}(\mu\text{-}AuPPh_3)(\mu\text{-}Ph)$[13] that are related to $Os_3(CO)_{10}(\mu\text{–}H)_2$.

We have now prepared and characterized the new dirhenium complex $Re_2(CO)_8(\mu\text{-}AuPPh_3)_2$, **3.1** that contains two bridging $Au(PPh_3)$ groups. The two rhenium atoms contain a total of 32 valence electrons leaving the metal atoms formally unsaturated by the amount of two electrons. In accord with this, the Re – Re interaction is unusually short. The metal – metal bonding in **3.1** was investigated by DFT computational analyses which have provided evidence for

bonding directly between the two rhenium atoms. For comparisons, the electronic structure of $Re_2(CO)_8(\mu\text{-}H)_2$, **3.2** was also investigated. Reactions of **3.1** with I_2 were investigated and were found to provide the new electronically-saturated compound $Re_2(CO)_8(\mu\text{-}AuPPh_3)(\mu\text{-}I)$, **3.3** and the previously reported complex $Re_2(CO)_8(\mu\text{-}I)_2$, **3.4**. The bonding in **3.3** and **3.4** was also investigated by computational methods. Details of these studies are provided in this report.

Experimental

General Data. Reagent grade solvents were dried by the standard procedures and were freshly distilled prior to use. Infrared spectra were recorded on a Thermo Nicolet Avatar 360 FT-IR spectrophotometer. Room temperature ^1H NMR and $^{31}P\{^1H\}$ NMR were recorded on a Bruker Avance/DRX 400 NMR spectrometer operating at 400.3 and 162.0 MHz, respectively. Positive/negative ion mass spectra were recorded on a Micromass Q-TOF instrument by using electrospray (ES) ionization or electron impact (EI) ionization. UV–vis spectra were recorded on a (Agilent/Varian Cary 50) UV–vis spectrometer in methylene chloride solvent at a concentration of 0.46×10^{-4} M $Re(CO)_5(AuPPh_3)$,[14] $Re_2(CO)_8(\mu\text{-}H)(\eta^2\text{-}CH{=}CHC_4H_9)$,[15] and $Au(PPh_3)I$[16] was prepared by the previously reported procedures. Product separations were performed by TLC in air on Analtech 0.25 mm silica gel 60 Å F254 glass plates.

Synthesis of $Re_2(CO)_8(\mu\text{-}AuPPh_3)_2$, 3.1.

45.0 mg (0.0572 mmol) of $Re(CO)_5Au(PPh_3)$ was dissolved in 25 mL of benzene and irradiated for 30 min. and the solution turned to brown. The solvent was removed in *vacuo*. The residue separated by TLC by using a 4:1 hexane/methylene chloride (v/v) solvent mixture to yield in order of elution: 1) a colorless band of $Re_2(CO)_{10}$, 0.7 mg (4 % yield), 2) a colorless band identified as $Re_2(CO)_8(PPh_3)_2$,[15] 6.7 mg (21 % yield) and 3) a red band of $Re_2(CO)_8(\mu\text{-}AuPPh_3)_2$, **3.1**, 7.6 mg (18 % yield). Spectral data for **3.1**: IR ν_{CO} (cm^{-1} in methylene chloride): 2065(w), 2028(s), 1976(vs), 1942(m), 1917(s). ^1H NMR (CD_2Cl_2, in ppm) δ = 7.20-7.36 (m, 30H, Ph). ^{31}P NMR (CD_2Cl_2, in ppm) δ = 76.17 (s). Mass Spec. EI/MS *m*/*z*. 1514, M^+, 1486, M^+-CO. The isotope distribution pattern is consistent with the presence of two gold atoms and two rhenium atoms. The UV-vis absorption spectrum in CH_2Cl_2 solvent: λ_{max} = 327 nm, ϵ = 6692 $cm^{-1}M^{-1}$, λ_{max} = 420 nm, ϵ = 2820 $cm^{-1}M^{-1}$ and λ_{max} = 493 nm, ϵ = 5836 $cm^{-1}M^{-1}$.

Synthesis of $Re_2(CO)_8(\mu\text{-}AuPPh_3)(\mu\text{-}I)$, 3.3

3.2 mg (0.0126 mmol) of I_2 was added to 19.0 mg (0.0125 mmol) of **3.1** in 10 mL of benzene. The solution was stirred at room temperature for 15 min. During this time the solution turned from orange to yellow. The solvent was removed in *vacuo* and the products were separated by TLC by using a 4:1 (v/v) hexane/methylene chloride solvent mixture to yield in order of elution: 1) a yellow band of 1.9 mg of $Re_2(CO)_8(\mu\text{-}AuPPh_3)(\mu\text{-}I)$, **3.3**, (13 % yield) and 2) a colorless

band of $Au(PPh_3)I$, 4.9 mg (33 % yield). Spectral data for **3.3**: IR ν_{CO} (cm^{-1} in methylene chloride): 2094(w), 2064(m), 2005(s), 1972(m), 1935(m). ^{31}P NMR (CD_2Cl_2, in ppm) δ = 76.79 (s). Mass Spec. EI/MS *m*/*z*. 1182, M^+, 1154, M^+-CO. The isotope distribution pattern is consistent with the presence of one gold atom and two rhenium atoms.

Alternative Synthesis of 3.3.

45.0 mg (0.0661 mmol) of $Re_2(CO)_8(\mu\text{-}H)(\eta^2\text{-}CH{=}CHC_4H_9)$ was added to 38.8 mg (0.0661 mmol) of $Au(PPh_3)I$ in 20 mL of hexane. The solution was refluxed for 30 min. After cooling, the solvent was removed in *vacuo* and the product was isolated by TLC by using hexane solvent to give a yellow band of **3.3**, 65.0 mg (83 % yield).

Synthesis of $Re_2(CO)_8(\mu\text{-}I)_2$, 3.4 from the reaction of 3.1 with I_2.

6.6 mg (0.026 mmol) of I_2 was added to a solution of 20.0 mg (0.0125 mmol) of **3.1** in 10 mL of benzene. The solution was stirred at room temperature for 15 min. During this time the solution turned from orange to colorless. The solvent was removed in *vacuo* and the residual was separated by TLC by using a 4:1 (v/v) hexane/methylene chloride solvent mixture to give two products in order of elution: 1) a colorless band containing 3.6 mg of $Re_2(CO)_8(\mu\text{-}I)_2$,[17] **3.4** (32 % yield) and 2) a colorless band of $Au(PPh_3)I$, 4.0 mg (26 % yield).

Reaction of 3.3 with I_2.

3.2 mg (0.0126 mmol) of I_2 was added to 30.0 mg (0.0125 mmol) of **3.2** that was dissolved in 10 mL of benzene. The solution was then stirred for 15 min. at room temperature. During this time the color of the solution turned from yellow to colorless. The solvent was removed in *vacuo*. The products were isolated by TLC by using a 4:1 hexane/methylene chloride (v/v) solvent mixture to give products in order of elution: 1) a colorless band that contained 5.0 mg of **3.4** (23 % yield) and 2) a colorless band of $Au(PPh_3)I$, 9.8 mg (66 % yield). Spectral data for **3.4**: IR ν_{CO} (cm^{-1} in methylene chloride): 2107(m), 2030(s), 1997(m), 1960(m). Mass Spec. EI/MS *m*/*z*. 850, M^+.

Crystallographic Analyses: Red crystals of **3.1** suitable for x-ray diffraction analyses were obtained from a methylene chloride/hexane solution by slow evaporation of a solvent at 25 °C. Yellow crystals of **3.3** suitable for x-ray diffraction analyses were obtained from a benzene/octane solution by slow evaporation of a solvent at 15 °C. X-ray intensity data were measured by using a Bruker SMART APEX CCD-based diffractometer by using Mo Kα radiation (λ = 0.71073 Å). The raw data frames were integrated with the SAINT+ program by using a narrow-frame integration algorithm.[18] Correction for Lorentz and polarization effects were also applied using SAINT+. An empirical absorption correction based on the multiple measurement of equivalent reflections was applied using the program SADABS. All structures were solved by a combination of direct methods and difference Fourier syntheses, and were refined by full-

matrix least-squares on F^2 by using the SHELXTL software package.[19] Crystal data, data collection parameters, and results of the analyses are available in the Supporting Information.

Computational Details.

Density functional theory (DFT) calculations were performed with the Amsterdam Density Functional (ADF) suite of programs[20] by using the PBEsol functional[21] with valence quadruple-ζ + 4 polarization function, relativistically optimized (QZ4P) basis sets for rhenium and gold, valence triple-ζ + 2 polarization function (TZ2P) basis set for iodide and double-ζ function (DZ) basis sets for the phosphorus, carbon, oxygen, and hydrogen atoms with none frozen cores. The molecular orbitals for **3.1** – **3.4** and $Re_2(CO)_{10}$ and their energies were determined by geometry-optimized calculations, with scalar relativistic corrections, that were initiated by using the atom positional parameters as determined from the crystal structure analyses. Electron densities at the bond critical points and Mayer bond orders were calculated by using the Bader Quantum Theory of Atoms In a Molecule (QTAIM) model.[22, 23] Natural bond orbital (NBO) analyses were performed using GENNBO 6.0 package embedded in ADF 2013.[24] Time-dependent DFT (TDDFT) calculations were performed for models in the gas phase by using the PBEsol functional with the same basis sets.

Results and Discussion

Photolytic decarbonylation of the compound $Re(CO)_5[(AuPPh_3)]$ led to formation of the new complex dirhenium complex $Re_2(CO)_8(\mu\text{-}AuPPh_3)_2$, **3.1** in 18 % yield. A coproduct in this reaction was the compound dirhenium complex $Re_2(CO)_8(PPh_3)_2$[15] (21 % yield). Both compounds were characterized crystallographically. An ORTEP diagram of the molecular structure of **3.1** is shown in Figure 3.1. In the solid state the complex sits upon a crystallographic center of symmetry. The molecule contains two $Re(CO)_4$ groups linked by two bridging $AuPPh_3$ groups. The two independent Re – Au bond distances, Re1 – Au1 = 2.7914(2) Å and Re1 – Au1* = 2.7977(2) Å are similar to those found in the compounds $Re_2(CO)_8[\mu\text{-}Au(PPh_3)](\mu\text{-}C_2Ph)$,[25] 2.744(1) Å and 2.844(2) Å and $Re_2(CO)_8[\mu\text{-}Au(PPh_3)](\mu\text{-}C_4Fc)$,[26] Fc = ferrocenyl, 2.7369(3) Å and 2.8268(3) Å. The Re – Re distance in **3.1** is 2.9070(3) Å, which is significantly shorter than the Re – Re single bond distance found in $Re_2(CO)_{10}$, Re – Re = 3.041(1) Å.[27] Compound **3.1** is structurally similar to $Re_2(CO)_8(\mu\text{-}H)_2$, **3.2** which has two bridging hydrido ligands in the locations of the bridging $Au(PPh_3)$ groups. Compound **3.2** is also formally unsaturated and has a similarly short Re – Re distance, 2.876(1) Å.[4] Compound **3.2** also contains 32 valence electrons and has been variously described as having no direct bonding between the two Re atoms, a Re – Re single bond, or an Re – Re double bond (Scheme 3.2).[4b]

Likewise, the dirhenium center in **3.1** contains only 32 valence electrons. King reported MPW1PW91 and BP86 geometry-optimized DFT structures for

3.2.[4c] In order to delve deeper into the nature of the Re – Re bonding in **3.1** and **3.2**, we have performed geometry-optimized PBEsol DFT molecular orbital calculations for both of these molecules.

Selected DFT MOs that show the bonding interactions between the Re and Au atoms in **3.1** are illustrated in Figure 3.2. There is evidence for direct Re - Re bonding in the HOMO, the HOMO-5 and the HOMO-25. The HOMO-5 is a totally symmetric A_{1g} orbital that is dominated by a 4-center bonding interaction that lies principally in the plane of the Re_2Au_2 core of the molecule. The HOMO-2 is dominated by a delocalized 4-center interaction about the Re_2Au_2 core of the molecule with a node along the Re – Re vector. The HOMO-7 provides evidence for a significant d - d π-bonding interaction that lies perpendicular to the Re_2Au_2 plane of the molecule. The low lying HOMO-25 shows evidence of direct σ-bonding interaction between the two Re atoms.

Figure 3.3 shows the QTAIM analyzed bond paths about the Re_2Au_2 core and lists the electron densities at selected bond critical points (BCPs) that were obtained from the DFT optimized structure of **3.1**. Interestingly, there is a significant electron density of 0.051 e/bohr^3 at the Re – Re BCP. It is almost as large as the electron density at the Re – Au BCPs, 0.055 and 0.056 e/bohr^3. This supports the idea of a significant direct Re – Re bonding interaction in **3.1**. Within the framework of the isolobal analogy, $Re_2(CO)_{10}$ probably provides the best example of a Re – Re σ-type single bond.[28,29] For comparison, we have also

calculated the QTAIM electron density at the Re – Re BCP for our PBEsol DFT optimized analysis of $Re_2(CO)_{10}$. The HOMO is consistent with the presence of a strong Re – Re σ-bond, however the calculations also show that there are two orbitals, HOMO-3 and HOMO-4, that do exhibit some supplementary Re – Re π-type bonding interactions, see figure 3.9. The QTAIM electron density for $Re_2(CO)_{10}$ at the Re – Re BCP obtained by this calculation was 0.038 e/bohr^3. A comparison with that of **3.1** would lead one to the conclusion that the Re – Re bonding interaction in **3.1** is significantly greater than that in $Re_2(CO)_{10}$. Indeed, the π-interaction represented in the HOMO-7 of **3.1** supports the idea of a partial multiple bonding character for its Re – Re bonding. To pursue the Re – Re bonding analysis further, we have also performed NBO analyses of **3.1**. These calculations provided Mayer indices, Natural Atomic Orbitals (NAOs), Natural Localized Molecular Orbitals (NLMOs) and a natural population analysis (NPA). These results are presented in Table 3.4 together with the corresponding results for $Re_2(CO)_{10}$ and for compounds **3.2**, **3.3** and **3.4**. The Mayer, NAO, NLMO/NPA and Wiberg indices for **3.1** are 0.777, 0.192, 0.624 and 0.224, respectively. The corresponding values for $Re_2(CO)_{10}$, 0.264, 0.324, 0.284 and 0.0922, are all considerably smaller than those in **3.1**. If we assume that the Re – Re bond order in $Re_2(CO)_{10}$ is formally 1.0, then it must be concluded that the Re – Re bond order in **3.1** is greater than 1.0 by all measures.

Compound **3.1** is intensely red in color. Accordingly, a UV-vis spectrum of **3.1** was obtained. This spectrum is shown in Figure 3.4a. It exhibits three

absorptions in the visible region of the spectrum , λ_{max} = 327 nm, ϵ = 6692 $cm^{-1}M^{-1}$, λ_{max} = 420 nm, ϵ = 2820 $cm^{-1}M^{-1}$ and λ_{max} = 493 nm, ϵ = 5836 $cm^{-1}M^{-1}$, that correlate to electronic transitions between the orbitals in the Re_2Au_2 core of the molecule. A time-dependent DFT (TDDFT) analysis of the electronic transitions has provided the spectrum shown in Figure 3.4b. The major visible transition at 493 nm (calculated at 525 nm) and is attributed to two closely spaced allowed transitions: 1) from the HOMO (74 %) and the HOMO-2 (22 %) to LUMO (f = 0.074) and 2) from the HOMO-2 (75 %) and the HOMO (22 %) to LUMO (f = 0.032). The observed shoulder at 420 nm, calculated to be at 476 nm, is attributed to the HOMO-4 (98 %, f = 0.0043) to LUMO. The absorption at 327 nm, calculated to be at 372 nm, is attributed to the HOMO-2 (94 %, f = 0.155) to LUMO+1 transition, see Figure 3.2 for the MOs.

In order to compare the $Au(PPh_3)$ group with H, we have also performed a geometry-optimized DFT analysis of **3.2**. Selected MOs that focus on the bonding in the Re_2H_2 core of the molecule are shown in Figure 3.5. The HOMO-3 and HOMO-7 show evidence for direct Re – Re interactions although they also include substantial overlaps with the two hydrogen atoms. The HOMO-28 is a low-lying symmetric orbital with a significant component delocalized about the the Re_2H_2 core, but this orbital also contains significant contributions from the σ-bonding from the four in-plane CO ligands which are largely responsible for its low energy. The HOMO-5 shows that there is significant out of plane Re – Re π-bonding as also found in the HOMO-7 in **3.1**. The HOMO-23 is another low-lying

orbital that includes delocalized bonding between the rhenium atoms and the hydride ligands. Figure 3.6 shows the QTAIM analyzed bond paths about the Re_2H_2 core and includes selected electron densities at the BCPs obtained from the optimized structure of **3.2**. Most interestingly, the electron density along the Re – Re vector (calculated at the ring point of the Re_2H_2 core) is even larger 0.058 e/bohr^3 than that in **3.1**. The Mayer, NAO, NLMO/NPA and Wiberg indices for the Re – Re interaction in **3.2** are similar to those for **3.1**, see Table 3.4, and lead to the conclusion that the Re – Re bonding in **3.2** is also partially multiple in character and very similar to that in **3.1**.

In order to investigate the reactivity of **3.1**, vis-à-vis, its electronic unsaturation, the reaction of **3.1** with I_2 was performed. When compound **3.1** was allowed to react with I_2, the new compound $Re_2(CO)_8(\mu\text{-}AuPPh_3)(\mu\text{-}I)$, **3.3** was obtained in 13 % yield. Compound **3.3** was obtained independently in a much better yield (83%) from the reaction of $Re_2(CO)_8(\mu\text{-}H)(\eta^2\text{-}CH{=}CHC_4H_9)$ with $Au(PPh_3)I$. Compound **3.3** was found to react with I_2 to yield $Re_2(CO)_8(\mu\text{-}I)_2$, **3.4** in 23 % yield. Compound **3.4** can be obtained directly from **3.1** in 32 % yield by using an excess of I_2.

Compound **3.3** was characterized by a single-crystal X-ray diffraction analysis and an ORTEP diagram of the molecular structure is shown in Figure 3.7. The two rhenium atoms are held together by one bridging $AuPPh_3$ group and one bridging iodide ligand. The Re – Re bond distance in **3.3** at 3.1890(12) Å is

approx. 0.3 Å longer than that in **3.1** and **3.2** and approx. 0.15 Å longer than that in $Re_2(CO)_{10}$. Because the iodide ligand serves formally as a three electron donor, the two rhenium atoms in **3.3** contain a total of 34 valence electrons, and a Re – Re single bond is anticipated. This is consistent with the increased length of the Re – Re distance relative to that of **3.1** and **3.2**. The Re – Au distances are similar to those found in **3.1**, Re2 – Au1 = 2.7871(9) Å and Re1 - Au1 = 2.7935(9) Å. The Re – I distances are Re1 - I1 = 2.7566(14) Å and Re2 - I1 = 2.7845(14) Å, but both are significantly shorter than the distances found in the di-iodide complex **3.4**, 2.827(2) Å, 2.826(2) Å, 2.813(2) Å and 2.814 (2) Å, which contains no formal Re – Re bond.[17]

NBO analyses of **3.3** and **3.4** were also performed, see Table 3.4. Assuming that the iodide ligand is a 3-electron donor and all bonds are of a 2 center – 2 electron type, the Re – Re bond order in **3.3** should be 1. The NBO bond orders for **3.3** are slightly larger than for those of $Re_2(CO)_{10}$ but smaller that for those of **3.1** and **3.2**. The QTAIM electron density at the Re – Re BCP in **3.3** at 0.0357 e/bohr^3 is only slightly larger than that in $Re_2(CO)_{10}$. Perhaps, the notion of the iodide ligand as a 3-electron donor having two 2 center – 2 electron σ-bonds to the Re atoms is too simple. Indeed, the HOMO-14, HOMO-15 and HOMO-16 obtained for **3.3** in our DFT calculations show both delocalized σ- and π-bonding interactions between the iodide ligand and the two rhenium atoms, see Figure 3.8. The effect of this bonding on the formal Re – Re bond order is difficult to evaluate, but the 3-center σ-bonding of the Re_2I group shown in the

HOMO-16 could lead to a slight increase in the electron density at the Re – Re BCP as observed.

Formally, there is no need for the formation of a Re – Re bond in compound **3.4**. With two bridging iodide ligands serving as three-electron donors, both Re atoms have 18 electron configurations. The observed Re – Re distance in **3.4** is long at 4.218(2) Å[17] and is consistent with the absence of a Re – Re bond. Consistent with this the Mayer, NAO, NLMO/NPA and Wiberg indices that were obtained after a geometry-optimized PBEsol MO refinement of the structure of **3.4** were all close to zero as expected.

Conclusions

The doubly-Au(PPh_3) bridged unsaturated complex **3.1** has been prepared and characterized by the photodecarbonylation of $Re(CO)_5[Au(PPh_3)]$. It is analogous to the doubly-hydride bridged unsaturated complex **3.2**. Both compounds possess short Re – Re bond distances. Computational analyses suggest the existence of partial multiple Re – Re bonds in both **3.1** and **3.2**. It can be concluded that Au(PPh_3) and H have similar effects on the Re – Re bonding in these two compounds. Compound **3.1** reacts with I_2 to yield the compounds **3.3** and **3.4**. This reaction appears to follow the sequence of two steps shown in scheme 3.3. Indeed, we have found that **3.3** also reacts with I_2 to yield **3.4**. The sequential replacement of the bridging one electron Au(PPh_3)

groups with three electron bridging iodide ligands reduces the Re – Re bonding until it is virtually eliminated in compound **3.4**.

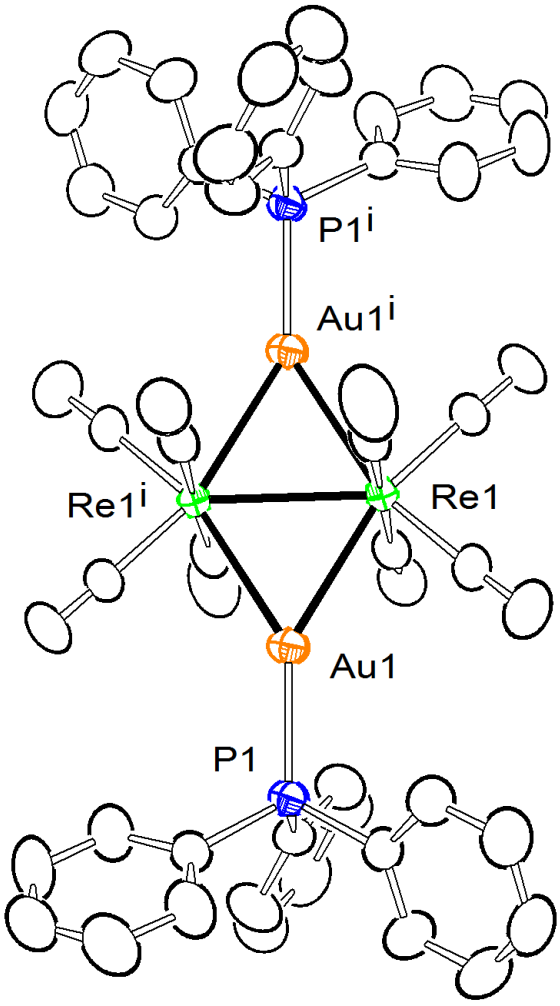

Figure 3.1. An ORTEP diagram of the molecular structure of $Re_2(CO)_8(\mu\text{-}AuPPh_3)_2$, **3.1** showing 40% thermal ellipsoid probability.

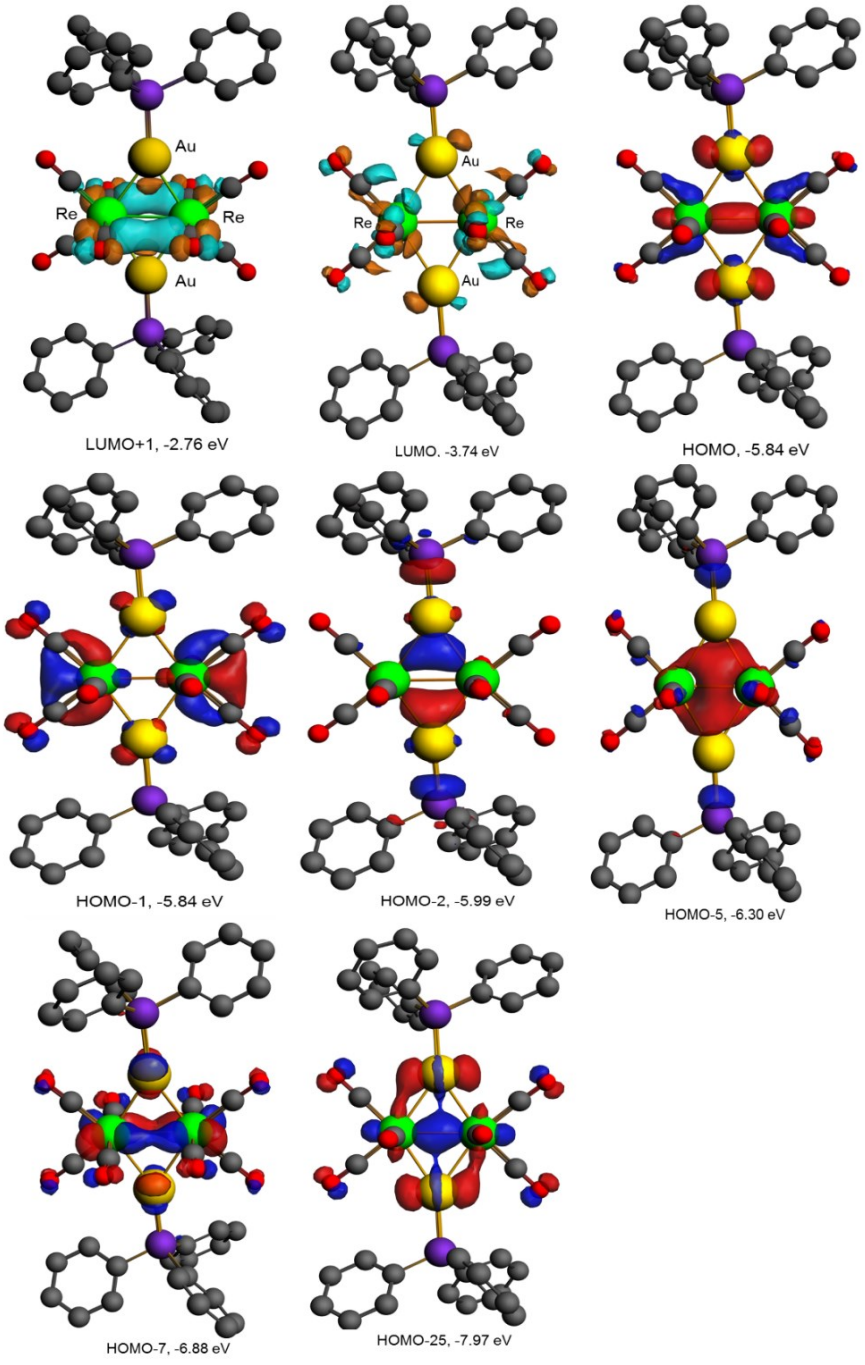

Figure 3.2. Molecular orbital diagrams of the LUMO+1, LUMO, HOMO, HOMO-1, HOMO-2, HOMO-5, HOMO-7 and HOMO-25, Isovalue = 0.04, with calculated energies showing the nature of the bonding in the Re_2Au_2 core of the structure of **3.1**.

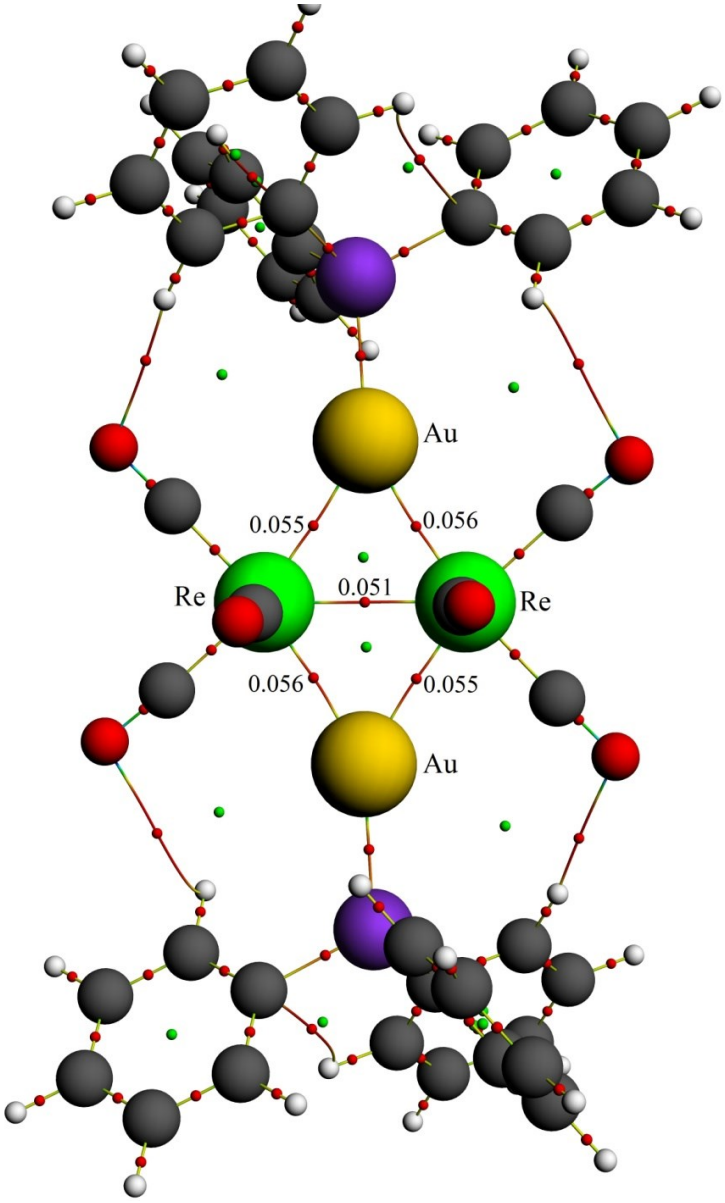

Figure 3.3. Selected electron densities at bond critical points shown in red calculated by the QTAIM method by using the DFT optimized structure of **3.1**.

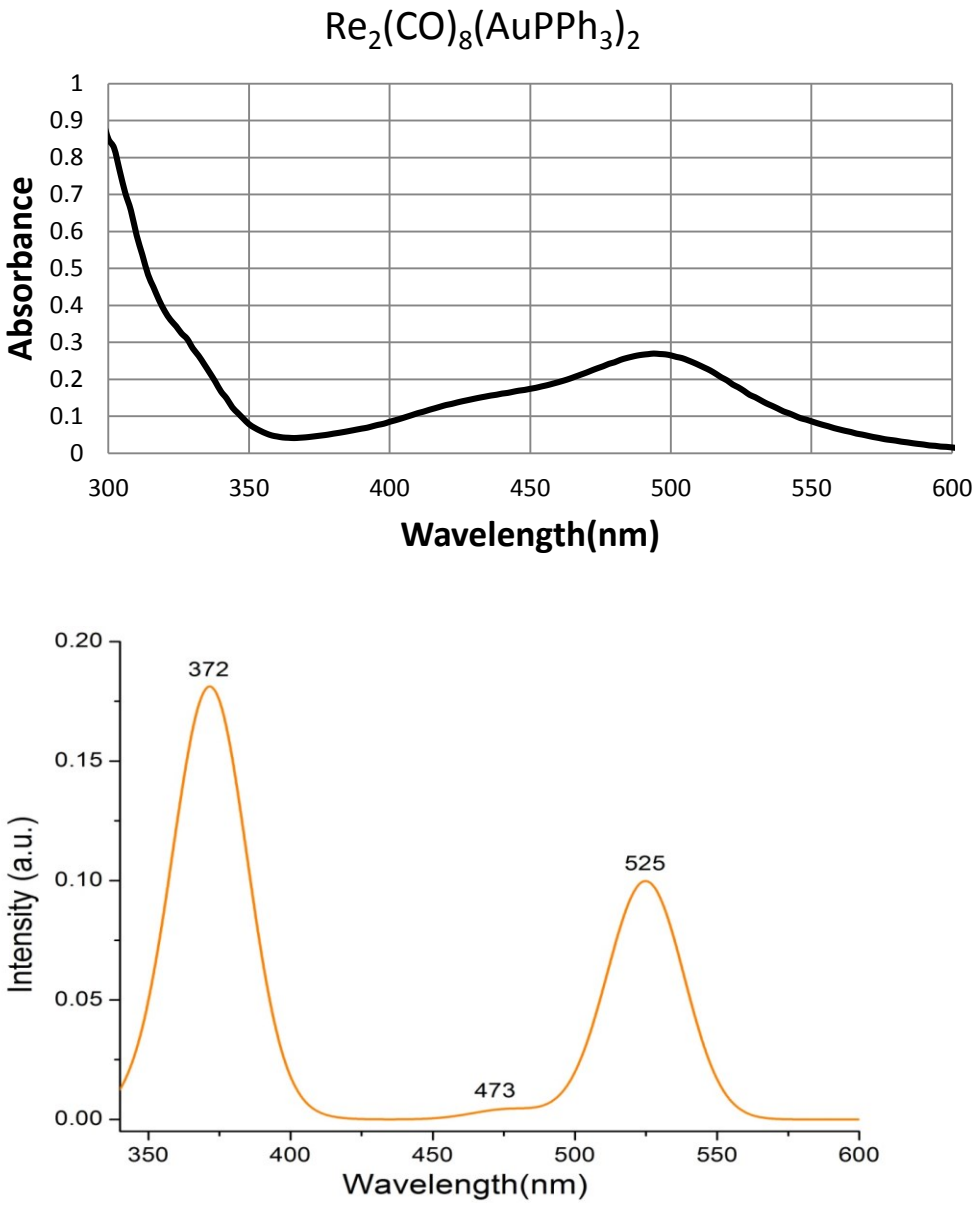

Figure 3.4. a) UV–vis absorption spectrum of **3.1** in CH_2Cl_2 solvent. b) TDDFT calculated UV–vis absorption spectrum of **3.1**.

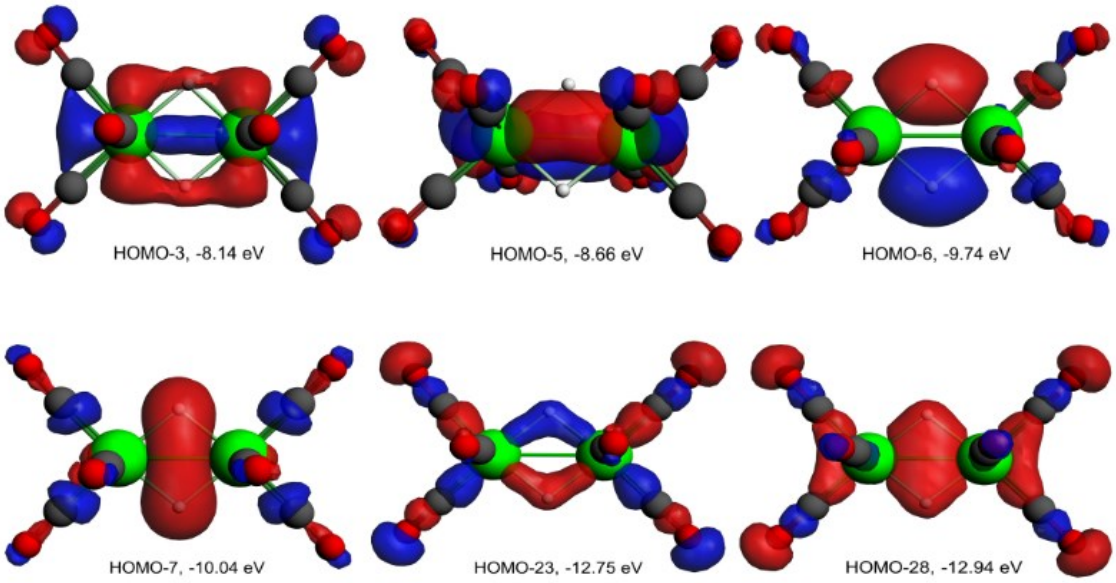

Figure 3.5. Molecular orbital diagrams of the HOMO-3, HOMO-5, HOMO-6, HOMO-23 and HOMO-28, Isovalue = 0.04, with calculated energies showing the bonding in the Re_2H_2 core of the structure of **3.2**.

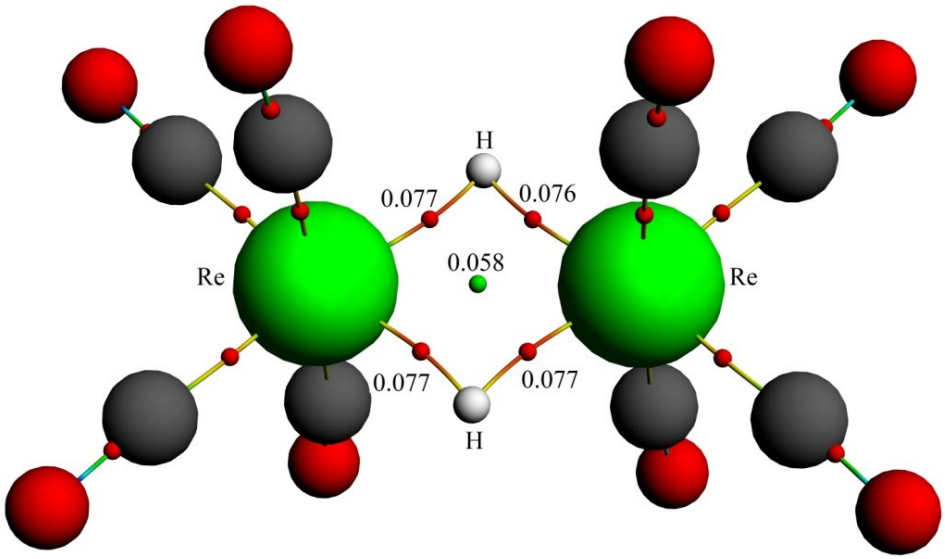

Figure 3.6. Selected electron densities at bond critical points shown in red and the Re_2H_2 ring point (in green) calculated by the QTAIM method by using the DFT optimized structure of **3.2**.

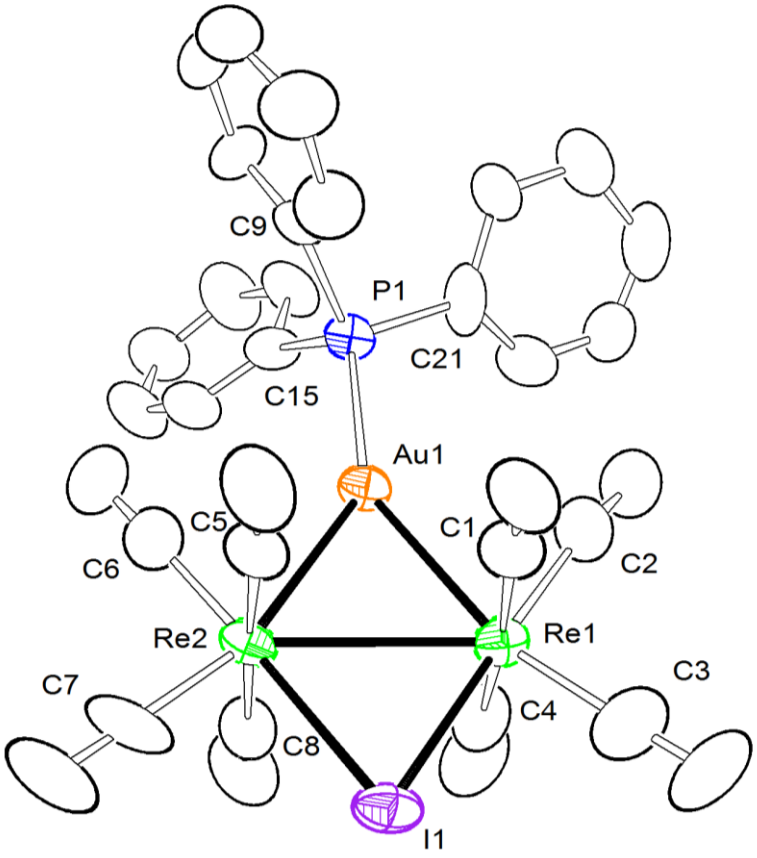

Figure 3.7. An ORTEP diagram of the molecular structure of $Re_2(CO)_8(\mu\text{-}AuPPh_3)(\mu\text{-}I)$, **3.3** showing 30% thermal ellipsoid probability.

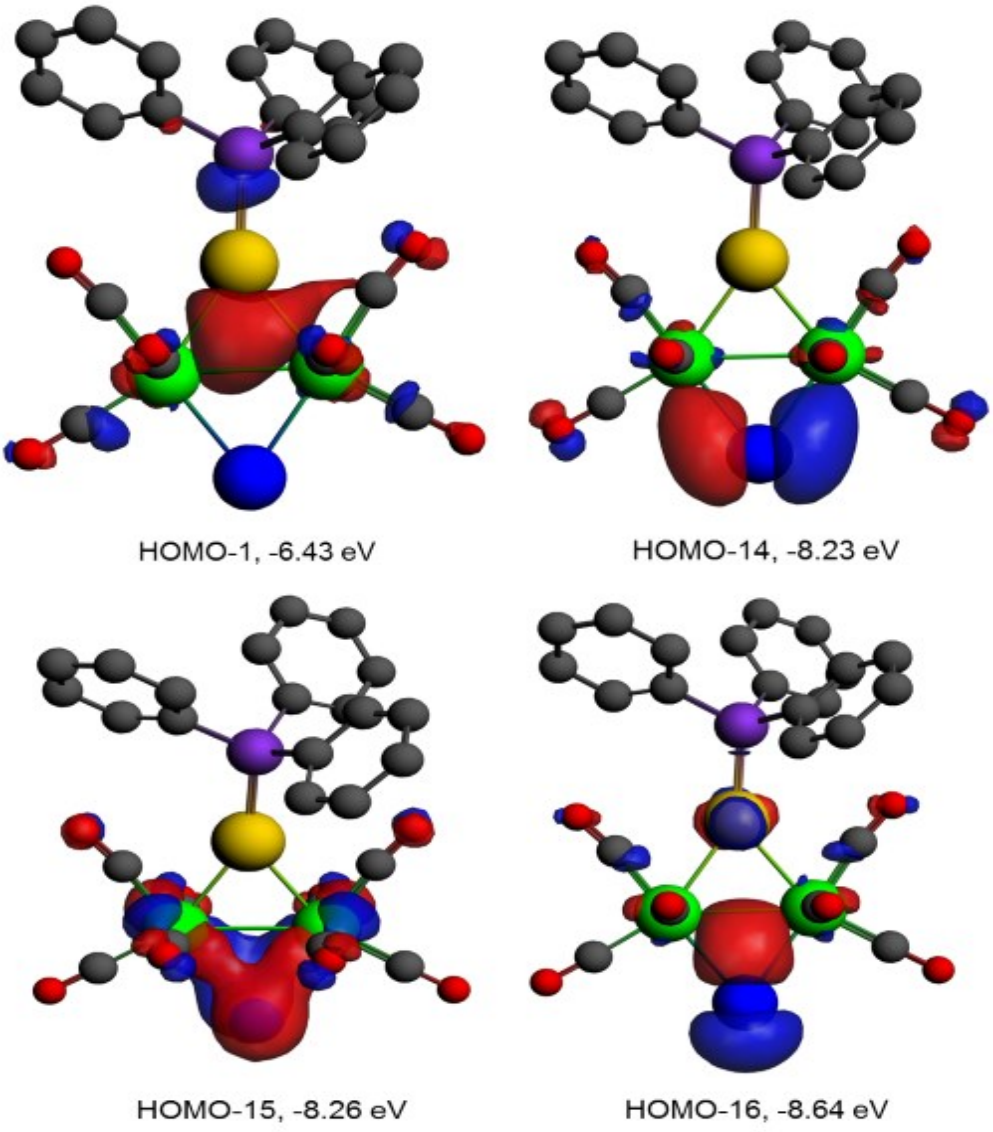

Figure 3.8. Molecular orbital diagrams of the HOMO-1, HOMO-14, HOMO-15 and HOMO-16, Isovalue = 0.04, with calculated energies showing the bonding in the Re_2AuI core of the molecule of **3.3**.

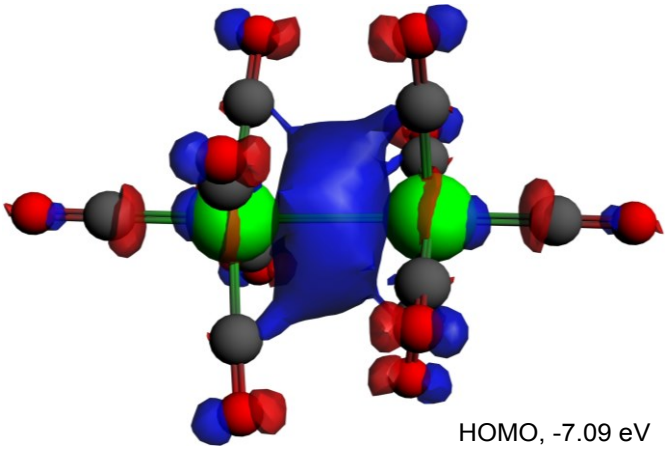

HOMO, -7.09 eV

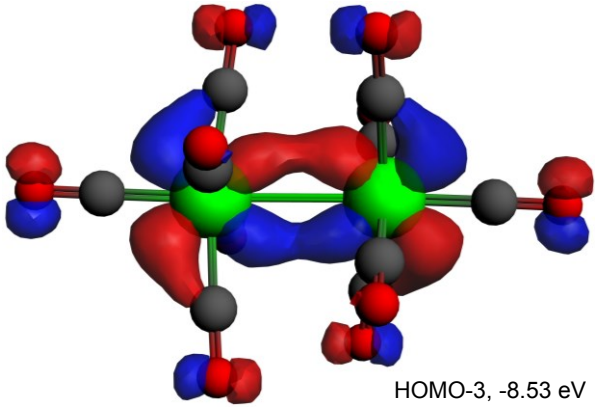

HOMO-3, -8.53 eV

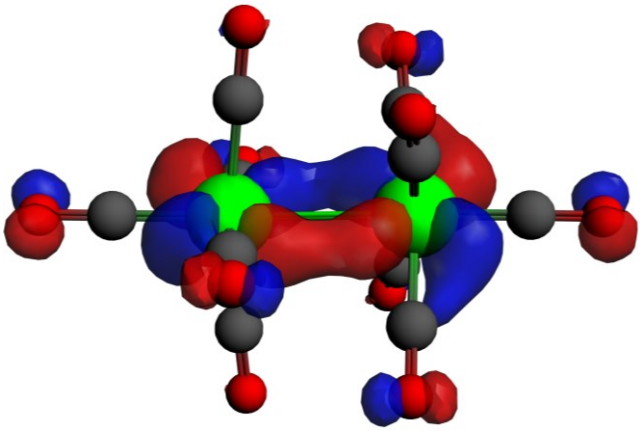

HOMO-4, -8.57 eV

Figure 3.9. Selected PBEsol molecular orbital diagrams with calculated energies for $Re_2(CO)_{10}$ showing the Re – Re bonding: HOMO, HOMO-3 and HOMO-4. Isovalue = 0.04.

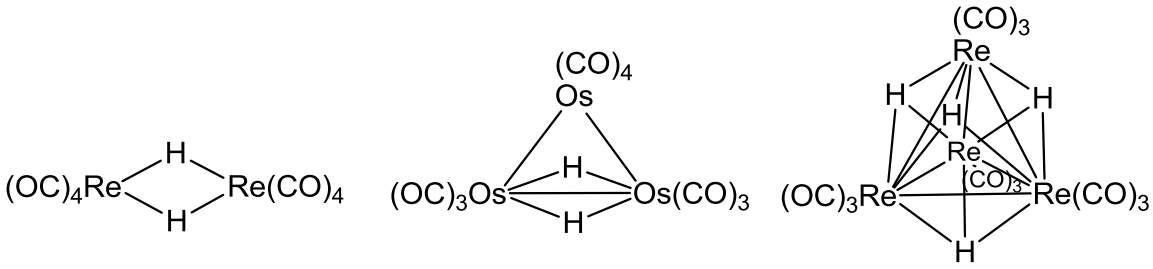

Scheme 3.1.Hydride-Bridged Metal Carbonyl Cluster complexes: $Re_2(CO)_8(\mu–H)_2$, $Os_3(CO)_{10}(\mu–H)_2$ and $Re_4(CO)_{12}(\mu–H)_4$

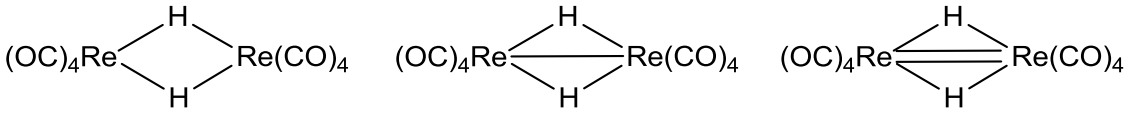

Scheme 3.2. Different bond order for the Re–Re bond in $Re_2(CO)_8(\mu\text{–}H)_2$, **3.2**.

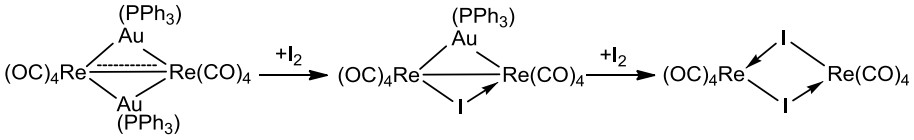

3.1 **3.3** **3.4**

Scheme 3.3. Sequential addition of I_2 to compounds **3.1** and **3.3**.

Table 3.1. Crystallographic data for **3.1** and **3.3**[a]

Compound	**3.1**	**3.3**
Empirical formula	$Au_2Re_2P_2O_8C_{44}H_{30}$	$AuRe_2IPO_8C_{26}H_{15}$
Formula weight	1514.95	1182.62
Crystal system	Monoclinic	Triclinic
Lattice parameters		
a (Å)	9.2034(2)	9.2417(10)
b (Å)	14.6713(2)	12.3747(14)
c (Å)	16.4820(3)	14.8012(16)
α (deg)	90.00	68.142(2)
β (deg)	101.35	79.951(2)
γ (deg)	90.00	70.977(2)
V (Å^3)	2181.98(7)	1482.5(3)
Space group	P21/n	$P\bar{1}$
Z value	2	2
ρ_{calc} (g/cm^3)	2.306	2.656
μ (Mo Kα) (mm^{-1})	12.356	14.221
Temperature (K)	294(2)	294(2)
$2\theta_{max}$(°)	56.48	56.58
No. Obs. (I>2σ(I))	3559	4785
No. Parameters	262	352
Goodness of fit (GOF)	1.078	1.089
Max. shift in cycle	0.004	0.001
Residuals*: R1; wR2	0.0192: 0.0434	0.0302; 0.0740
Absorption Correction, Max/min	Multi-Scan 1.000/0.533	Multi-Scan 1.000/0.523
Largest peak in Final Diff. Map (e$^-$/ Å^3)	0.790	0.993

[a] $R = \Sigma_{hkl}(\,|\,|F_{obs}|-|F_{calc}|\,|\,)/\Sigma_{hkl}|F_{obs}|$; $R_w = [\Sigma_{hkl}w(\,|F_{obs}|-|F_{calc}|\,)^2/\Sigma_{hkl}wF^2_{obs}]^{1/2}$; $w = 1/\sigma^2(F_{obs})$; GOF = $[\Sigma_{hkl}w(\,|F_{obs}|-|F_{calc}|\,)^2/(n_{data} - n_{vari})]^{1/2}$.

Table 3.2. Selected intramolecular angles and bond distances for **3.1**[a]

Atom	Atom	Distance(Å)	Atom	Atom	Atom	Angle(°)
Re1	Au1	2.7914(2)	Au1	Re1	Au1*	117.320(6)
Re1	Au1*	2.7977(2)	Re1	Au1	Re1*	62.681(6)
Re1	Re1*	2.9070(3)	P1	Au1	Re1	145.57(3)
Au1	P1	2.3308(11)	P1	Au1	Re1	147.68(3)

[a] Estimated standard deviations in the least significant figure are given in parentheses.

Table 3.3. Selected intramolecular angles and bond distances for **3.3**[a]

Atom	Atom	Distance(Å)	Atom	Atom	Atom	Angle(°)
Re1	Re2	3.1890(2)	I1	Re1	Au1	110.31(4)
Re2	Au1	2.7871(9)	Au1	Re2	I1	109.68(4)
Re1	Au1	2.7935(9)	Re2	Au1	Re1	69.70(3)
Re1	I1	2.7566(14)	Re1	I1	Re2	70.27(3)
Re2	I1	2.7845(14)	Re1	Au1	P1	146.92(11)
Au1	P1	2.322(4)	Re2	Au1	P1	143.27(11)

[a] Estimated standard deviations in the least significant figure are given in parentheses.

Table 3.4. NBO Analyses of the Re - Re bond orders calculated for **3.1** – **3.4** and $Re_2(CO)_{10}$.

Compound	Mayer bond order[a]	NAO bond order[b]	NLMO/NPA bond order[b]	Wiberg bond index[c]
3.1	0.777	0.192	0.624	0.224
3.2	0.522	0.134	0.480	0.180
3.3	0.457	0.0888	0.319	0.118
3.4	0.124	-8.8×10^{-3}	1.32×10^{-2}	6.4×10^{-3}
$Re_2(CO)_{10}$	0.264	0.0324	0.284	0.0922

[a] Mayer, I. *J. Comput. Chem.* **2007**, *28*, 204 - 221. [b] NAO = natural atomic orbital, NLMO = Natural localized molecular orbitals, NPA = natural population analysis. [c] Wiberg, K. B. *Tetrahedron* **1968**, *24*, 1083 - 1096.

REFERENCES

1) (a) Raubenheimer, H. G.; Schmidbaur, H. *Organometallics* **2012**, *31*, 2507 - 2522. (b) Stone, F. G. A. *Angew. Chem. Int. Ed. Engl.* **1984**, *23*, 89 - 99. (c) Evans, D. G.; Mingos, D. M. P. *J. Organomet. Chem.* **1982**, *232*, 171 – 191.

2) Bau, R.; Drabnis, M. H. *Inorg. Chim. Acta* **1997**, *259*, 27 - 50. (b) Teller, R. G.; Bau, R., *Struc. Bonding* **1981**, 41, 1 - 82. (c) Humphries, A. P.; Kaesz, H. D. *Prog. Inorg. Chem.*145 – 222.

3) (a) Salter, I. D. in *Comprehensive Organometallic Chemistry II,* Abel, E. W.; Stone, F. G. A.; Wilkinson, G., Oxford, UK, **1995**, Vol. 10, Ch. 5, pp 255 – 322. (b) Salter, I. D. in *Metal Clusters in Chemistry*, Braunstein, P.; Oro, L. A.; Raithby, P. R., Wiley-VCH, Weinheim, 1999, Vol. 1, Ch. 1.27, pp 509-534. (c) Salter, I. D. *Adv. Organomet. Chem.* **1989**, *29*, 249 – 343.

4) (a) Bennett, M. J.; Graham, W. A. G.; Hoyano, J. K.; Hutcheon, W. L. *J. Am. Chem. Soc.* **1972**, *94*, 6232 – 6233. (b) Masciocchi, N.; Sironi, A.; D'Alfonso, D. *J. Am. Chem. Soc.* **1990,** 112, 9395 – 9397. (c) Li, N.; Xie, Y.; King, R. B.; Schaefer III, H. F. *J. Phys. Chem. A* **2010,** *114,* 11670 – 11680.

5) (a) Broach, R. W.; Williams, J. M. *Inorg. Chem.* **1979**, *18*, 314 – 319. (b) Churchill, M. R.; Hollander, F. J.; Hutchinson, J. P. *Inorg. Chem.* **1977**, *16*, 2697 - 2700; (c) Allen, V. F.; Mason, R.; Hitchcock, P. B. *J. Organomet. Chem.* **1977**, *140*, 297 - 307.

6) Wilson, R. D.; Bau, R. *J. Am. Chem. Soc.* **1976**, *98*, 4687 – 4689.

7) Adams, R. D.; Captain, B.; Beddie, C.; Hall, M. B. *J. Am. Chem. Soc.* **2007**, *129*, 986 – 1000.

8) Adams, R. D.; Kan, Y.; Zhang, Q.; Hall, M. B.; Trufan, E. *Organometallics* **2012**, *31,* 50-53.

9) (a) Deeming A. J. *Adv. Organomet. Chem.* **1986**, *26*, 1 – 96. (b) Keister, J. B.; Shapley, J. R. *J. Am. Chem. Soc.* **1976**, *98*, 1056 – 1057. (c) Hudson, R. H. E.; Poe, A. J. *Organometallics* **1995**, *14,* 3238 - 3248.

10) Wang, S. R.; Wang, S.-L.; Cheng, C. P. *J. Organomet. Chem,* **1992**, *431*, 215-226.

11) Burgess, K.; Johnson, B. F. G.; Kaner, D. A.; Lewis, J.; Raithby, P. R.; Syed,-Mustaffa, S. N. A. B. *J. Chem. Soc., Chem. Commun.* **1983**, 455 – 457.

12) Johnson, B. F. G.; Kaner, D. A.; Lewis, J.; Raithby, P. R. *J. Organomet. Chem.* **1981**, *215*, C33 – C37.

13) Adams, R. D; Rassolov, V.; Zhang, Q. *Organometallics* **2012**, *31,* 2961−2964.

14) Nicholson, B. K.; Bruce, M. I.; bin Shawkataly, O.; Tiekink, E. R. T. *J. Organomet. Chem.* **1992**, *440*, 411 – 418.

15) Nubel, P. O.; Brown, T. L. *J. Am. Chem. Soc.* **1984**, 106, 644-652.

16) Westland, A.D. *Canad. J. Chem.*, 47, **1969**, 4135-4140.

17) Darst, K. P.; Lenhert, P. G.; Lukehart, C. M.; Warfield, L. T. *J. Organomet. Chem.* **1980**, *195*, 317 – 324.

18) SAINT+ Version 6.2a. Bruker Analytical X-ray System, Inc., Madison, Wisconsin, USA, 2001.

19) Sheldrick, G. M., SHELXTL Version 6.1; Bruker Analytical X-ray Systems, Inc., Madison, Wisconsin, USA, 1997.

20) ADF2013; SCM Theoretical Chemistry, Vrije Universiteit, Amsterdam, The Netherlands, http://www.scm.com.

21) Perdew, J. P.; Ruzsinszky, A.; Csonka, G. I.; Vydrov, O. A.; Scuseria, G. E. *Phys. Rev. Lett.* **2008**, *100*, 136406.

22) (a) Bader, R. F. W. *Atoms in Molecules: A Quantum Theory*, Oxford, Clarendon, 1990. (b) Cortés-Guzmán, F.; Bader, R. F. W. *Coord. Chem. Rev.* **2005**, *249*, 633 - 662.

23) AIMAll, Version 12.11.09, Keith, T. A. TK Gristmill Software, Overland Park KS, USA, 2012 (aim.tkgristmill.com).

24) a) Glendening, E. D.; Badenhoop, J. K.; Reed, A. E.; Carpenter, J. E.; Bohmann, J. A.; Morales, C. M.; Weinhold, F. *NBO 5.0*. Theoretical Chemistry Institute, University of Wisconsin, Madison, 2001. b) Weinhold, F.; Landis, C. R., Valency and Bonding: A Natural Bond Order Donor-

Acceptor Perspective; Cambridge University Press: Cambridge, U.K., 2005; pp 32−36.

25) Bruce; M. I.; Paul J. Low, P. J.; Skelton, B. W.; White, A. H. *J. Organomet. Chem.* **1996**, *515*, 65 – 79.

26) Chedia, R. V.; Dolgushin, F. M.; Smolyakov, A. F.; Lekashvili, O. I.; Kakulia, T. V.; Janiashvili, L. K.; Sheloumov, A. M.; Ezernitskaya, M. G.; Peregudova, S. M.; Petrovskii, P. V.; Koridze, A. A. *Inorg. Chim. Acta* **2011**, *378*, 264 – 268.

27) Churchill, M. R.; Amoh, K. N.; Wasserman, H. J. *Inorg. Chem.*, **1981**, *20*, 1609–1611.

28) Hoffmann, R. *Angew Chem. Int. Ed. Engl.* **1982**, *21*, 711-724.

29) Xu, B.; Li, Q.-S.; Xie, Y.; King, R. B.; Schaefer III, H. F. *Dalton Trans.*, **2008**, 2495–2502.

CHAPTER 4

FACILE C–H BOND FORMATION BY REDUCTIVE ELIMINATION AT A DINUCLEAR METAL SITE

INTRODUCTION

The making and breaking of CH bonds is fundamental to the transformations of organic molecules into new compounds.[1] In many cases, these transformations are facilitated by metal atoms via oxidative-addition and reductive-elimination processes.[2,3] The mechanisms of these processes at single metal atoms have been the subject of intense scrutiny over the years.[3,4] The nature of these processes on metal surfaces and at polynuclear metal centers is certainly more complex and is not as well understood, but it is certainly of no less importance.[5-7] Multicenter metal-based transformations of hydrocarbons are believed to be important in heterogeneous catalytic hydrogenations,[8] petroleum reforming[9] and Fischer-Tropsch chemistry.[10]

There are strong similarities between the reductive-elimination of C-H bonds and the reductive-elimination of the H-H bond to form H_2. In 1984, Trinquier and Hoffmann showed that the concerted symmetric C_{2v} intramolecular, 1,2-reductive elimination of H_2 from a dinuclear metal center(1) is a symmetry-forbidden processes, but an unsymmetrical elimination via the planar C_s geometric form(2) is symmetry-allowed (Scheme 4.1).[11]

In this work we have synthesized the complexes $Re_2(CO)_8(\mu\text{-}AuPPh_3)(\mu\text{-}Ph)$, **4.1** and $Re_2(CO)_8(\mu\text{-}H)(\mu\text{-}Ph)$, **4.2** containing a bridging phenyl ligand and a bridging gold-phosphine group, **4.1** a bridging hydrido ligand, **4.2**. When allowed to react with NCMe at room temperature, compound **4.2** readily eliminates benzene by a C-H bond forming reductive elimination of the bridging phenyl ligand and the bridging hydrido ligand. The mechanism of this elimination has been investigated and ascertained by DFT computational analyses and is reported herein.

Experimental Details

General Data. Reagent grade solvents were dried by the standard procedures and were freshly distilled prior to use. Infrared spectra were recorded on a Thermo Nicolet Avatar 360 FT-IR spectrophotometer. ^1H NMR and $^{31}P\{^1H\}$ NMR were recorded on a Varian Mercury 400 spectrometer operating at 400.1 and 161.9 MHz respectively. $^{31}P\{^1H\}$ NMR spectra were externally referenced against 85% *ortho*-H_3PO_4. Mass spectrometric (MS) measurements performed by a direct-exposure probe using electron impact ionization (EI) were made on a VG 70S instrument. $Re_2(CO)_{10}$ was obtained from STREM and was used without further purification. $Re_2(CO)_8[\mu\text{-}\eta^2\text{-}C(H)=C(H)Bu^n](\mu\text{-}H)$[12] and $Au(PPh_3)Ph$[13] were prepared according to previously reported procedures. Product separations were performed by TLC in air on Analtech 0.25 and 0.5 mm silica gel 60 Å F_{254} glass plates.

Reaction of $Re_2(CO)_8[\mu\text{-}\eta^2\text{-}C(H)=C(H)Bu^n](\mu\text{-}H)$ with $AuPPh_3Ph$

40.0 mg (0.0745 mmol) of $AuPPh_3Ph$ was added to 38.0 mg (0.0558 mmol) of $Re_2(CO)_8[\mu\text{-}\eta^2\text{-}C(H)=C(H)Bu^n](\mu\text{-}H)$ dissolved in 25 mL of hexane. The solution was then refluxed for 3h. An orange solution was formed and the solvent was then removed in *vacuo*. The residue was extracted in methylene chloride and separated by TLC by using a 4:1 hexane/methylene chloride (v/v) solvent mixture to give a yellow band of $Re_2(CO)_8(\mu\text{-}AuPPh_3)(\mu\text{-}Ph)$, **4.1**, 55.2 mg (87% yield). Spectral data for **4.1**: IR ν_{CO} (cm^{-1} in methylene chloride): 2080(w), 2052(s), 1987(vs), 1963(s), 1933(s). ^1H NMR (CD_2Cl_2, in ppm) δ = 7.03-7.07 (t, 2H, Ph, J_{H-H}=7.6 Hz), δ = 7.46-7.56 (m, 30H, Ph), δ = 8.03-8.04 (d, 2H, Ph, J_{H-H}=6.4 Hz), δ = 8.15-8.19 (t, 1H, Ph, J_{H-H}=7.2 Hz). ^{31}P NMR (CD_2Cl_2, in ppm) δ = 71.48(s). Mass Spec. EI/MS *m*/*z*. 1132, M^+. The isotope pattern is consistent with the presence of one gold atom and two rhenium atoms.

Reaction of $Re_2(CO)_8)(\mu\text{-}AuPPh_3)(\mu\text{-}Ph)$ with $HSnPh_3$.

20.4 mg (0.0581 mmol) of $HSnPh_3$ was added to 44.0 mg (0.0388 mmol) of $Re_2(CO)_8(\mu\text{-}AuPPh_3)(\mu\text{-}Ph)$ dissolved in 25 mL of methylene chloride and stirred at room temperature for 1h. The solution turned from yellow to orange and the solvent was then removed in *vacuo*. The residue was extracted in methylene chloride and separated by TLC by using a 4:1 hexane/methylene chloride (v/v) solvent mixture to give a yellow band of $Re_2(CO)_8(\mu\text{-}H)(\mu\text{-}Ph)$, **4.2**, 11.6 mg (44%) , $[(\mu\text{-}AuPPh_3)(\mu\text{-}SnPh_3)]_2$, **5.1**, 7.2 mg (22.9%) [this metal complex will be discussed in Chapter 5] and a colorless band of Sn_2Ph_6, 4.7 mg (23%) Spectral

data for **4.2**: IR ν_{CO} (cm^{-1} in methylene chloride): 2110(w), 2084(m), 2010(vs), 1990(s), 1959(s). ^1H NMR (CD_2Cl_2, in ppm) δ = 7.19-7.23 (t, 2H, Ph, J_{H-H}=8.0 Hz), δ = 8.03-8.07 (t, 1H, Ph, J_{H-H}=8.0 Hz), δ = 8.20-8.22 (d, 2H, Ph, J_{H-H}=8.0 Hz), δ = -11.67 (s, 1H, hydride). Mass Spec. EI/MS *m*/*z*. 674. The isotope distribution pattern is consistent with the presence of two rhenium atoms.

Benzene Formation by the Addition of NCMe to 4.2.

10.0 mg (0.0148 mmol) of **4.2** and 2.0 mg (0.0123 mmol) of hexamethylbenzene (as Internal Standard) were dissolved in 0.8 mL of NCMe-d_3 in a 5 mm NMR tube. The NMR tube was evacuated and filled with N_2 five times. The NMR tube was left to sit for 24 h and a ^1H NMR spectra was recorded. ^1H NMR spectra of this solution showed a singlet at δ = 7.37 indicating the formation of benzene in solution (~100%). The solvent was removed in vacuo and the residue was extracted in methylene chloride and separated by TLC using a 4:1 hexane/methylene chloride (v/v) solvent mixture to give a yellow band of $Re_2(CO)_8(NCMe\text{-}d_3)_2$, 5.4 mg (53% isolated yield).

Reaction of $Re_2(CO)_8(\mu\text{-}H)(\mu\text{-}C_6H_5)$ with C_6D_6.

5.0 mg (0.0074 mmol) of **4.2** was dissolved in 1.0 mL of C_6D_6 in a 5 mm NMR tube. The NMR tube was evacuated and filled with N_2 five times. The NMR tube was left to sit for 11 h at 60 °C and a mass spectrum was obtained. The mass spectrum of this solution showed a parent molecular ion peak of 680 *m*/*z*. This corresponds to $Re_2(CO)_8(\mu\text{-}D)(\mu\text{-}C_6D_5)$ with a conversion factor of ~100%.

Reaction of $Re_2(CO)_8)(\mu\text{-}H)(\mu\text{-}Ph)$ with $(C_2H_5)_2NC_6H_5$.

20 µL (0.1250 mmol) of N,N-Diethylaniline was added to 30.0 mg (0.0444 mmol) of $Re_2(CO)_8(\mu\text{-}H)(\mu\text{-}Ph)$, **4.2** dissolved in 2 mL of deuterated methylene chloride and stirred at 50 °C for 5.5 h. The solution was light yellow and the solvent was then removed in *vacuo*. The residue was extracted in methylene chloride and separated by TLC by using a 4:1 hexane/methylene chloride (v/v) solvent mixture to give a yellow band of $Re_2(CO)_8(\mu\text{-}H)[\mu\text{-}(C_2H_5)_2NC_6H_4]$, **4.3**, 20.2 mg (61.0%) and trace amounts of $[Re(CO)_3(\mu\text{-}OH)]_4$. Spectral data for **4.3**: IR ν_{CO} (cm^{-1} in methylene chloride): 2100(w), 2077(m), 2000(vs), 1981(s), 1946(s). ^1H NMR (CD_2Cl_2, in ppm) δ = 6.42-6.45 (d, 2H, Ph, J_{H-H}=8.7 Hz), δ = 8.04-8.06 (d, 2H, Ph, J_{H-H}=8.6 Hz), δ = -11.96 (s, 1H, hydride). Mass Spec. EI/MS *m*/*z*. 745. The isotope distribution pattern is consistent with the presence of two rhenium atoms.

Crystallographic Analyses: Orange single crystals of **4.1** suitable for x-ray diffraction analyses were obtained by slow evaporation of a benzene/octane solvent mixture at 15 °C. Yellow single crystals of **4.2** suitable for x-ray diffraction analyses were obtained by slow evaporation of a benzene/octane solvent mixture at 15 °C. Yellow single crystals of **4.3** suitable for x-ray diffraction analyses were obtained by slow evaporation of benzene at 25 °C. Each data crystal was glued onto the end of a thin glass fiber. X-ray intensity data were measured by using a Bruker SMART APEX CCD-based diffractometer using Mo Kα radiation (λ = 0.71073 Å). The raw data frames were integrated with the SAINT+ program by using a narrow-frame integration algorithm.[14] Correction for Lorentz and

polarization effects were also applied with SAINT+. An empirical absorption correction based on the multiple measurement of equivalent reflections was applied using the program SADABS. All structures were solved by a combination of direct methods and difference Fourier syntheses, and refined by full-matrix least-squares on F^2, using the SHELXTL software package.[15] All non-hydrogen atoms were refined with anisotropic displacement parameters. Hydrogen atoms were placed in geometrically idealized positions and included as standard riding atoms during the least-squares refinements. Crystal data, data collection parameters, and results of the analyses are listed in Table 4.1.

Computational Analyses.

All calculations were performed with ADF2013 program by using the PBEsol functional with ZORA scalar relativistic correction[16] and valence triple-ζ + 2 polarization, relativistically optimized (TZ2P) Slater-type basis set, with small frozen cores. All computations were performed by using gas phase models. This choice of computational model was based on prior testing of various functionals and basis sets.[17] The PBEsol functional was originally developed primarily for use with solid state materials, but has been shown to be superior to other functionals in the PBE family in simulating the structural parameters of large organic systems [18] and metal clusters.[19] This is also consistent with our own testing of various functionals for the structural parameters and relative energetics in organometallic cluster complexes. The energy profile was computed by scanning the defined reaction coordinate with full geometry optimization of other

degrees of freedom. The transition states are defined as energy maxima along the reaction coordinate scan. They are approximate transition states, since the backward scan along the same reaction coordinate starting with the products has an energy maximum at slightly different coordinates. The search for the exact transition state is very difficult to absence of analytic Hessians for PBEsol functional in ADF. Nevertheless, our approximate transition state energies are the upper bounds to the true ones. The intermediates are defined as energy minima along the scan coordinate and are exact within the computational model.

For the first reaction step, which is reactants to first intermediate portion of the reaction, the R(N-Re) distance was used as the reaction coordinate. For the second step the R(H-C) distance between the hydrogen on the metal cluster and the phenyl carbon bonded to rhenium was used as reaction coordinate.

The orbitals of the compounds at selected geometries were analyzed by fragment analysis, by orbital decomposition to the orbitals of the interacting fragments. The orbitals participating in the bonding of the fragments were used to understand the nature of chemical interaction in the compounds. The Cartesian coordinates of the species at selected geometries through the course of the C – H forming transformation are shown in Tables 4.4-4.8.

Results, Discussion.

The complex $Re_2(CO)_8(\mu\text{-}AuPPh_3)(\mu\text{-}Ph)$, **4.1** was obtained in 87% yield from the reaction of $Re_2(CO)_8[\mu\text{-}\eta^2\text{-}C(H)=C(H)Bu^n](\mu\text{-}H)$ with $Au(PPh_3)(Ph)$. Compound **4.1** was characterized by a single-crystal X-ray diffraction analysis.

An ORTEP diagram of the molecular structure of **4.1** is shown in Figure 4.1. The molecule contains two $Re(CO)_4$ groups held together by a bridging $AuPPh_3$ group, an η^1-bridging phenyl ligand and a strong Re-Re bonding interaction. The Re-Au distances, Au(1)-Re(1) = 2.7567(3) Å, Au(1)-Re(2) = 2.8080(4) Å, and the Re-C distances to the bonded carbon atom of the bridging phenyl ligand, Re(1)-C(1) = 2.292(5) Å, Re(2)-C(1) = 2.396(5) Å are slightly, but significantly different in the solid state. Compound **4.1** contains only 32 valence electrons at the two metal atoms and is thus formally electronically unsaturated by the amount of two electrons. Accordingly, the Re-Re distance is short, Re(1)-Re(2) = 2.9690(4) Å, and is similar to that found in a related unsaturated complex, $Re_2(CO)_8(\mu\text{-}AuPPh_3)_2$, Re(1)-Re(2) = 2.9070(3) Å.[20]

To further explore the bonding in **4.1**, a gas-phase PBEsol geometry optimized DFT calculation was performed on the structure of **4.1**. [21] The computed HOMO-LUMO gap is 2.31 eV, a value smaller than the typical computed gaps in stable molecules, consistent with unsaturated electronic structure (Figure 4.4).

The HOMO shows predominantly π back donation from the rhenium atoms to the carbonyl ligands. HOMO-4, shows a 3-center σ-type bonding between the phenyl carbon atom, C(1) and the two rhenium atoms. HOMO-18 displays a 4-center interaction that includes the gold atom, C(1) and the two rhenium atoms. HOMO-12 and HOMO-16 show electron donations from the filled

π-orbitals of the phenyl ligand to the rhenium atoms which helps to reduce some of the electronic unsaturation at the Re atoms resulting in a Re–Re bond length that is longer than that in the related compound $Re_2(CO)_8(\mu\text{-}AuPPh_3)_2$.[20]

When treated with $HSnPh_3$, compound **4.1** was converted to the new compound $Re_2(CO)_8(\mu\text{-}H)(\mu\text{-}Ph)$, **4.2** in 44% yield by replacement of the bridging $Au(PPh_3)$ group with a bridging hydrido ligand. Compound **4.2** was also characterized by single-crystal X-ray diffraction analysis and an ORTEP diagram of the derived molecular structure is shown in Figure 4.2. Like **4.1**, compound **4.2** also has only 32 valence electrons and is also electronically unsaturated by the amount of two electrons. The Re-Re bond distance is only slightly longer than that in **4.1**, Re(1)-Re(2) = 2.9924(3) Å. The phenyl and hydrido ligands bridge the Re-Re bond asymmetrically in the solid state, Re(1) - H(1) = 2.23(10) Å, Re(2) - H(1) = 2.08(10) Å, Re(1) - C(1) = 2.397(5) Å and Re(2) – C(1) = 2.266(5) Å**.**

In order to understand the bonding in **4.2**, a gas-phase PBEsol geometry-optimized DFT calculation of the structure of **4.2** was performed. This analysis provided a structure with equivalent Re - H distances, 1.87 Å, equivalent Re-C distances, 2.32 Å, to the carbon atom of the bridging phenyl ligand. The plane of the C_6 ring of the bridging phenyl ligand was perpendicular to that Re-Re vector. Molecular orbitals generated from these calculations show delocalized bonding across the *ipso*-carbon atom C(1) of the phenyl ring, the two rhenium atoms and the bridging hydride ligand, see Figure 4.5. The computed HOMO-LUMO gap is

2.62 eV, a value smaller than the typical computed gaps in stable molecules, consistent with an unsaturated electronic structure.

The HOMO-2, -6.77 eV, shows a closed 3-center σ–type bond involving the phenyl carbon atom C(1) and the two rhenium atoms. The HOMO-8 is predominantly a 4-center σ–type bond interaction that includes the hydrido ligand, C(1) and the two rhenium atoms. The HOMO-5 and HOMO-7 show the existence of electron donations from the filled π-orbitals of the phenyl ligand to the rhenium atoms which helps to reduce some of the electronic unsaturation at the Re atoms resulting in the longer Re – Re distances versus that in $Re_2(CO)_8(\mu\text{-}AuPPh_3)_2$. Note: the Re – Re distance in the unsaturated dirhenium compound $Re_2(CO)_8(\mu\text{-}H)_2$ is 2.876(1) Å which is significantly shorter than that in **4.1** and **4.2**.[22]

When treated with NCMe-d_3 in an NMR tube, compound **4.2** was converted to $Re_2(CO)_8(NCMe\text{-}d_3)_2$ and benzene (C_6H_6) in essentially quantitative yield after 19 h at 25° C.

A series of DFT computational analyses were performed in order to establish a mechanism for the formation of the benzene from the bridging H and Ph ligands. This analysis shows a transformation that is initiated by the approach of an NCMe ligand to one of the metal atoms and proceeds via a transition state

TS1, +15.6 kcal/mol as the nitrogen atom approaches the rhenium atom Re(1) at 2.73 Å, see top of Figure 4.6.

At the same time, the Re(1)-C(1) bond lengthens to 2.48 Å and the phenyl ligand begins to shift towards Re(2), Re(2) - C(1)= 2.28 Å. The Re-Re bond also weakens to 3.02 Å, as the addition of electron density from the NCMe ligand reduces some of the electronic unsaturation at the metal atoms. The transformation proceeds to an intermediate, **I1**, -8.86 kcal/mol from **4.2**, as the Re-N bond, 2.09 Å, to the NCMe ligand becomes fully established on Re(1). At this time, the phenyl ligand has been shifted completely to a terminal coordination site on Re(2), Re(2)-C(1) = 2.22 Å, see Figure 4.6.

The hydride ligand remains as a bridge across the two Re atoms, but it has shifted to the other side of the Re-Re bond and lies *cis* to the phenyl ligand. The Re-Re bond has lengthened to 3.23 Å. The formation of the C-H bond proceeds by a shift of the bridging hydride ligand from the metal-metal bond to the carbon atom C(1). This shift passes over a low energy transition state **TS2**, -4.30 kcal/mol and would be virtually spontaneous in a solution at room temperature, i.e. the addition of the second NCMe ligand to the complex is not needed to drive the formation of the CH bond at this stage of the process. In **TS2**, the C(1)-H distance is 1.61 Å and the Re-Re bond has shortened to 3.08 Å as the hydride moves toward C(1). The product, **P**, $Re_2(CO)_8(NCMe)(\eta^2\text{-}C_6H_6)$, contains a η^2- CH bound benzene ligand terminally coordinated to Re(2), C(1)-H

= 1.15 Å, Re(2)-C(1) = 2.49 Å, Re(2)-H = 1.98 Å and Re(1)-Re(2) = 3.03 Å. The Re(1)···H distance, 2.94 Å, is a nonbonding interaction in this species, see Figure 4.6. An energy profile of the transformations along the reaction coordinate is shown in Figure 4.7.

Views of the molecular orbitals that show transformations in the bonding in the course of the C-H bond forming process are shown in Figure 4.8. The symmetric nature of the Re - C bonding to the phenyl ring at the beginning is nicely represented by the HOMO-2 shown in Figure 4.5. As the NCMe ligand begins to donate electron density to Re(1), the Re-C bonding weakens as **TS1** is traversed, see the **TS1**-HOMO-4, Figure 4.8. The HOMO-12 in **I1** shows the formation of an C(1)-H-Re(1) overlap which is the predecessor to the C-H bond shown by the HOMO-15 in **TS2**. Finally, the C-H bond is fully formed as shown in the HOMO-10 in the η^2-benzene product complex **P**. Facile displacement of the benzene ligand by a second equivalent NCMe (not shown in Figure 4.8) would complete the transformation as it occurs in solution.

Although the C-H bond forming process takes place predominantly at one metal atom only, Re(2), the second Re atom is not completely a spectator, as the H atom is delivered to the carbon atom C(1) from the Re-Re bond. It can be seen that the C-H bond forming process upon the addition of NCMe to **4.2**, at least in the final stages, strongly resembles that of the unsymmetric, planar reductive

elimination of H_2 (2) (Scheme 4.1) that was predicted by Trinquier and Hoffmann 30 years ago.[11]

Despite the fact that it has not yet been observed in this system, it should not go unnoticed that the microscopic reverse of the **4.2** to **P** reaction is tantamount to a C-H bond activation process[2] and in this process the cleavage of the C-H bond would be facilitated by the second metal atom when the hydrogen atom is "inserted" into the Re-Re bond via the **TS2** - **I1** rearrangement. Furthermore, these results also may have important implications for C-H bond cleavage processes at multinuclear metal sites on metal nanoparticles[6] and metal surfaces[7] as the complete sequence takes place with only small changes in the metal-metal bond distances.

CH BOND CLEAVAGE REACTIONS

The reaction of compound **4.2** with N,N-diethylaniline yielded the interesting new compound, $Re_2(CO)_8(\mu\text{-}H)[\mu\text{-}(C_2H_5)_2NC_6H_4]$, **4.3** in 61% yield. Compound **4.3** was characterized by a single-crystal X-ray diffraction analysis. An ORTEP diagram of the molecular structure of **4.3** is shown in Figure 4.3. Similarly, compound **4.3** like **4.1** and **4.2** also has only 32 valence electrons and is also electronically unsaturated by the amount of two electrons. The Re–Re bond distance is only slightly shorter than that in **4.2**, Re(1)–Re(2)=2.9720(4) Å and the N,N-diethylaniline and hydrido ligands bridge the Re–Re bond

asymmetrically in the solid state, Re(1)–H(1)=1.77(4)Å, Re(2)–H(1)=1.86(4)Å, Re(1)–C(1)=2.338(5)Å and Re(2)–C(1)=2.269(4)Å.

A proposed mechanism for the formation of **4.3** from **4.2** is given in scheme 4.2. The initiation step involves the coordination of the N,N-diethylaniline ligand to a rhenium atom (**I1-N**). Subsequently, the phenyl ligand shifts to a terminal coordination site on the opposing rhenium atom and even though the hydrido ligand still remains as a bridge across the rhenium atoms, it now lies *cis* to the phenyl ligand (**I2-N**). In **I3-N**, the bridging hydride moves closer to the phenyl carbon atom coordinated to a rhenium atom. A C-H bond is formed and a η^2-CH bound benzene ligand terminally coordinated to a rhenium atom is observed in **I4-N**. The reductive elimination of benzene followed by activation of a C-H bond on N,N-diethylaniline results in an η^2-CH bound N,N-diethylaniline ligand terminally coordinated to a rhenium atom **I5-N**. The phenyl carbon-hydrogen bond is broken and a bridging hydride between the rhenium atoms is formed (**I6-N**). To form product **4.3**, an N,N-diethylaniline ligand dissociates from the rhenium atom.

An alternative mechanism for the transformation of **4.3** from **4.2** is given in scheme 4.3. The initiation step involves the formation of the N,N-diethylaniline carbanion at the para position. Since the carbanion is a nucleophile, it will attack a rhenium atom (**I1-C**). An η^2-CH bound N,N-diethylaniline is formed with the coordination of a cis –phenyl and a bridging hydrido ligand (**I2-C**).The formation

of an η^2-CH bound benzene ligand and the η^2-CH bound N,N-diethylaniline carbanion is then observed in **I3-C**. To form **4.3**, benzene is reductively eliminated.

Interestingly, when compound **4.2** was heated in deuterated benzene at 60 °C for 11 h, $Re_2(CO)_8(\mu\text{-}D)(\mu\text{-}C_6D_5)$ was formed quantitatively as determined by mass spectrometric analysis. A C-D bond on deuterated benzene was activated under these conditions. An η^2-$(\mu\text{-}C_6D_5)(\mu\text{-}D)$ intermediate is formed at the dirhenium site. The absence of $Re_2(CO)_8(\mu\text{-}H)(\mu\text{-}C_6D_5)$ and $Re_2(CO)_8(\mu\text{-}D)(\mu\text{-}C_6H_5)$ indicates that the reductive elimination of C_6H_6 is a facile reaction and $Re_2(CO)_8(\mu\text{-}D)(\mu\text{-}C_6D_5)$ is energetically more stable than **4.2**.

Conclusion

Reaction of $Re_2(CO)_8[\mu\text{-}\eta^2\text{-}C(H)=C(H)Bu^n](\mu\text{-}H)$ with $Au(PPh_3)Ph$ yielded compound **4.1**, $Re_2(CO)_8(\mu\text{-}AuPPh_3)(\mu\text{-}Ph)$, an electronically unsaturated metal complex. By further reacting **4.1** with Ph_3SnH, $Re_2(CO)_8(\mu\text{-}H)(\mu\text{-}Ph)$, **4.2** another unsaturated dirhenium complex was formed by replacing the $AuPPh_3$ group in **4.1** with a bridging hydrido ligand. Upon addition of NCMe at 25 °C, compound **4.2** reductively eliminated benzene. Heating compound **4.2** at 60 °C in deuterated benzene yielded a fully deuterated $Re_2(CO)_8(\mu\text{-}D)(\mu\text{-}C_6D_5)$. The reaction of **4.2** with N,N-diethylaniline yielded $Re_2(CO)_8(\mu\text{-}H)[\mu\text{-}(C_2H_5)_2NC_6H_4]$, **4.3**. The formation of **4.3** indicates the activation of a C-H bond on the phenyl

ring of N,N-diethylaniline. The electronic structure of **4.1** and **4,2** were also investigated by DFT computational analyses.

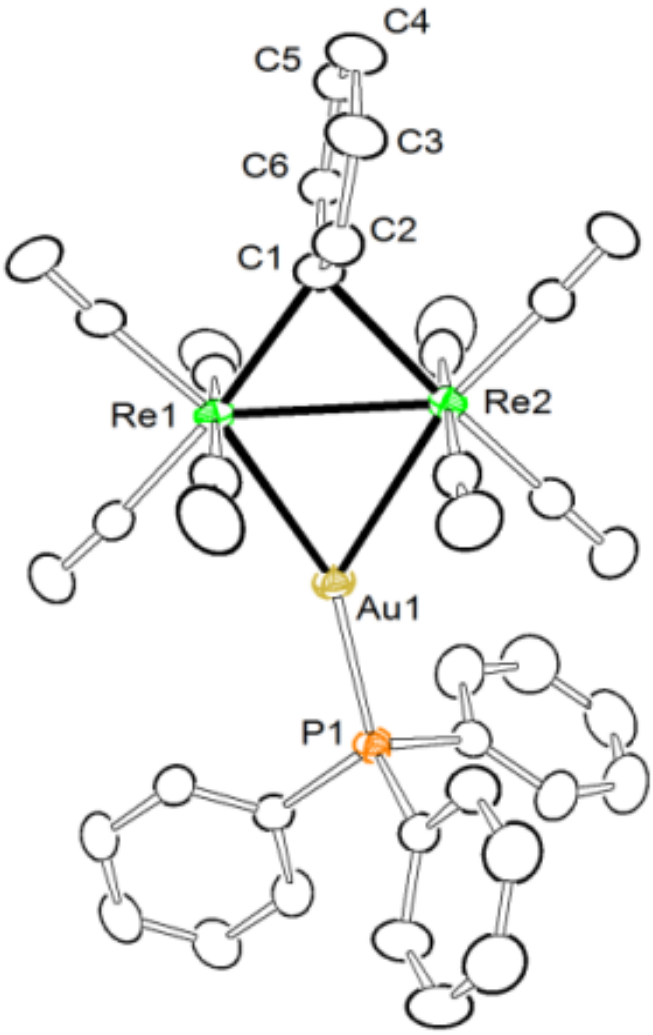

Figure 4.1. An ORTEP diagram of the molecular structure of $Re_2(CO)_8(\mu\text{-}AuPPh_3)(\mu\text{-}Ph)$, **4.1** showing 30% thermal ellipsoid probability.

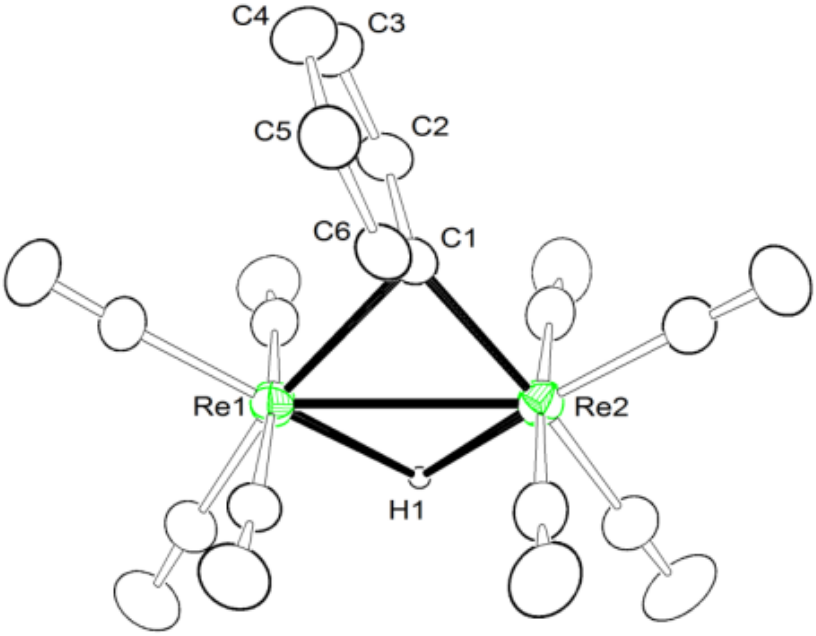

Figure 4.2. An ORTEP diagram of the molecular structure of $Re_2(CO)_8(\mu\text{-}H)(\mu\text{-}Ph)$, **4.2** showing 30% thermal ellipsoid probability.

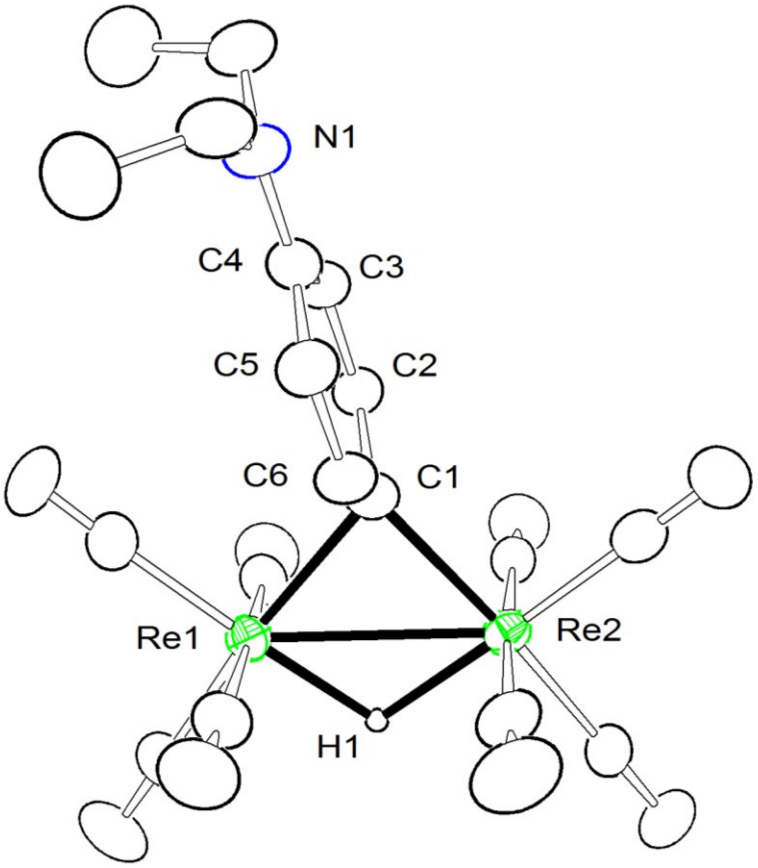

Figure 4.3. An ORTEP diagram of the molecular structure of $Re_2(CO)_8(\mu\text{-}H)[\mu\text{-}(C_2H_5)_2NC_6H_4]$, **4.3** showing 30% thermal ellipsoid probability.

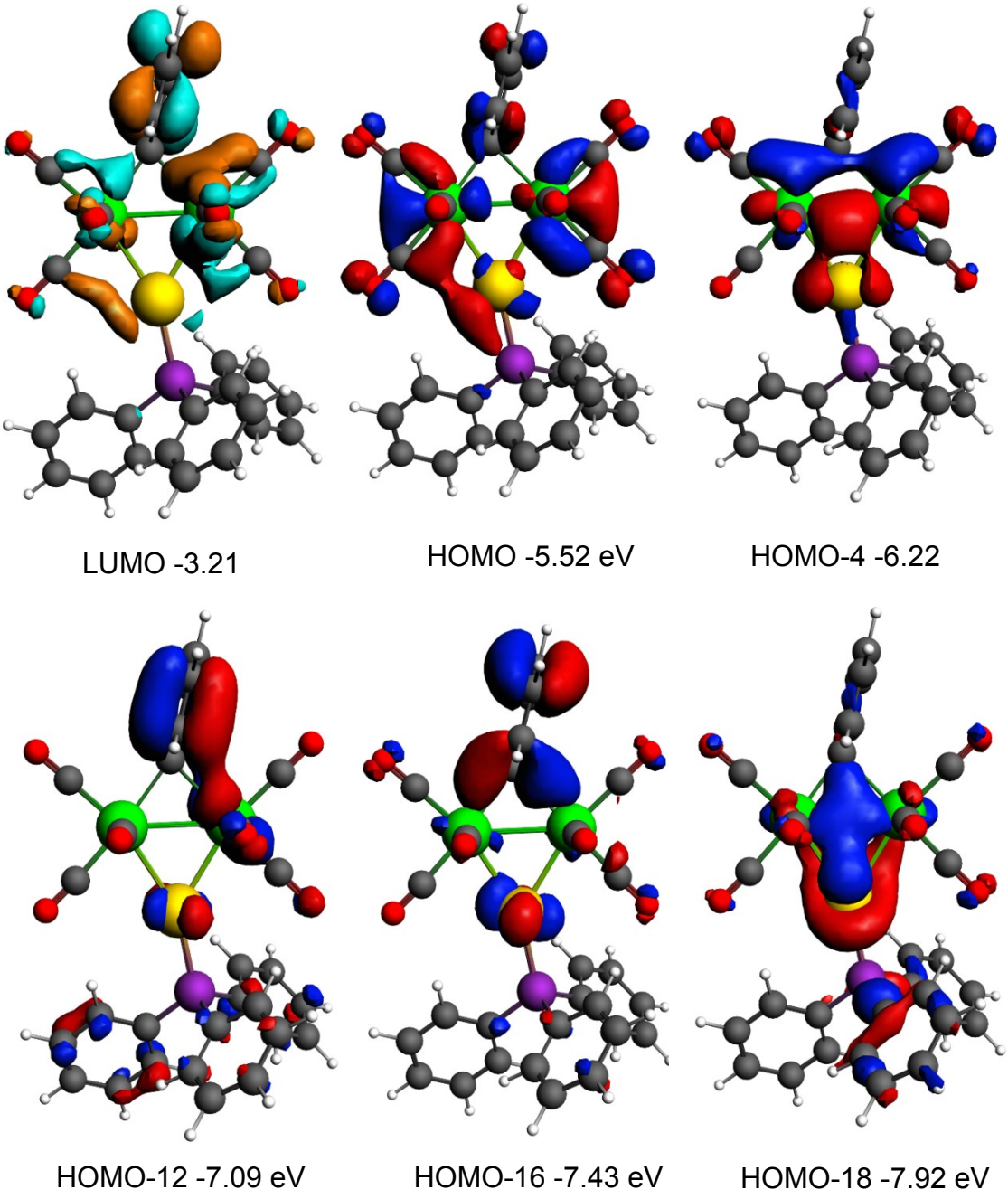

Figure 4.4. Calculated Energies for the LUMO, HOMO, HOMO-4, HOMO-12, HOMO-16 and HOMO-18 of **4.1**. The rhenium atoms are colored green.

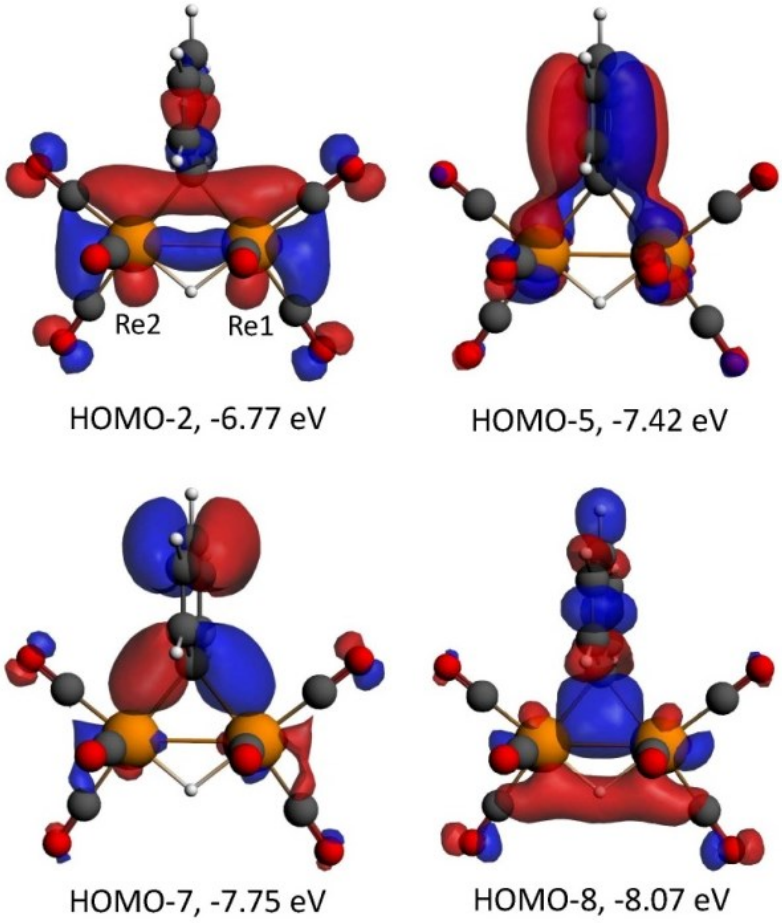

Figure 4.5. Selected molecular orbitals (MOs) with calculated energies in eV for compound **4.2** that show the nature of the bonding of the phenyl and hydrido ligands to the two rhenium atoms. The rhenium atoms are colored orange

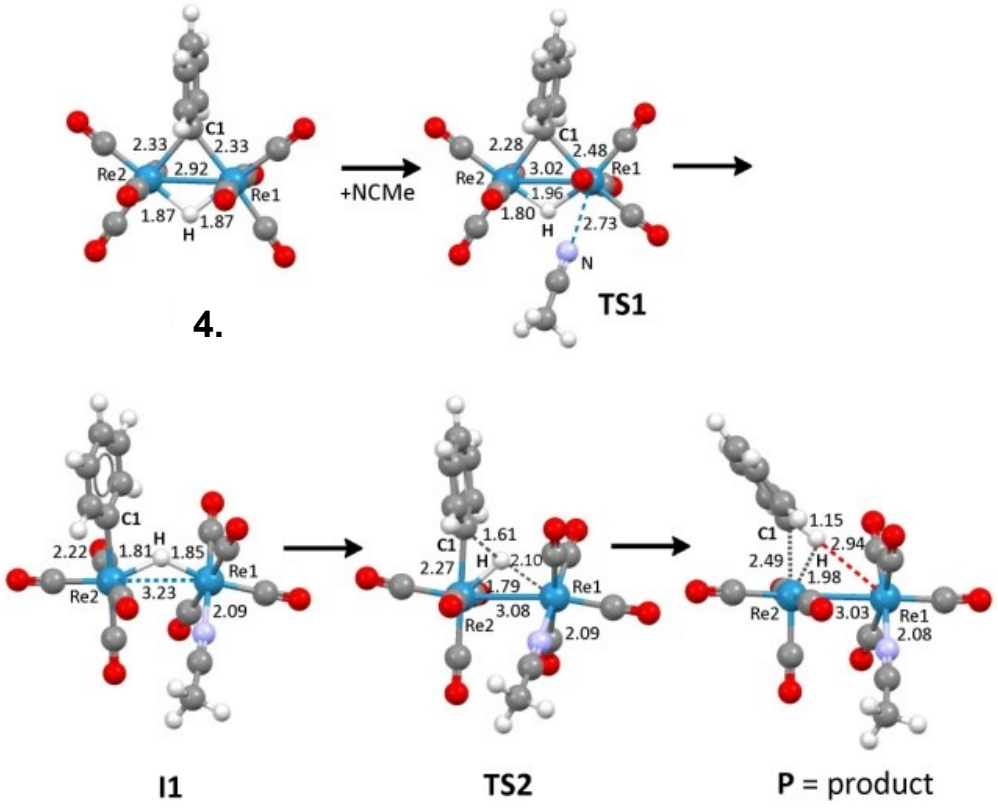

Figure 4.6. Structures of intermediates and transition states with selected interatomic distances that are traversed in the course of the NCMe-induced reductive elimination of benzene from **4.2**.

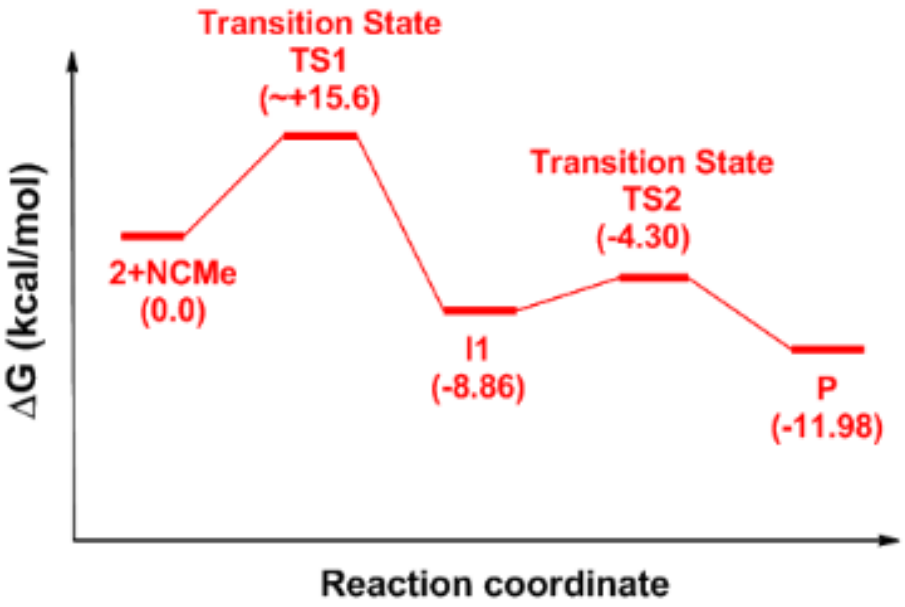

Figure 4.7. An energy profile of the transformations **4.2** along the reaction coordinate during the addition of NCMe. The energies in kcal/mol are given in parentheses.

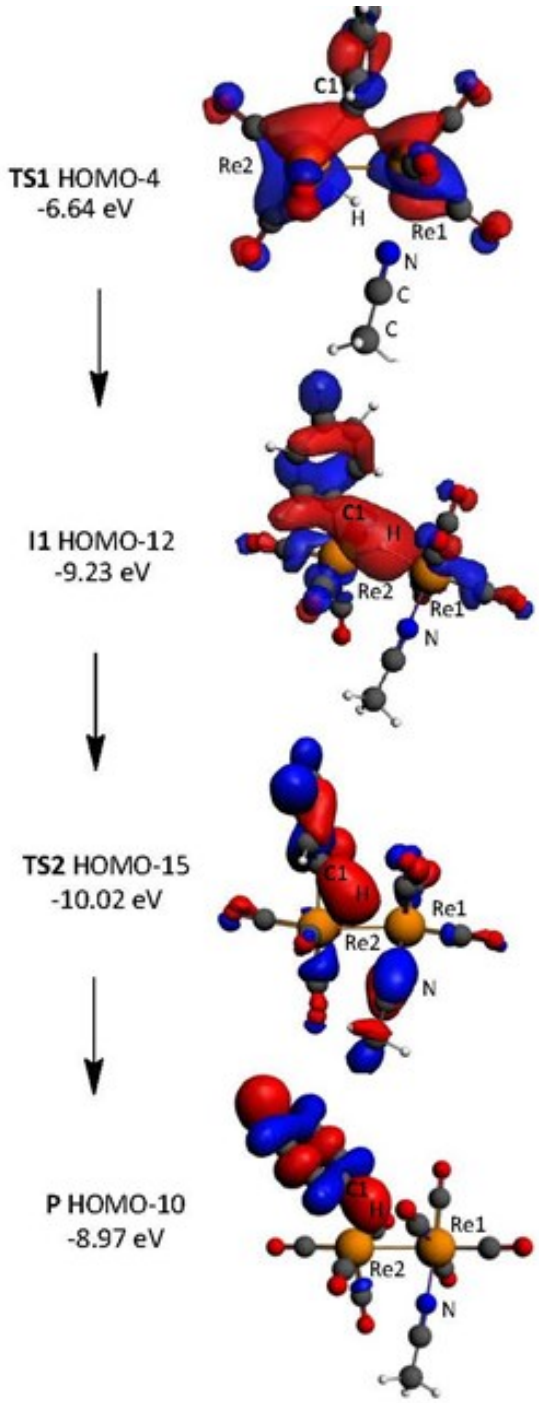

Figure 4.8. Selected molecular orbitals for **4.2** that emphasize the nature of the Re-C, Re-H and C-H bonding interactions in the course of the formation of the C-H bond during the reductive elimination process

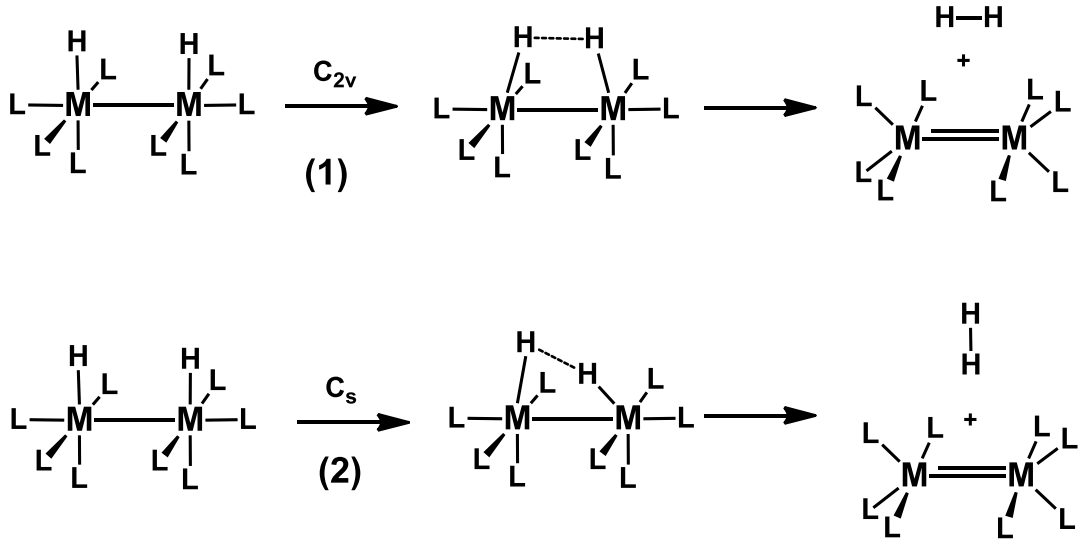

Scheme 4.1. Intramolecular dinuclear 1,2-reductive elimination.

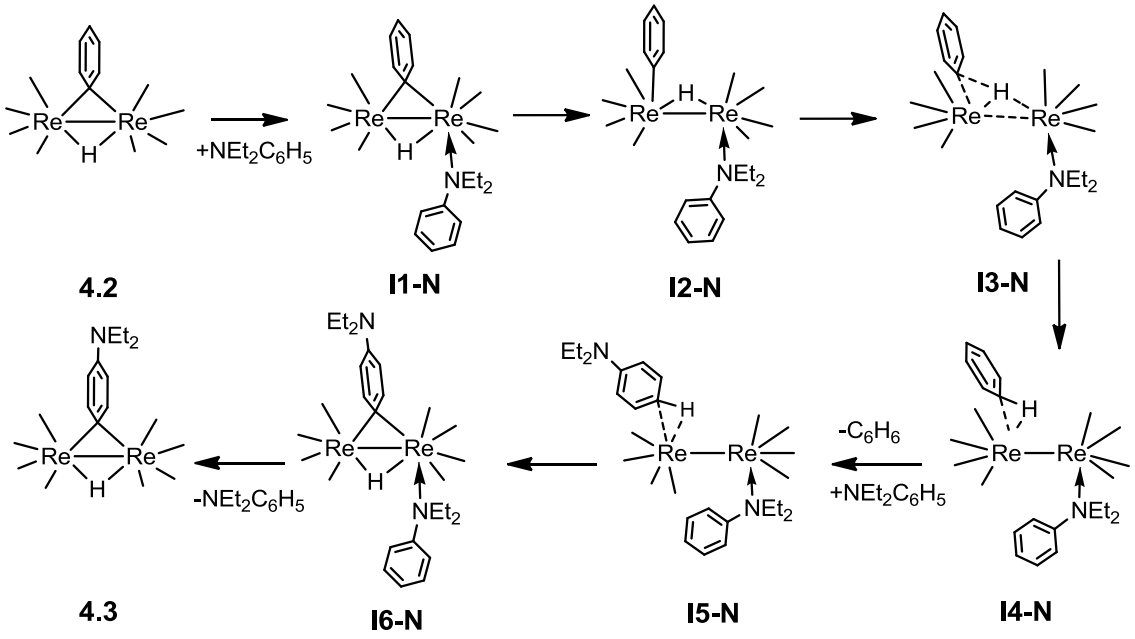

Scheme 4.2. First proposed mechanism for formation of compound **4.3**.

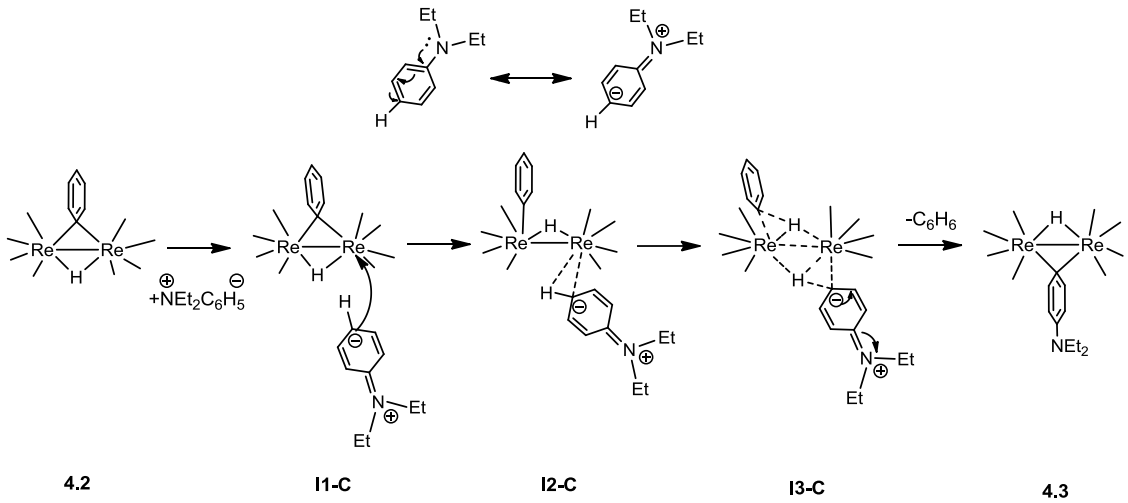

Scheme 4.3. Second proposed mechanism for formation of compound **4.3**.

Table 4.1. Crystallographic data for **4.1**, **4.2 and 4.3.**[a]

Compound	**4.1**	**4.2**	**4.3**
Empirical formula	$AuRe_2PO_8C_{32}H_{20}$	$Re_2O_8C_{14}H_6$	$Re_2O_8NC_{18}H_{15}$
Formula weight	1132.82	674.59	745.71
Crystal system	Monoclinic	Orthorhombic	Monoclinic
Lattice parameters			
a (Å)	14.401(2)	8.8587(4)	12.4057(14)
b (Å)	24.572(3)	12.7536(5)	11.9489(14)
c (Å)	9.1438(13)	14.7467(6)	14.8370(17)
α (deg)	90.00	90.00	90.00
β (deg)	95.440(3)	90.00	97.005(2)
γ (deg)	90.00	90.00	90.00
V ($Å^3$)	3221.0(8)	1666.09(12)	2182.9(4)
Space group	$P2_1/c$	$P2_12_12_1$	$P2_1/n$
Z value	4	4	4
ρ_{calc} (g/cm^3)	2.336	2.689	2.269
μ (Mo Kα) (mm^{-1})	12.139	14.555	11.122
Temperature (K)	294(2)	294(2)	294(2)
$2\theta_{max}(°)$	56.48	56.56	56.22
No. Obs. (I>2σ(I))	5685	2958	3204
No. Parameters	397	221	268
Goodness of fit (GOF)	1.072	1.051	1.044
Max. shift in cycle	0.002	0.001	0.002
Residuals*: R1; wR2	0.0208; 0.0542	0.0183; 0.0450	0.0214; 0.0470
Absorption Correction, Max/min	Multi-Scan 1.000/0.546	Multi-Scan 1.000/0.263	Multi-Scan 1.000/0.659
Largest peak in Final Diff. Map ($e^-/ Å^3$)	0.526	0.357	1.017

[a] $R = \Sigma_{hkl}(\,||F_{obs}| - |F_{calc}||\,)/\Sigma_{hkl}|F_{obs}|$; $R_w = [\Sigma_{hkl} w(|F_{obs}| - |F_{calc}|)^2/\Sigma_{hkl} w F^2_{obs}]^{1/2}$; $w = 1/\sigma^2(F_{obs})$; GOF = $[\Sigma_{hkl} w(|F_{obs}| - |F_{calc}|)^2/(n_{data} - n_{vari})]^{1/2}$.

Table 4.2. Selected intramolecular angles and bond distances for **4.1**[a]

Atom	Atom	Distance(Å)	Atom	Atom	Atom	Angle(°)
Re1	Re2	2.9690(4)	Re1	C1	Re2	78.55(13)
Au1	Re1	2.7567(3)	Re1	Au1	Re2	64.481(10)
Au1	Re2	2.8080(4)				
Re1	C1	2.292(5)				
Re2	C1	2.396(5)				

[a] Estimated standard deviations in the least significant figure are given in parentheses.

Table 4.3. Selected intramolecular angles and bond distances for **4.2**[a]

Atom	Atom	Distance(Å)	Atom	Atom	Atom	Angle(°)
Re1	Re2	2.9924(3)	Re2	H1	Re1	87.9(2)
Re1	H1	2.23(10)	Re2	C1	Re1	79.80(17)
Re2	H1	2.08(10)				
Re1	C1	2.397(5)				
Re2	C1	2.266(5)				

[a] Estimated standard deviations in the least significant figure are given in parentheses.

Table 4.4. Selected intramolecular angles and bond distances for **4.3**[a]

Atom	Atom	Distance(Å)	Atom	Atom	Atom	Angle(°)
Re1	Re2	2.9720(4)	Re1	C1	Re2	80.34(14)
Re1	H1	1.77(4)	Re1	H1	Re2	110.37(15)
Re2	H2	1.86(4)				
Re1	C1	2.338(5)				
Re2	C1	2.269(4)				

[a] Estimated standard deviations in the least significant figure are given in parentheses.

Table 4.5. Cartesian Coordinates for geometry optimized of **4.1**

Atom	x	y	z	Atom	x	y	z
Au	2.3303	1.5054	-0.0678	H	7.2042	1.1750	1.3170
Re	0.0091	3.0010	-0.0154	C	5.2100	0.5939	-1.7315
Re	-0.0587	0.0149	-0.0420	C	6.2489	1.2782	-2.3678
P	4.5976	1.0688	-0.0874	H	6.7473	2.1082	-1.8584
C	-1.7826	1.6415	0.0849	C	6.6438	0.9063	-3.6519
C	-2.5963	1.4570	-1.0684	H	7.4537	1.4493	-4.1468
H	-2.1585	1.6161	-2.0589	C	6.0097	-0.1488	-4.3020
C	-3.9372	1.1017	-0.9895	H	6.3188	-0.4356	-5.3108
H	-4.5227	0.9764	-1.9047	C	4.9751	-0.8367	-3.6672
C	-4.5310	0.9025	0.2557	H	4.4720	-1.6641	-4.1748
H	-5.5856	0.6197	0.3211	C	4.5692	-0.4641	-2.3909
C	-3.7773	1.0621	1.4171	H	3.7507	-0.9988	-1.8971
H	-4.2368	0.9054	2.3970	C	5.0409	-0.3158	1.0017
C	-2.4372	1.4198	1.3295	C	6.0191	-1.2544	0.6605
H	-1.8730	1.5506	2.2583	H	6.5257	-1.1855	-0.3070
C	-1.2750	4.4330	0.0658	C	6.3333	-2.2840	1.5447
C	0.2533	2.9872	1.9470	H	7.0936	-3.0204	1.2703
C	1.4410	4.3090	-0.1025	C	5.6788	-2.3780	2.7708
C	0.0252	3.0109	-1.9932	H	5.9237	-3.1904	3.4604
C	0.2316	-0.0347	1.9159	C	4.7012	-1.4447	3.1132
C	-1.3588	-1.3918	0.0272	H	4.1764	-1.5222	4.0691
C	1.3227	-1.2998	-0.1708	C	4.3783	-0.4198	2.2303
C	-0.0490	0.0192	-2.0230	H	3.5949	0.3028	2.4849
C	5.6789	2.4324	0.4370	O	-2.0447	5.2952	0.1187
C	5.2797	3.7445	0.1615	O	0.4433	3.0472	3.0837
H	4.3144	3.9310	-0.3196	O	2.2383	5.1517	-0.1613
C	6.0984	4.8128	0.5169	O	0.0817	3.0937	-3.1426
H	5.7751	5.8348	0.3021	O	0.4691	-0.1540	3.0383
C	7.3131	4.5774	1.1581	O	-2.1383	-2.2468	0.0745
H	7.9510	5.4173	1.4468	O	2.1333	-2.1275	-0.2670
C	7.7092	3.2716	1.4437	O	0.0184	-0.0758	-3.1696
H	8.6576	3.0853	1.9553				
C	6.8970	2.1993	1.0845				

Table 4.6. Cartesian Coordinates for geometry optimized of **4.2**

Atom	x	y	z	Atom	x	y	z
C	-0.588370	5.214415	1.294227	O	5.789304	0.599309	1.442274
H	-1.139916	6.157584	1.345642	Re	0.483989	0.485140	0.848784
H	-0.746092	4.827912	3.413812	O	0.038168	-0.121085	3.887171
C	-0.368626	4.471618	2.451482	C	0.294492	-1.414504	0.602286
C	0.331789	3.275265	2.381916	O	-2.553786	0.946780	0.559960
H	0.962022	3.223148	-0.964161	C	2.884594	1.633950	3.256389
H	-0.275035	5.335300	-0.839784	C	3.319863	2.106225	-0.648580
O	0.197714	-2.558313	0.456012	C	3.730610	3.666521	1.591945
Re	2.999951	1.904048	1.296650	C	4.746461	1.098055	1.390487
H	2.318573	0.189120	1.020774	C	-1.418165	0.760334	0.666621
O	3.601306	2.221787	-1.758583	C	0.234572	0.151407	2.786363
H	0.489055	2.713771	3.307824	C	0.678122	0.614026	-1.119275
O	2.912442	1.477499	4.396267	C	0.844484	2.764504	1.160664
O	4.147299	4.729874	1.768970	C	0.594328	3.558046	0.010502
O	0.738961	0.607506	-2.268562	C	-0.105110	4.755457	0.071485

Table 4.7. Cartesian Coordinates for geometry optimized of **TS1**

Atom	x	y	z	Atom	x	y	z
C	-0.356731	4.742320	1.207280	C	0.847191	-2.010610	1.514830
H	-0.824435	5.720230	1.062320	O	-2.233220	0.061881	0.960542
H	-0.962429	4.578650	3.273950	C	2.573640	1.878890	4.235630
C	-0.432605	4.105150	2.442440	C	3.878750	1.494480	0.506295
C	0.162706	2.862870	2.621970	C	3.358290	3.531660	2.210240
H	1.441280	2.433890	-0.501964	C	4.944770	1.538220	2.948800
H	0.388320	4.619480	-0.817062	C	-1.100710	0.000074	1.184090
O	0.908591	-3.168880	1.520100	C	0.466592	-0.210520	3.480600
Re	3.141100	1.656160	2.336780	C	1.206070	-0.123873	-0.400623
H	2.596790	-0.117179	1.716270	C	0.859656	2.194590	1.582700
O	4.365320	1.424020	-0.533827	C	0.915446	2.886920	0.344445
H	0.069663	2.383130	3.601600	C	0.321718	4.127090	0.157320
O	2.363520	2.082520	5.348260	H	3.731380	-3.714830	4.405680
O	3.443630	4.679940	2.067630	N	3.639090	-0.646177	3.723270
O	1.422190	-0.227072	-1.527410	C	4.087730	-2.866180	5.009230
O	6.042870	1.499430	3.319910	H	5.163640	-2.991790	5.202540
Re	0.807953	-0.079206	1.540290	H	3.551650	-2.864810	5.970680
O	0.249351	-0.373142	4.602200	C	3.846010	-1.626990	4.310070

Table 4.8. Cartesian Coordinates for geometry optimized of **I1**

Atom	x	y	z	Atom	x	y	z
C	-0.970124	4.774229	1.429222	C	1.721183	-1.702125	1.688280
H	-1.397524	5.780531	1.403458	O	-1.852649	-0.729794	0.842618
H	-2.323045	4.051317	2.948371	C	3.637897	2.503952	3.555626
C	-1.483814	3.808828	2.288789	C	4.341706	-0.415007	0.944901
C	-0.935899	2.527327	2.317068	C	4.209257	2.337761	0.857526
H	1.474937	2.935542	-0.033445	C	5.923788	1.161443	2.646068
H	0.512234	5.177753	-0.088660	C	-0.763537	-0.446995	1.105738
O	2.083286	-2.800280	1.816162	C	0.620451	0.060218	3.491793
Re	4.031679	1.034882	2.275046	C	1.493116	0.290012	-0.353970
H	2.221033	1.366796	2.079643	C	0.143939	2.157839	1.497874
O	4.583530	-1.216229	0.157879	C	0.637041	3.152824	0.637912
H	-1.378518	1.798431	3.004992	C	0.094833	4.436418	0.600046
O	3.424604	3.372645	4.274630	H	2.309066	-1.895976	6.111425
O	4.328779	3.114797	0.013299	N	3.742144	-0.382407	3.780308
O	1.766298	0.388649	-1.468205	C	3.236855	-2.174090	5.585774
O	7.054452	1.273595	2.860753	H	3.087644	-3.147794	5.091968
Re	1.020536	0.115729	1.566119	H	4.055389	-2.261477	6.316970
O	0.418108	0.004801	4.628653	C	3.543022	-1.177885	4.597166

Table 4.9. Cartesian Coordinates for geometry optimized of **TS2**

Atom	x	y	z	Atom	x	y	z
C	-0.748169	4.888410	1.510850	C	1.589120	-1.744690	1.637390
H	-1.184040	5.890570	1.473400	O	-1.917090	-0.335303	0.741722
H	-1.328890	4.528030	3.558830	C	3.147270	2.509680	3.717090
C	-0.828448	4.127270	2.672510	C	4.261490	-0.275875	1.119710
C	-0.271053	2.852100	2.719780	C	3.920210	2.482750	1.041530
H	0.978933	2.711560	-0.435104	C	5.624300	1.458090	2.908600
H	-0.013411	4.946700	-0.519069	C	-0.809214	-0.211103	1.046520
O	1.920420	-2.853080	1.732890	C	0.613942	0.004334	3.488670
Re	3.787630	1.143510	2.430370	C	1.597780	0.217858	-0.326928
H	1.813030	1.667020	1.963160	C	0.371781	2.288890	1.606110
O	4.588060	-1.074760	0.357214	C	0.460662	3.085950	0.452644
H	-0.352197	2.289750	3.654930	C	-0.096507	4.360580	0.400710
O	2.794530	3.310680	4.464890	H	2.401390	-1.922300	6.316740
O	4.021250	3.283820	0.215554	N	3.599950	-0.321130	3.906720
O	1.940900	0.241378	-1.427530	C	3.314810	-2.137090	5.738880
O	6.731690	1.672040	3.171370	H	3.206180	-3.123910	5.260960
Re	1.020540	0.115729	1.566120	H	4.177110	-2.163290	6.423310
O	0.410769	-0.112854	4.621920	C	3.495100	-1.128310	4.730910

Table 4.10. Cartesian Coordinates for geometry optimized of **P**

Atom	x	y	z	Atom	x	y	z
C	-1.593405	4.406584	0.931697	O	6.851182	1.153753	3.157313
H	-2.392527	5.123169	0.722928	Re	1.024585	0.152266	1.605731
H	-2.036306	4.303919	3.043372	O	0.637095	0.044623	4.704230
C	-1.398356	3.944722	2.231852	C	1.350997	-1.713146	1.703597
C	-0.384026	3.035189	2.500387	O	-1.939426	-0.288871	0.888442
H	0.925375	2.745603	-0.640123	C	3.191104	1.952977	3.692721
H	-0.900484	4.360548	-1.113418	C	4.333640	-0.721256	1.025578
H	1.434594	2.087523	1.725053	C	3.997380	2.014741	1.044581
H	-0.210736	2.687337	3.521751	C	5.742712	0.938504	2.890076
C	0.422018	2.567023	1.456821	C	-0.825789	-0.103685	1.149790
C	0.254766	3.066145	0.160930	C	0.764901	0.133190	3.555619
C	-0.761522	3.976241	-0.099681	C	1.696635	0.166965	-0.255449
O	1.550829	-2.855038	1.793475	H	2.318246	-2.647055	6.012043
Re	3.911551	0.645377	2.399249	N	3.659229	-0.887296	3.785965
O	4.589198	-1.505967	0.219800	C	3.244883	-2.839817	5.447757
O	2.759096	2.731811	4.430006	H	3.123525	-3.778094	4.883010
O	4.042877	2.832642	0.224148	H	4.079207	-2.953859	6.157613
O	2.100856	0.140482	-1.337144	C	3.493027	-1.756038	4.536190

REFERENCES

1) Olah, G. A.; Molnar, A. In *Hydrocarbon Chemistry*; Wiley, New York, **1995**.

2) (a) Crabtree, R. H. *J. Organomet.Chem.* **2004**, *689*, 4083-4091. (b) Vastine, B. A.; Hall, M. B. *Coord. Chem. Rev.* **2009**, *253*, 1202-1218. (c) Hall, C.; Perutz, R. N. *Chem.Rev.* **1996**, *96*, 3125-3146. (d) Labinger, J. A.; Bercaw, J. E. *Nature* **2002**, *417*, 507-514.

3) Kubas, G. J. In Metal Dihydrogen and Sigma Bond Complexes; Kluwer Academic, New York, **2002**.

4) (a) Jones, W. D. *Acc. Chem. Res.* **2003**, *36*, 140-246. (b) Parkin, G.; Bercaw, J. E. *Organometallics* **1989**, *8*, 1172-1179. (c) Gould, G. L.; Heinekey, D. M. *J. Am. Chem. Soc.* **1989**, *111*, 5502-5504.

5) Ritleng, V.; Checuti, M. *Chem. Rev.* **2007**, *107*, 797-858.

6) (a)Vines, F.; Lykhach, Y.; Staudt, T.; Lorenz, M. P. A.; Papp, C.; Steinrück, H.-P.; Libuda, J.; Neyman, K. M.; Görling, A. *Chem. Eur. J.* **2010**, *16*, 6530-6539. (b) Chin, Y.-H.; Buda, C.; Neurock, M.; Iglesia, E. *J. Catal.* **2011**, *283*, 10-24. (c) Chin, Y.-H.; Buda, C.; Neurock, M.; Iglesia, E. *J. Am. Chem. Soc.* **2013**, *135*, 15425-15442.

7) Saillard, J.-Y.; Hoffmann, R. *J. Am. Chem. Soc.* **1984**, *106*, 2006-2026.

8) Reference (1), Ch. 11. Reduction-Hydrogenation.

9) Reference (2), Ch. 2. Hydrocarbon from Petroleum and Natural Gas

10) Brady, R. C.; Pettit, R. *J. Am. Chem. Soc.* **1980**, *102*, 6181-6182.

11) Trinquies, G.; Hoffmann, R. *Organometallics* **1984**, *3*, 370-380.

12) Nubel, P. O.; Brown, T.L., *J. Am. Chem. Soc.* **1984**, *106*, 644 – 652.

13) Partyka, D.V.; Zeller, M.; Hunter, A.D.; Gray, T.G. *Angew. Chem. Int. Ed.* **2006**, *45*, 8188-8191.

14) SAINT+, version 6.2a, Bruker Analytical X-ray Systems, Inc., Madison, WI, 2001.

15) Sheldrick, G. M. SHELXTL, version 6.1, Bruker Analytical X-ray Systems, Inc., Madison, WI, 1997.

16) (a) Velde, G. te; Bickelhaupt, F.M.; van Gisbergen, S.J.A.; Fonseca Guerra, C; Baerends, E.J.; Snijders, J.G.; Ziegler, T. *J. Comp. Chem.* **2001**, *22*, 931-967. (b) Fonseca Guerra, C.; Snijders, J.G.; Velde, G. te; Baerends, E.J. *Theoret. Chem. Accts.* **1998**, *99*, 391-403. (c) Perdew, J.P.; Ruzsinszky, A.; Csonka, G.I.; Vydrov, O.A.; Scuseria, G.E.; Constantin, L.A.; Zhou, X.; Burke, K. *Phys. Rev. Lett.* **2008**, *100*, 136406. (d) Perdew, J.P.; Ruzsinsky, A.; Csonka, G.I.; Vydrov, O.A.; Scuseria, G.E.; Constantin, L.A.; Zhou, X.; Burke,K. *Phys. Rev. Lett,* **2009**, *102*, 039902. (e) van Lenthe, E.; Baerends, E.J.; Snijders, J.G. *J. Chem. Phys.* **1993**, *99*, 4597. (f) van Lenthe, E.; Baerends, E.J.; Snijders, J.G.; *J. Chem. Phys.* **1994**, *101*, 9783. (g) van Lenthe, E.; Ehlers, A.E.; Baerends ,E.J. *J. Chem. Phys.* **1999**, *110*, 8943.

17) Adams, R. D.; Kan, Y.; Rassolov, V.; Zhang, Q. *Organometallics* **2013**, *730*, 20 - 31.

18) Csonca, G.I.; Ruzisinsky, A.; Perdew, J.P.; Grimme, S. *J. Chem. Theor. Comp.* **2008**, *4*, 888-891

19) (a) Koitz, R.; Soini, T.M.; Genest, A.; Trickey, S.B.; Rosch, N. *J. Chem. Phys.* **2008**, *137*, 034102. (b) Johansson, M.P.; Lechtken, A.; Schooss, D.; Kappes, M.M.; Furche, F. *Phys. Rev. A* **2008**, *77*, 035202.

20) Adams, R. D.; Wong, Y. O.; Zhang, Q. *Organometallics* **2013**, *32*, 7540-7546.

21) *ADF, SCM, Theoretical Chemistry*; Vrije Universiteit: Amsterdam, The Netherlands. *http://www.scm.com.*

22) Bennett, M.J.; Graham, W.A.G,; Hoyano, J.K.; Hutcheon, W.L., *J. Am. Chem. Soc.* **1972**, *94*, 6232-6233. (b) Masciocchi, N.; Sironi, A.; D'Alfonso, D. *J. Am. Chem. Soc.* **1990**, *112*, 9395-9397.

CHAPTER 5

SYNTHESIS AND STRUCTURE OF A NOVEL GOLD TIN METAL COMPLEX

Introduction

Recently, gold nanoparticles supported on metal oxides have been reported to exhibit surprisingly high catalytic activity for low-temperature CO oxidation.[1,2] A recent example includes an Au/SnO_2 catalyst which displayed activity comparable to Au/TiO_2, one of the most active catalytic gold oxidation systems.[3] Among the synthetic studies on tin derivatives of transition metals that can be found in the chemical literature, examples that involve group 11 metals especially gold are exceedingly rare. These examples include halide[4], triaminometalate[5] and dodecarborate[6] ligands on tin. In the previous chapter, it was shown that compound **4.1** reacted with Ph_3SnH to yield a new Au–Sn compound. The characterization of this new Au–Sn complex including an improved synthesis is described in this chapter. This compound is the first example of an X-ray crystallographic characterization of a gold-tin cluster complex having phenyl substituents.

Experimental Details

General Data. Reagent grade solvents were dried by the standard procedures and were freshly distilled prior to use. Infrared spectra were recorded on a Thermo Nicolet Avatar 360 FT-IR spectrophotometer. ^1H NMR and $^{31}P\{^1H\}$ NMR

were recorded on a Varian Mercury 400 spectrometer operating at 400.1 and 161.9 MHz respectively. $^{31}P\{^{1}H\}$ NMR spectra were referenced externally by using 85% *ortho*-H_3PO_4. Solid state ^{119}Sn CP-MAS spectra were collected on a Bruker Avance III-HD 500 MHz spectrometer fitted with a 1.9 mm MAS probe. The spectra was collected at ambient temperature with a sample rotation rate of 20 KHz. Mass spectrometric (MS) measurements were performed by using a direct-exposure probe with electron impact ionization (EI) on a VG 70S instrument. Ph_3SnH was obtained from SIGMA-ALDRICH and was used without further purification. $Au(PPh_3)Ph$ was prepared according to the previously reported procedure.[9] Product separations were performed by TLC in air on Analtech 0.25 mm alumina 60 Å F_{254} glass plates.

Reaction of Ph_3SnH with $Au(PPh_3)Ph$

30.0 mg (0.026 mmol) of $Au(PPh_3)Ph$ was added to 18.6 mg (0.052 mmol) of Ph_3SnH dissolved in 10 mL of benzene. The solution was allowed to stir for 7h at room temperature. A red-orange solution was formed and the solvent was then removed *in vacuo*. The residue was extracted in methylene chloride and separated by TLC by using hexane solvent to elute a yellow band of $[(AuPPh_3)(\mu\text{-}SnPh_3)]_2$, **5.1**, 18.8 mg (52%) and Sn_2Ph_6, 8.6 mg (46.4%). Spectral data for **5.1**: ^{1}H NMR (CD_2Cl_2, in ppm) δ = 7.50(m) 15H, 7.35(m) 15H. ^{119}Sn CP-MAS (in ppm) δ = 121.01. ^{31}P NMR (CD_2Cl_2, in ppm) δ = 43.33(s). Anal. Calcd for **5.1**: C, 53.42; H, 3.73. Found: C, 56.65; H, 4.10.

Crystallographic Analysis

Orange single crystals of **5.1** cocrystallized with Sn_2Ph_6 (a decomposition product) upon slow evaporation of solvent from a solution in methylene chloride at 15 °C. The orange crystals of pure **5.1** can be physically separated from the colorless crystals of the Sn_2Ph_6. The orange data crystal was glued onto the end of a thin glass fiber. X-ray intensity data were measured by using a Bruker SMART APEX CCD-based diffractometer by using Mo Kα radiation (λ = 0.71073 Å). The raw data frames were integrated with the SAINT+ program by using a narrow-frame integration algorithm.[7] Correction for Lorentz and polarization effects were also applied using SAINT+. An empirical absorption correction based on the multiple measurement of equivalent reflections was applied by using the program SADABS. The structure was solved by a combination of direct methods and difference Fourier syntheses, and refined by full-matrix least-squares on F^2, using the SHELXTL software package.[8] All non-hydrogen atoms were refined with anisotropic displacement parameters. The hydrogen atoms were placed in geometrically idealized positions and included as standard riding atoms during the least-squares refinements. Compound **5.1** crystallized in the orthorhombic crystal system with one equivalent of CH_2Cl_2 cocrystallized from the crystallization solvent The space group $P2_12_12$ was uniquely identified by the pattern of systematic absences observed in the data. Crystal data, data collection parameters, and results of the analyses are listed in Table 5.1.

Computational Details.

Density functional theory (DFT) calculations were performed with the Amsterdam Density Functional (ADF) suite of programs[10] by using the PBEsol functional[11] with valence quadruple-ζ + 4 polarization function, relativistically optimized (QZ4P) basis sets for the gold, tin, phosphorus, carbon and hydrogen atoms with frozen cores. The molecular orbitals for compound **5.1** and their energies were determined by geometry-optimized calculations with scalar relativistic corrections that were initiated by using the atom positional parameters as determined from the crystal structure analysis. The geometry-optimized coordinates of **5.1** are given in Table 5.4

Results and Discussion

The reaction of $Au(PPh_3)Ph$ and Ph_3SnH led to formation of the new gold-tin complex, $[(AuPPh_3)(\mu–SnPh_3)]_2$, **5.1** in 52% yield. Sn_2Ph_6 is a major coproduct that was obtained in 46% yield. The Sn_2Ph_6 is believed to be formed by the decomposition of **5.1.** Compound **5.1** was characterized structurally by a single-crystal X-ray diffraction analysis. An ORTEP diagram of the molecular structure of **5.1** is shown in Figure 5.1. The molecule contains two $SnPh_3$ groups that bridge two $Au(PPh_3)$ groups that are linked by and Au – Au bond. In the solid state the molecule lies on a crystallographic two-fold rotation axis. The two independent Au – Sn distances, Au1–Sn1 = 2.8207(16) Å and $Au1–Sn1^i$ = 2.9038(6) Å are significantly different in length, but are similar to those found in the compound $[Au_4(PPh_3)_4(\mu_2–SnCl_3)_2]$, 2.8150(7) Å and 2.9725(8) Å, (Scheme

5.2).[12] The Au1–Au1^{i} distance in **5.1** is 2.5590(5) Å which is shorter than the Au–Au bond distance found in the related compound $[Bu_3NH]_2[(Ph_3P)Au(SnB_{11}H_{11})]_2$, Au–Au= 2.625(1)Å (Scheme 5.3).[13] The Au1–Sn1–Au1^{i} angle (53.08°) observed in compound **5.1** is smaller than the Au–Sn–Au angle (57.03°) found in $[Bu_3NH][(Ph_3P)Au(SnB_{11}H_{11})]_2$. This indicates a stronger intramolecular Au^{I}–Au^{I} interaction in compound **5.1** as compared to $[Bu_3NH][(Ph_3P)Au(SnB_{11}H_{11})]_2$.

In order to probe further into the nature of the Au–Sn and Au–Au bonding in **5.1**, a geometry-optimized PBEsol DFT molecular orbital calculation was performed. Selected MOs that show bonding of the Au_2Sn_2 ring are shown in Figure 5.2. The LUMO showed delocalized bonding between the tin, gold and phosphorus atoms. The HOMO shows a σ–type gold-tin bonding interaction having a node along the Au – Au vector, because of the node this orbital contributes very little to direct bonding between the two gold atoms. The HOMO-1 is a symmetric 4 center – 2 electron orbital across both Au and both Sn atoms. It provides evidence both for direct Au – Au bonding interactions and also for direct Sn – Sn bonding interactions. The HOMO-62 is a low lying orbital that also reflects gold tin bonding interactions in **5.1.** It is a symmetric combination of the p orbitals of tin and the d orbitals of gold. The HOMO-74 and HOMO-75 both display gold-gold π bonding interactions. The interactions consist mainly of overlapping d-d orbitals from the gold atoms. In the absence of an Au – Au bond, each Au atom would formally contain 14 valence electrons. In the presence of an Au – Au single bond, each Au atom would have an odd 15 valence electron

count which would make it paramagnetic. With an Au – Au double bond, each Au atom would have a 16 electron configuration which is more consistent with the very short Au – Au distance observed in the crystal structure analysis of **5.1**.

Conclusion

Compound **5.1** was also obtained as a side production in the reaction of compound **4.1** with Ph_3SnH, see Chapter 4. Compound **5.1** contains a strong Au – Au interactions consisting of a combination of σ–bonding and some π-bonding that might be construed as partial multiple bonding between the two gold atoms.

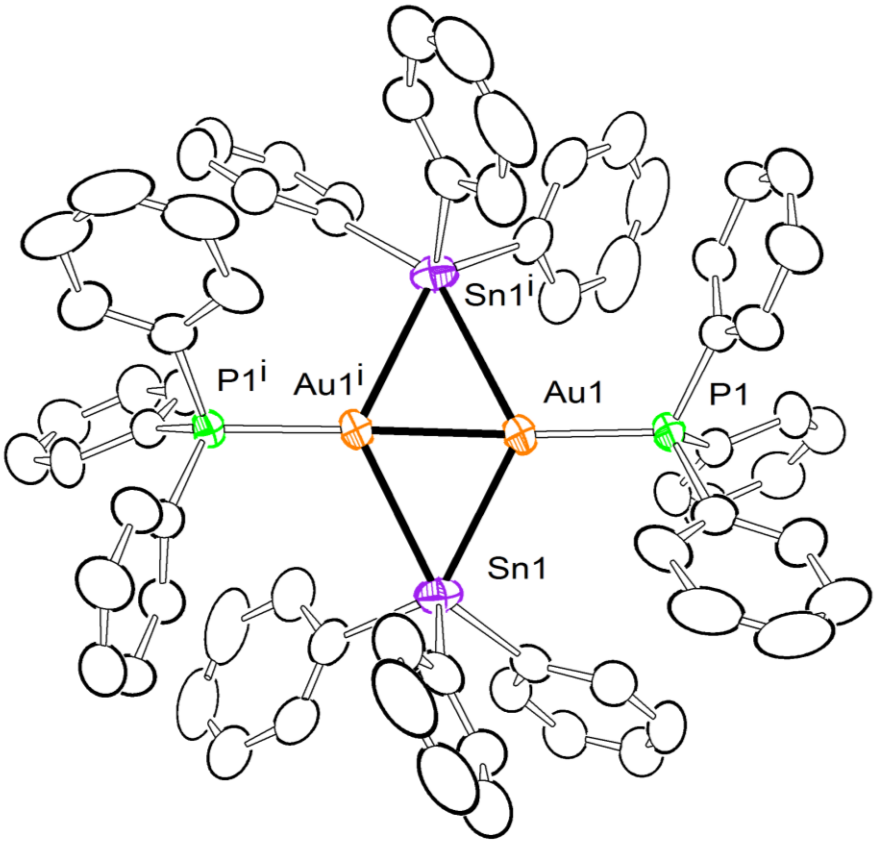

Figure 5.1. An ORTEP diagram of the molecular structure of $[(AuPPh_3)(\mu\text{-}SnPh_3)]_2$, **5.1**, showing 30% thermal ellipsoid probability.

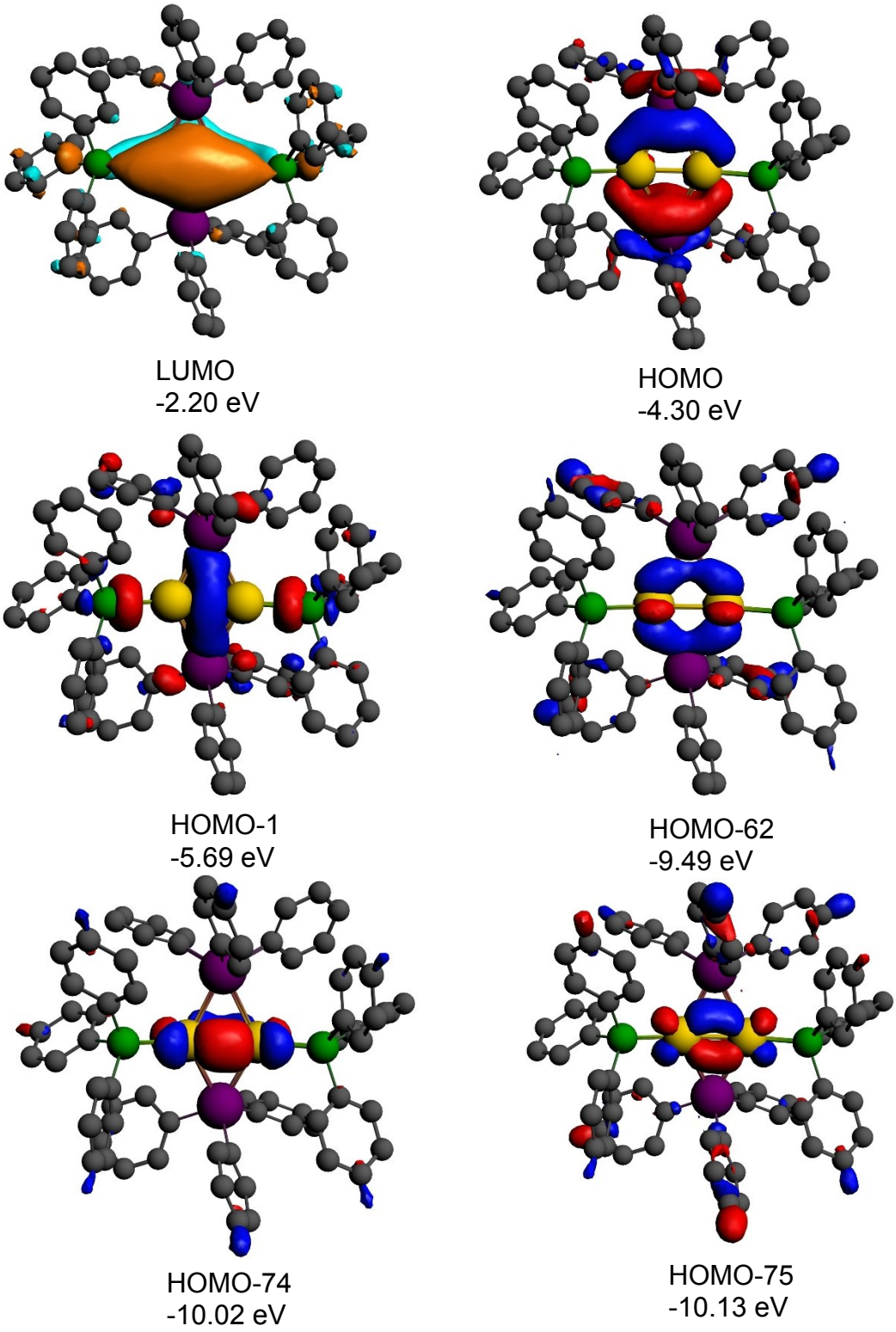

Figure 5.2. Calculated Energies for the LUMO, HOMO, HOMO-1, HOMO-62, HOMO-74 and HOMO-75 of **5.1**.

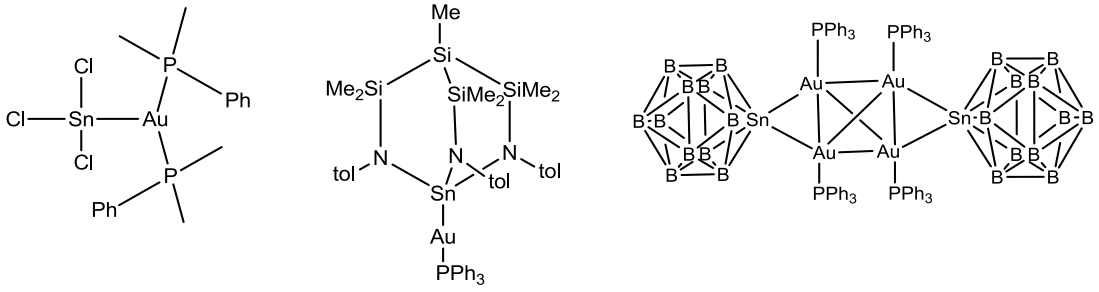

Scheme 5.1. Halide, Triaminometalate and dodecarborate ligand derivatives of tin respectively.

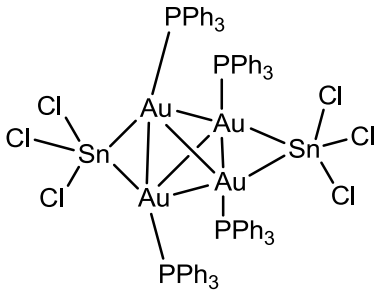

Scheme 5.2. Structure of $[Au_4(PPh_3)_4(\mu\text{-}SnCl_3)_2]$

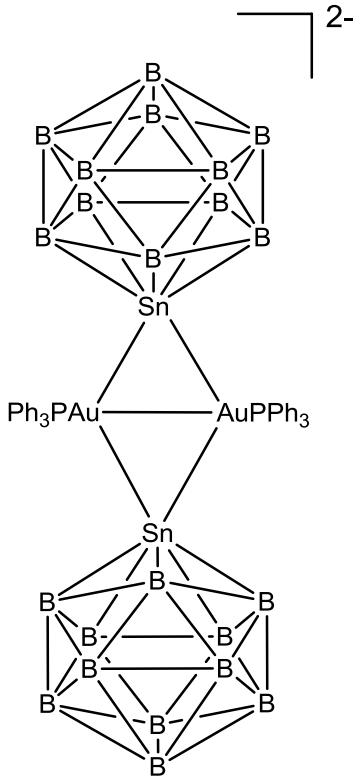

Scheme 5.3. Structure of $[Bu_3NH]_2[(Ph_3P)Au(SnB_{11}H_{11})]_2$

Table 5.1. Crystallographic data for **5.1**[a]

Compound	**5.1**
Empirical formula	$Au_2Sn_2P_2C_{72}H_{60}{\cdot}CH_2Cl_2$
Formula weight	1618.54
Crystal system	Orthorhombic
Lattice parameters	
a (Å)	14.2638(6)
b (Å)	22.9477(9)
c (Å)	9.8436(4)
α (deg)	90.00
β (deg)	90.00
γ (deg)	90.00
V (Å^3)	3222.0(2)
Space group	$P2_12_12$
Z value	2
ρ_{calc} (g/cm^3)	1.711
μ (Mo Kα) (mm^{-1})	5.437
Temperature (K)	294(2)
$2\theta_{max}$(°)	47.50
No. Obs. (I>2σ(I))	7132
No. Parameters	364
Goodness of fit (GOF)	1.119
Max. shift in cycle	0.001
Residuals*: R1; wR2	0.0424; 0.1092
Absorption Correction, Max/min	Multi-Scan 1.000/0.699
Largest peak in Final Diff. Map (e$^-$/ Å^3)	2.019

[a] $R = \Sigma_{hkl}(\,|\,|F_{obs}|-|F_{calc}|\,|\,)/\Sigma_{hkl}|F_{obs}|$; $R_w = [\Sigma_{hkl}w(|F_{obs}|-|F_{calc}|)^2/\Sigma_{hkl}wF^2_{obs}]^{1/2}$; $w = 1/\sigma^2(F_{obs})$; GOF = $[\Sigma_{hkl}w(|F_{obs}|-|F_{calc}|)^2/(n_{data}-n_{vari})]^{1/2}$.

Table 5.2. Selected intramolecular angles and bond distances for **5.1** from structural analysis.[a]

Atom	Atom	Distance(Å)	Atom	Atom	Atom	Angle(°)
Au1	Sn1	2.8207(6)	Au1	Sn1	Au1i	53.083(13)
Au1	Sn1i	2.9038(6)	Sn1	Au1	Sn1i	124.613(15)
Au1	Au1i	2.5590(5)				

[a] Estimated standard deviations in the least significant figure are given in parentheses.

Table 5.3. Interatomic Distances from the Geometry-Optimized structure of **5.1**.

Atom	Atom	Distance(Å)	Atom	Atom	Atom	Angle(°)
Au1	Sn1	2.806	Au1	Sn1	Au1i	53.7
Au1	Sn1i	2.835	Sn1	Au1	Sn1i	124.1
Au1	Au1i	2.552				

Table 5.4. Cartesian Coordinates for geometry optimized of **5.1**

Atom	x	y	z	Atom	x	y	z
Au	0.0000	2.5520	0.0000	H	5.4031	2.5020	-0.4744
Sn	2.4916	1.3076	-0.3456	C	6.1100	3.1044	1.4691
P	0.0194	4.9202	-0.1706	H	7.0883	3.4143	1.0895
C	2.6996	2.4478	-2.1884	C	5.8233	3.2085	2.8350
C	3.2990	3.7184	-2.2494	H	6.5774	3.5931	3.5274
H	3.7237	4.1787	-1.3486	C	4.5760	2.7920	3.3158
C	3.3736	4.4168	-3.4619	H	4.3532	2.8532	4.3851
H	3.8533	5.3996	-3.4901	C	3.6205	2.2774	2.4297
C	2.8466	3.8610	-4.6319	H	2.6577	1.9425	2.8260
H	2.9256	4.4014	-5.5792	C	1.7126	5.6857	0.0126
C	2.2381	2.6021	-4.5871	C	2.5211	5.2615	1.0718
H	1.8448	2.1481	-5.5019	H	2.1620	4.5078	1.7778
C	2.1618	1.9073	-3.3741	C	3.8044	5.7917	1.2233
H	1.6929	0.9198	-3.3680	H	4.4362	5.4438	2.0457
C	3.6663	-0.4529	-0.8445	C	4.2792	6.7437	0.3143
C	3.3372	-1.2940	-1.9196	H	5.2876	7.1499	0.4266
H	2.4671	-1.0877	-2.5482	C	3.4648	7.1716	-0.7391
C	4.1168	-2.4163	-2.2215	H	3.8296	7.9218	-1.4451
H	3.8454	-3.0466	-3.0734	C	2.1764	6.6483	-0.8907
C	5.2320	-2.7290	-1.4371	H	1.5470	6.9745	-1.7248
H	5.8399	-3.6075	-1.6704	C	-1.0079	5.9699	0.9801
C	5.5752	-1.8997	-0.3643	C	-0.4221	7.0087	1.7137
H	6.4604	-2.1214	0.2397	H	0.6541	7.1976	1.6457
C	4.8043	-0.7671	-0.0759	C	-1.2229	7.8136	2.5326
H	5.0980	-0.1266	0.7635	H	-0.7642	8.6209	3.1085
C	3.8939	2.1691	1.0557	C	-2.6005	7.5878	2.6089
C	5.1523	2.5912	0.5871	H	-3.2234	8.2188	3.2478
C	-3.1794	6.5510	1.8689	C	-3.6663	3.0049	-0.8445
H	-4.2554	6.3662	1.9184	C	-3.3372	3.8460	-1.9196
C	-2.3870	5.7366	1.0556	H	-2.4671	3.6397	-2.5482
H	-2.8525	4.9321	0.4761	C	-4.1168	4.9682	-2.2215
C	-0.4923	5.5600	-1.8459	H	-3.8454	5.5986	-3.0734
C	-1.2029	6.7572	-1.9677	C	-5.2320	5.2810	-1.4371
H	-1.5181	7.3074	-1.0756	H	-5.8399	6.1594	-1.6704
C	-1.5234	7.2423	-3.2398	C	-5.5752	4.4517	-0.3643
H	-2.0741	8.1810	-3.3361	H	-6.4604	4.6734	0.2397
C	-1.1394	6.5311	-4.3805	C	-4.8043	3.3191	-0.0759
H	-1.3908	6.9127	-5.3735	H	-5.0980	2.6786	0.7635

C	-0.4264	5.3337	-4.2499	C	-3.8939	0.3829	1.0557
H	-0.1109	4.7777	-5.1364	C	-5.1523	-0.0393	0.5871
C	-0.0965	4.8464	-2.9824	H	-5.4031	0.0500	-0.4744
H	0.4800	3.9193	-2.8857	C	-6.1100	-0.5524	1.4691
Au	0.0000	0.0000	0.0000	H	-7.0883	-0.8623	1.0895
Sn	-2.4916	1.2444	-0.3456	C	-5.8233	-0.6565	2.8350
P	-0.0194	-2.3683	-0.1706	H	-6.5774	-1.0412	3.5274
C	-2.6996	0.1042	-2.1884	C	-4.5760	-0.2401	3.3158
C	-3.2990	-1.1664	-2.2494	H	-4.3532	-0.3012	4.3851
H	-3.7237	-1.6267	-1.3486	C	-3.6205	0.2746	2.4297
C	-3.3736	-1.8648	-3.4619	H	-2.6577	0.6095	2.8260
H	-3.8533	-2.8476	-3.4901	C	-1.7126	-3.1337	0.0126
C	-2.8466	-1.3090	-4.6319	C	-2.5211	-2.7095	1.0718
H	-2.9256	-1.8495	-5.5792	H	-2.1620	-1.9559	1.7778
C	-2.2381	-0.0501	-4.5871	C	-3.8044	-3.2397	1.2233
H	-1.8448	0.4039	-5.5019	H	-4.4362	-2.8918	2.0457
C	-2.1618	0.6446	-3.3741	C	-4.2792	-4.1917	0.3143
H	-1.6929	1.6322	-3.3680	H	-5.2876	-4.5980	0.4266
C	-3.4648	-4.6197	-0.7391	C	2.3870	-3.1847	1.0556
H	-3.8296	-5.3698	-1.4451	H	2.8525	-2.3802	0.4761
C	-2.1764	-4.0964	-0.8907	C	0.4923	-3.0081	-1.8459
H	-1.5470	-4.4225	-1.7248	C	1.2029	-4.2052	-1.9677
C	1.0079	-3.4179	0.9801	H	1.5181	-4.7555	-1.0756
C	0.4221	-4.4567	1.7137	C	1.5234	-4.6903	-3.2398
H	-0.6541	-4.6457	1.6457	H	2.0741	-5.6291	-3.3361
C	1.2229	-5.2616	2.5326	C	1.1394	-3.9791	-4.3805
H	0.7642	-6.0689	3.1085	H	1.3908	-4.3608	-5.3735
C	2.6005	-5.0358	2.6089	C	0.4264	-2.7817	-4.2499
H	3.2234	-5.6668	3.2478	H	0.1109	-2.2258	-5.1364
C	3.1794	-3.9990	1.8689	C	0.0965	-2.2944	-2.9824
H	4.2554	-3.8142	1.9184	H	-0.4800	-1.3673	-2.8857

REFERENCES

1) Royer,S. and Duprez,D. *ChemCatChem*, **2011**,*3*,24-65.

2) (a) Haruta,M.; Kobayashi,T.;Sano,H. and Yamada,N. *Chem Lett*, **1987**, *16*, 405-408. (b) Haruta, M., *Gold Bull.* **2004***, 37*, 27 – 36. (c) Haruta, M., *Catal. Today* **1997**, *36*, 153 – 166. (d) Haruta, M.; Date, M., *Appl. Catal. A: Gen.* **2001**, *222*, 427 – 437.

3) Maeda,Y.;Akita,T. and Kohyama,M. *Catal. Lett,* **2014**, 10.1007/s10562-014-1376-4.

4) Clegg,W. *Acta Crystallogr.,Sect.B:Struct.Crystallogr.Cryst.Chem,* **1978**,*34*,278.

5) Findeis, B.; Contel, M.; Gade, L.H.; Laguna, M.; Gimeno, I.J. and McPartlin,M. *Inorg.Chem*,**1997**,*36*,2386.

6) Joosten,D.;Weissinger,I.;Kirchmann,M.;Maichle-Mossmer,C.;Schappacher,F.M.;Pottgen,R.and Wesemann,L. *Organometallics*, **2007**, *26*, 5696.

7) SAINT+, version 6.2a, Bruker Analytical X-ray Systems, Inc., Madison, WI, 2001.

8) Sheldrick, G. M. SHELXTL, version 6.1, Bruker Analytical X-ray Systems, Inc., Madison, WI, 1997.

9) Partyka, D. V.; Zeller, M.; Hunter, A. D.; Gray,T. G. *Angew. Chem*. *Int. Ed.* **2006**, *45*, 8188-8191.

10) ADF2013; SCM Theoretical Chemistry, Vrije Universiteit, Amsterdam, The Netherlands, http://www.scm.com.

11) Perdew, J. P.; Ruzsinszky, A.; Csonka, G. I.; Vydrov, O. A.; Scuseria, G. E. *Phys. Rev. Lett.* **2008**, *100*, 136406.

12) Mingos, D.M.P.; Powell,H.R. and Stolberg,T.L. *Transition Met. Chem.*, **1992**, *17*, 334-337.

13) Hagen,S.; Pantenburg,I.;Weigend,F.; Wickleder,C. and Wesemann,L. *Angew.Chem.Int.Ed.,***2003**,*42*,1501-1505.

CHAPTER 6

New Rhenium Carbonyl Cluster Complexes Containing Bridging Mercury Groups

INTRODUCTION

In recent studies it has been shown that arylgoldphosphine compounds, such as $(PPh_3)Au(C_6H_5)$, can be readily oxidatively added to activated 3rd row polynuclear metal carbonyl cluster complexes to yield arylmetalcarbonyl cluster complexes containing bridging gold phosphine groupings, e.g. Eqs. (1) – (3).[1-3] In certain cases, the aryl ligands have adopted an unusual bridging coordination mode that can result in interesting physical and chemical properties such as hindered rotation about the metal-metal bond.[4]

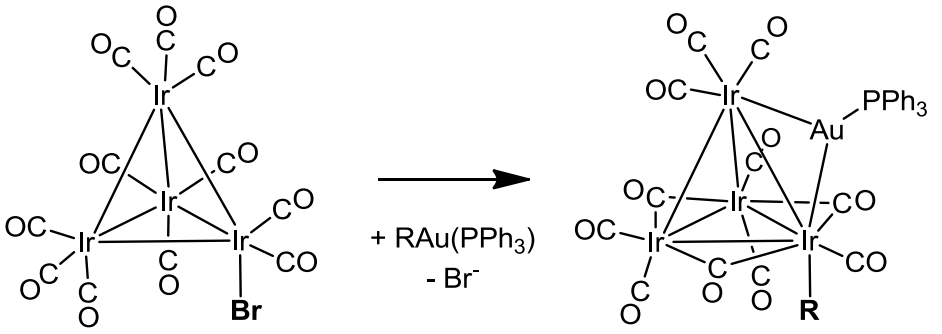

$[Ir_4(CO)_{11}Br]^-$ $Ir_4(CO)_{11}(R)[\mu\text{-}Au(PPh_3)]$, R = CH_3, C_6H_5, 2-$C_{16}H_9$ (1)

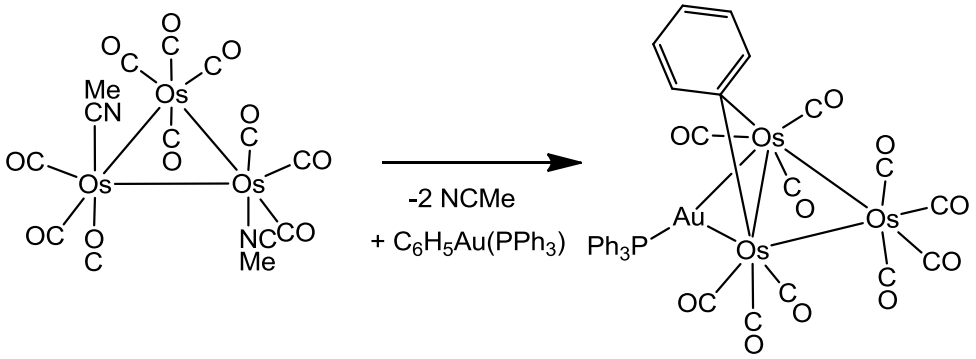

(2)

$Os_3(CO)_{10}(NCMe)_2$ $Os_3(CO)_{10}(\mu\text{-}C_6H_5)[\mu\text{-}Au(PPh_3)]$

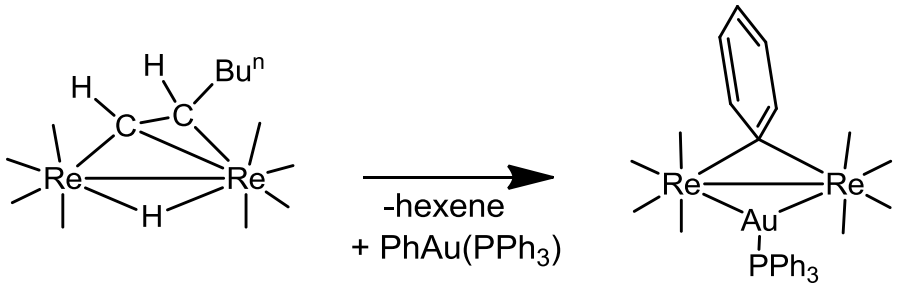

(3)

$Re_2(CO)_8[\mu\text{-}HCC(H)Bu](\mu\text{-}H)$ $Re_2(CO)_8[\mu\text{-}Au(PPh_3)](\mu\text{-}C_6H_5)$, **4.1**

We have found that the gold phosphine group can be replaced in some of these complexes in reactions with mercuric halides, eq. (4).[5]

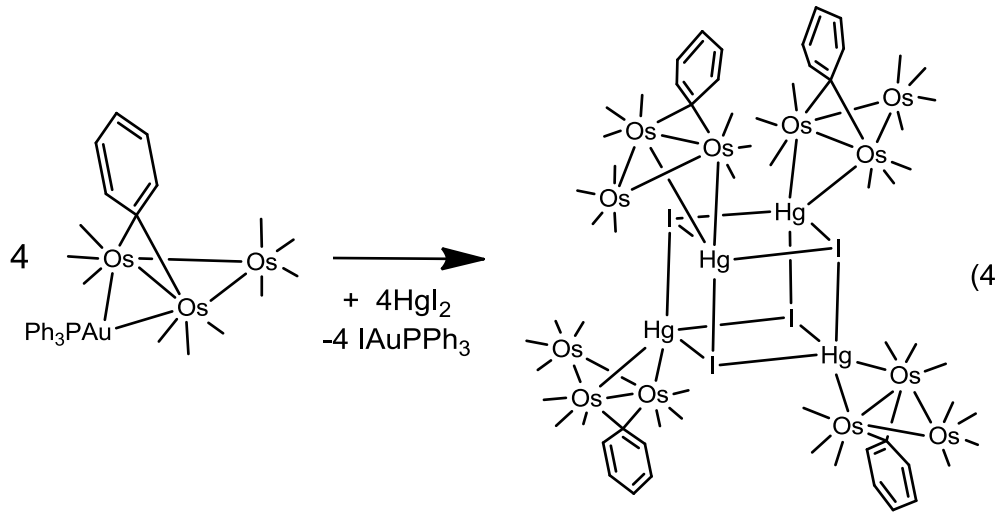

(4)

$[Os_3(CO)_{10}(\mu\text{-}C_6H_5)[\mu\text{-}HgI]_4$

We have now investigated the reaction of $Re_2(CO)_8[\mu\text{-}Au(PPh_3)](\mu\text{-}\eta^1\text{-}C_6H_5)$, **4.1** with HgI_2. We have found that the $AuPPh_3$ group is replaced by a bridging HgI group with concomitant formation of $IAu(PPh_3)$ and the dirhenium product $Re_2(CO)_8(\mu\text{-}HgI)(\mu\text{-}\eta^1\text{-}C_6H_5)$ which condenses to form a dimer having the formula $[Re_2(CO)_8(\mu\text{-}HgI)(\mu\text{-}\eta^1\text{-}C_6H_5)]_2$, **6.1** in the solid state. The dimer is held together by two bridging iodide ligands between the two mercury atoms. In an effort to synthesize other phenyldirheniummercury complexes we also investigated the reaction of $Re_2(CO)_8[\mu\text{-}HCC(H)C_4H_9](\mu\text{-}H)$ with $Hg(C_6H_5)_2$. The product of this reaction turned out to be the new compound $[Re_2(CO)_8[\mu\text{-}HCC(H)C_4H_9]_2(\mu_4\text{-}Hg)$, **6.2** which contains a spiro-mercury atom bridging two hexenyl-bridged $Re_2(CO)_8$ groupings. The synthesis and structures of these two new mercury containing rhenium complexes are described in this chapter.

Experimental Section

General Data. Reagent grade solvents were dried by the standard procedures and were freshly distilled prior to use. All the reactions were performed under a nitrogen atmosphere using the standard Schlenk techniques, unless otherwise stated. Once they were formed, all of the products were air stable, and they were isolated, stored and analyzed in air. Infrared spectra were recorded on an AVATAR 360 FT-IR spectrophotometer. ^1H NMR spectra were recorded on a Varian Mercury 400 spectrometer operating at 399 MHz. Mass spectrometric measurements were performed by direct exposure probe using electron impact ionization (EI) on a VG 70S instrument. HgI_2 and $HgPh_2$ were

purchased from SIGMA-ALDRICH and were used without further purification. $Re_2(CO)_8(\mu\text{-}AuPPh_3)(\mu\text{-}C_6H_5)$, **4.1**[3] and $Re_2(CO)_8[\mu\text{-}\eta^2\text{-}C(H)=C(H)Bu^n]$[6] were prepared according to previously reported procedures. Product separations were performed by TLC in air on Analtech 0.25 mm silica gel 60 Å F254 glass plates.

Synthesis of $Re_2(CO)_8(\mu\text{-}HgI)(\mu\text{-}C_6H_5)$, 6.1

16.0 mg (0.035 mmol) of HgI_2 was added to 45.0 mg (0.039 mmol) of **4.1** dissolved in 20 mL of benzene and stirred at room temperature for 1 h. The solution turned from orange to light yellow and the solvent was then removed in *vacuo*. The residue was extracted in methylene chloride and separated by TLC using a 4:1 hexane/methylene chloride (v/v) solvent mixture. The products listed in order of elution include to give a colorless band of $(Ph_3P)AuI$[7], 15.3 mg (66% yield) and a yellow band of $Re_2(CO)_8(\mu\text{-}HgI)(\mu\text{-}C_6H_5)$, **6.1**, 29.0 mg (73% yield). Spectral data for **6.1**: IR ν_{CO} (cm^{-1} in hexane): 2078(m), 2010(vs), 1999(s), 1978(m). ^1H NMR (CD_2Cl_2, in ppm) δ = 7.25-7.29 (t, 2H, $J_{H\text{-}H}$=8.0 Hz, Ph), δ = 8.13-8.15 (d, 2H, $J_{H\text{-}H}$=8.0 Hz,Ph), δ = 8.46-8.50 (t, 1H, $J_{H\text{-}H}$=8.0 Hz,Ph). Mass Spec. EI/MS *m/z* 1002, M^+. The isotope pattern is consistent with the presence of one mercury atom and two rhenium atoms.

Synthesis of $\{Re_2(CO)_8[\mu\text{-}\eta^2\text{-}C(H)=C(H)Bu^n]\}_2(\mu_4\text{-}Hg)$, 6.2

15.6 mg (0.044 mmol) of $Hg(C_6H_5)_2$ was added to 30.0 mg (0.044 mmol) of $Re_2(CO)_8[\mu\text{-}\eta^2\text{-}C(H)=C(H)Bu^n](\mu\text{-}H)$ dissolved in 20 mL of toluene. The solution was then refluxed for 1 h. A yellow solution was formed and the solvent was then

removed in *vacuo*. The residue was extracted in methylene chloride and separated by TLC by using a 4:1 hexane/methylene chloride (v/v) solvent mixture. The products, listed in order of elution, include a light yellow band of unreacted $Re_2(CO)_8[\mu\text{-}\eta^2\text{-}C(H)=C(H)Bu^n](\mu\text{-}H)$, 7.6 mg (25%), and a yellow band of $\{Re_2(CO)_8[\mu\text{-}\eta^2\text{-}C(H)=C(H)Bu^n]\}_2(\mu_4\text{-}Hg)$, **6.2** 15.4 mg (23%). Spectral data for **6.2**: IR ν_{CO} (cm^{-1} in methylene chloride): 2133(w), 2086(w), 2066(s), 2018(vs), 1984(s), 1955(m). ^1H NMR (CD_2Cl_2, in ppm) δ = 0.98 (t, 3H, $J_{H\text{-}H}$=7.0 Hz, CH_3), 1.48 (s, 2H, $J_{H\text{-}H}$=7.0 Hz, CH_2), 1.60 (q, 2H, $J_{H\text{-}H}$=8.0 Hz, CH_2), 2.29 (dt, 2H, $J_{H\text{-}H}$=8.0 Hz, CH_2), 4.89 (dt, 1H, $J_{H\text{-}H}$=16.0 Hz, =CH-CH_2), 6.96 (d, 1H, $J_{H\text{-}H}$=16.0 Hz, =CH) Mass Spec. EI/MS *m/z* 1560, M^+. The isotope pattern is consistent with the presence of one mercury atom and four rhenium atoms.

Crystallographic Structural Analyses.

Yellow single crystals of **6.1** and **6.2** suitable for x-ray diffraction analyses were obtained by slow evaporation of solvent from solutions of the pure compound in a hexane/methylene chloride solvent mixtures at room temperature. Each data crystal was glued onto the end of a thin glass fiber. X-ray intensity data were measured by using a Bruker SMART APEX CCD-based diffractometer using Mo Kα radiation (λ = 0.71073 Å). The raw data frames were integrated with the SAINT+ program by using a narrow-frame integration algorithm.[8] Correction for Lorentz and polarization effects were also applied with SAINT+. An empirical absorption correction based on the multiple measurement of equivalent reflections was applied by using the program SADABS. All structures were

solved by a combination of direct methods and difference Fourier syntheses, and were refined by full-matrix least-squares on F^2, using the SHELXTL software package.[9] All non-hydrogen atoms were refined with anisotropic displacement parameters. Hydrogen atoms were placed in geometrically idealized positions and included as standard riding atoms during the least-squares refinements. Crystal data, data collection parameters, and results of the analyses are listed in Table 6.1.

Results and Discussion

The reaction of **4.1** with HgI_2 in benzene at room temperature provided the new compound $Re_2(CO)_8(\mu\text{-}HgI)(\mu\text{-}C_6H_5)$, **6.1**, in 73% yield and the known compound $AuPPh_3I$, in 66% yield in 1 h. Compound **6.1** was characterized by a combination of IR, mass spec, ^1H NMR and a single-crystal X-ray diffraction analysis. An ORTEP diagram of the molecular structure of compound **6.1** is shown in Figure 6.1. In the solid state the structure compound **6.1** consists of a centrosymmetric dimer of empirical formula unit $Re_2(CO)_8(\mu\text{-}HgI)(\mu\text{-}C_6H_5)$ that is held together by bridging iodide ligands between the two Hg atoms. There are two independent Hg – I bond distances to each mercury atom and one Hg – I bond is considerably longer and presumably much weaker than the other, Hg(1)–I(1)=2.6754(10) Å and Hg(1)–$I(1)^i$=3.4506(13) Å. The Hg-I distance is 2.6764(16) Å in the complex $Pt(PCy_3)_3I(HgI)$ which contains a terminally coordinated HgI grouping.[10]

Asymmetric X-Hg-X bonding was also observed for the dimeric complexes of $[Ru_3(CO)_9(\mu_3\text{-}C_2C_4H_9)(\mu\text{-}HgBr)]_2$ [11] and $[Ru_5(C)(CO)_{14}(\mu\text{-}C_l)(\mu\text{-}HgCl)]_2$ [12] in the solid state. Large asymmetry in the Hg-I bonding was also observed for the HgI aggregation of the compound $Os_3(CO)_{10}(\mu\text{-}C_6H_5)(\mu\text{-}HgI)$ into a tetrameric form $[Os_3(CO)_{10}(\mu\text{-}C_6H_5)(\mu\text{-}HgI)]_4$, which contains a cubane-like Hg_4I_4 core having D_2 symmetry: Hg(1) – I(1) = 2.9112(8) Å, Hg(1) – $I(1^i)$ = 2.9645(8) Å and Hg(1) – $I(1^{ii})$ = 3.524(1) Å, see eq. (4).[5] The mercury atom in **6.1** is much more symmetrically bonded to the two rhenium atoms, Hg(1)–Re(1)=2.7843(8) Å, Hg(1)–Re(2)=2.8051(7) Å. The phenyl group is a η^1-coordinated, bridging ligand and is slightly asymmetrically bonded to the rhenium atoms, Re(1)–C(1)=2.302(14) Å, Re(2)–C(1)=2.380(13) Å. The η^1-bridging phenyl ligand in compound **4.1** is also asymmetrically coordinated to the two rhenium atoms, Re(1)-C(1)= 2.292(5) Å, Re(2)-C(1)= 2.396(5) Å.[3]

An electron impact mass spectrum of **6.1** did not show the parent ion. The highest mass ions were attributed to the monomeric fragment $Re_2(CO)_8(\mu\text{-}HgI)(\mu\text{-}C_6H_5)$. Evidently, the dimeric structure is split under the forcing conditions of the mass spectrometer to yield the monomeric fragment as the highest weight ion.

The dirhenium unit of **6.1** contains only 32 valence electrons including one electron donated from the phenyl ligand and one electron from the HgI grouping. The dirhenium center is isoelectronic to that of compound **4.1** which is also formally unsaturated at the metal atoms. The Re – Re distance in **6.1**, Re(1)–

Re(2) = 3.0134(8) Å, is only slightly longer than that in **4.1** Re(1)–Re(2) = 2.9690(4) Å. The Re – Re distance in $Re_2(CO)_{10}$ which is generally regarded to have an Re – Re single bond is 3.041(1) Å.[13]

The compound $Re_2(CO)_8[\mu\text{-}\eta^2\text{-}C(H)=C(H)Bu^n](\mu\text{-}H)$ is known to react with $(PPh_3)Au(C_6H_5)$ to form the compound **4.1** Eq. (3). [3] Accordingly we attempted to synthesize other rhenium complexes containing bridging phenyl ligands by the reaction of $Re_2(CO)_8[\mu\text{-}\eta^2\text{-}C(H)=C(H)Bu^n](\mu\text{-}H)$ with $Hg(C_6H_5)_2$ by heating a solution of the two compounds in toluene solvent to reflux for 1h. From this reaction solution, the new compound $\{Re_2(CO)_8[\mu\text{-}\eta^2\text{-}C(H)=C(H)Bu^n]\}_2(\mu_4\text{-}Hg)$, **6.2** was obtained in 23% yield. Compound **6.2** was characterized by a combination of IR, mass spec, ^1H NMR and a single-crystal X-ray diffraction analysis. An ORTEP diagram of the molecular structure of compound **6.2** is shown in Figure 6.2.

Compound **6.2** contains two $Re_2(CO)_8[\mu\text{-}\eta^2\text{-}C(H)=C(H)Bu^n]$ groupings linked by a μ_4-*spiro*-structured bridging mercury atom. The μ_4-*spiro* link has not been previously observed in the chemistry of rhenium carbonyls although there are a number of examples of this type of μ_4-mercury bonding in cluster complexes of the Group VIII transition metals.[14-15] The four independent Re – Hg distances in **6.2** are significantly longer than those in **6.1** and range from 2.8382(4) Å to 2.9574(5) Å. The two Re_2Hg triangles, Re(1)-Hg-Re(2) and Re(3)-Hg-Re(4) are nearly perpendicular to each other, 81.7(1)°. The two independent

Re – Re distances, Re(1)–Re(2)=3.1077(5), Re(3)–Re(4)=3.1132(5) Å are also significantly longer than that in **6.1** and even longer than the Re – Re single bond distance in $Re_2(CO)_{10}$, 3.041(1) Å.[13] Each pair of Re atoms contains an η^2-σ-π coordinated hexenyl, $C(H)=C(H)Bu^n$, ligand. The atoms C(1) and C(7) are coordinated to both rhenium atoms, Re(1)–C(1)=2.129(9), Re(2)–C(1)=2.324(9) Å, Re(3)-C(7)=2.151(11) Å, Re(4)-C(7)=2.411(11) Å, while C(2) and C(8) are coordinated to only one rhenium atom at significantly longer Re – C distances Re(2)–C(2)=2.481(9) Å, Re(4)-C(8)=2.505(15) Å. The C(1)-C(2) and C(7)-C(8) distances are short,1.382(13) Å and 1.417(17) Å, respectively and are indicative of partial C – C multiple bonding. The σ-π coordinated hexenyl ligands serve as 3-electron donors while the Hg atom donates one electron to each pair of rhenium atoms. Thus, each pair of rhenium atoms contains 34 valence electrons and is formally electronically saturated. This explains the longer length of the Re – Re bond distances compared to the unsaturated dirhenium complex **6.1**, see above.

Summary and Conclusions

A summary of the results of this study are shown in Scheme 6.1. It has been shown that the mercury halides HgI_2 can replace the $Au(PPh_3)$ group in the compound **4.1** to yield the unsaturated dirhenium carbonyl cluster complex **6.1** which contains an η^1-bridging phenyl ligand. Compound **6.1** is a dimer in the solid state due to weak bonding between the iodide ligands from two different molecules. The reaction of $Re_2(CO)_8[\mu\text{-}\eta^2\text{-}C(H)=C(H)Bu^n](\mu\text{-}H)$ with $Hg(C_6H_5)_2$

yielded the new compound **6.2** containing a spiro-bridging Hg atom between two $Re_2(CO)_8[\mu\text{-}\eta^2\text{-}C(H)=C(H)Bu^n$ groupings. Presumably, the hydride ligands in the original dirhenium complex were combined with the phenyl groups from the $Hg(C_6H_5)_2$ to form benzene. Farrugia showed that reactions of hydride containing cluster complexes with $Hg(C_6H_5)_2$ also yielded cluster complexes with *spiro* μ_4-bridging mercury atoms.[14c-15]

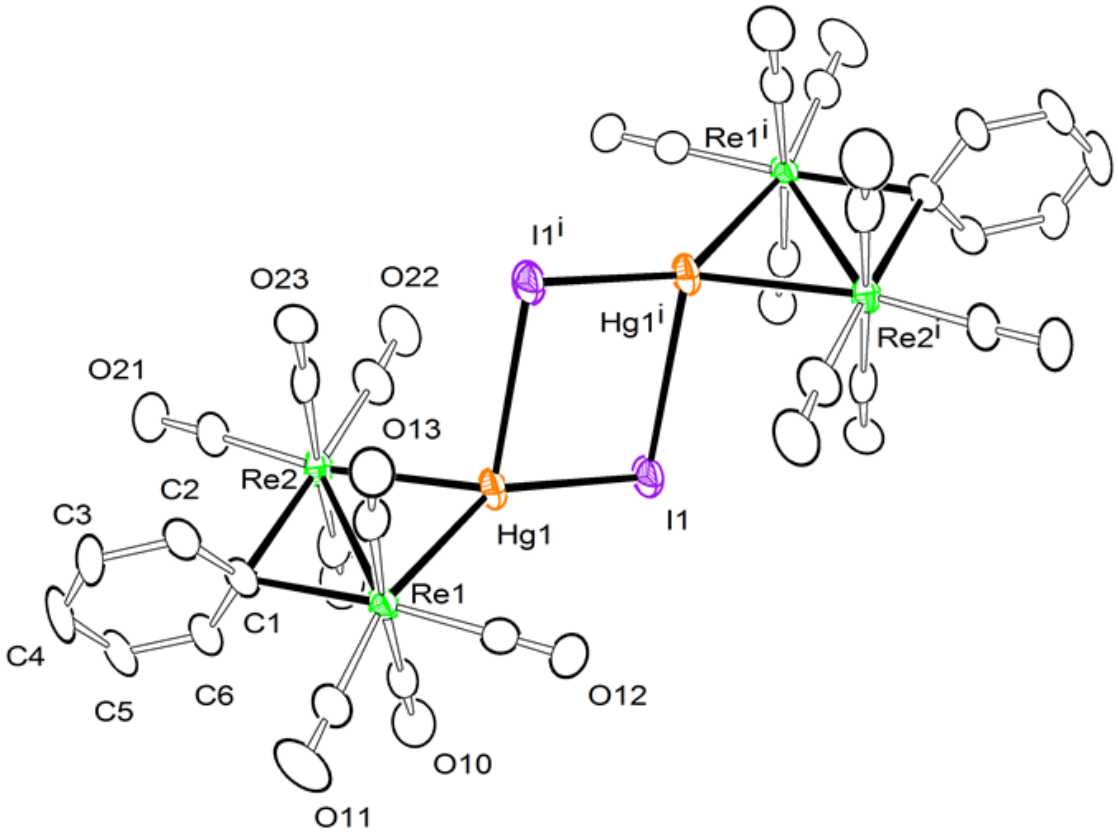

Figure 6.1. An ORTEP diagram of the molecular structure of $[Re_2(CO)_8(\mu\text{-HgI})(\mu\text{-Ph})]_2$, **6.1** showing 30% thermal ellipsoid probability.

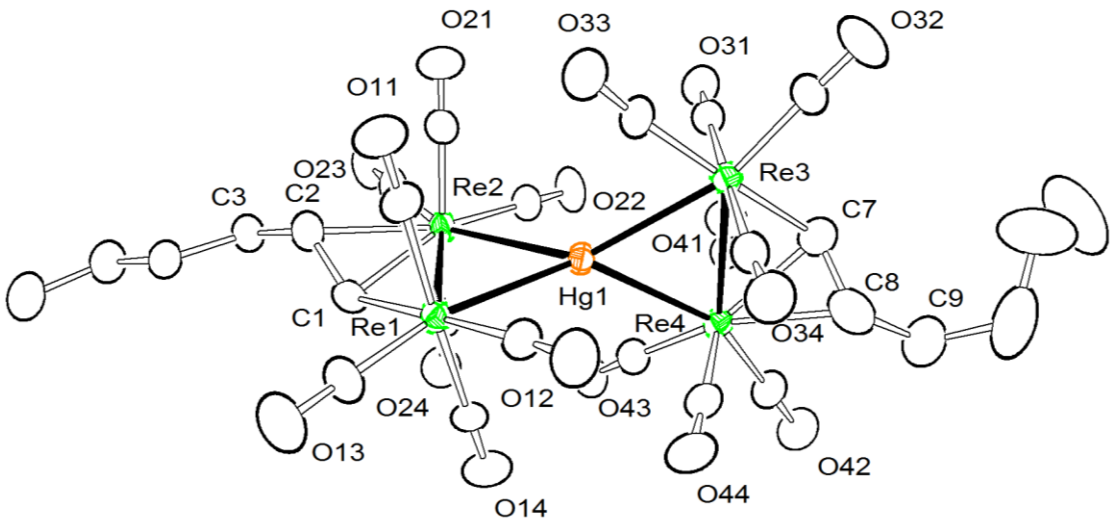

Figure 6.2. An ORTEP diagram of the molecular structure of $\{Re_2(CO)_8[\mu\text{-}\eta^2\text{-}C(H)=C(H)Bu^n]\}_2(\mu_4\text{-}Hg)$,**6.2** showing 30% thermal ellipsoid probability.

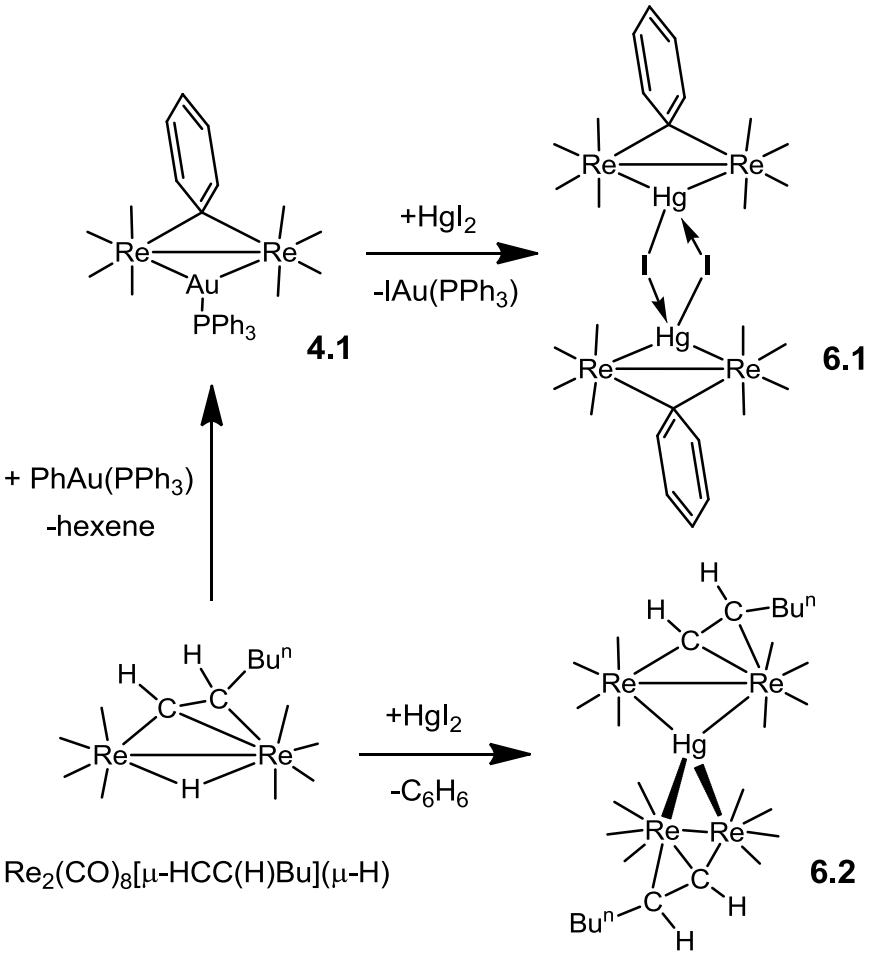

Scheme 6.1. Synthetic pathway for compounds **6.1** and **6.2**.

Table 6.1. Crystallographic data for **6.1** and **6.2**[a]

Compound	**6.1**	**6.2**
Empirical formula	$HgRe_4I_2O_{16}C_{28}H_{10}$	$HgRe_4O_{16}C_{28}H_{17}$
Formula weight	2002.18	1554.85
Crystal system	Monoclinic	Triclinic
Lattice parameters		
a (Å)	8.6924(10)	12.4882(5)
b (Å)	8.3395(9)	12.7552(5)
c (Å)	27.172(3)	13.5210(5)
α (deg)	90.00	95.123(1)
β (deg)	96.052(2)	105.110(1)
γ (deg)	90.00	113.953(1)
V (Å^3)	1958.7(4)	1853.17(12)
Space group	$P2_1/c$	$P\bar{1}$
Z value	2	2
ρ_{calc} (g/cm^3)	3.395	2.786
μ (Mo Kα) (mm^{-1})	21.760	17.209
Temperature (K)	294(2)	294(2)
$2\theta_{max}$(°)	55.74	50.06
No. Obs. (I>2σ(I))	2980	5870
No. Parameters	235	452
Goodness of fit (GOF)	1.114	1.058
Max. shift in cycle	0.001	0.002
Residuals*: R1; wR2	0.0420; 0.0958	0.0340; 0.0855
Absorption Correction, Max/min	Multi-Scan 1.000/0.493	Multi-Scan 1.000/0.344
Largest peak in Final Diff. Map (e$^-$/ Å^3)	1.287	1.738

[a] $R = \Sigma_{hkl}(\,|\,|F_{obs}|-|F_{calc}|\,|\,)/\Sigma_{hkl}|F_{obs}|$; $R_w = [\Sigma_{hkl}w(|F_{obs}|-|F_{calc}|)^2/\Sigma_{hkl}wF^2_{obs}]^{1/2}$; $w = 1/\sigma^2(F_{obs})$; GOF = $[\Sigma_{hkl}w(|F_{obs}|-|F_{calc}|)^2/(n_{data}-n_{vari})]^{1/2}$.

Table 6.2. Selected intramolecular angles and bond distances for **6.1**[a]

Atom	Atom	Distance(Å)	Atom	Atom	Atom	Angle(°)
Re(1)	Re(2)	3.0134(8)	Re(1)	Hg(1)	Re(2)	65.246(19)
Hg(1)	Re(1)	2.7843(8)	I(1)	Hg(1)	$I(1)^{i}$	86.25(3)
Hg(1)	Re(2)	2.8051(7)	Hg(1)	I(1)	$Hg(1)^{i}$	93.75(3)
Hg(1)	I(1)	2.6754(10)				
Hg(1)	$I(1)^{i}$	3.4506(13)				
Re(1)	C(1)	2.302(14)				
Re(2)	C(1)	2.380(13)				

[a] Estimated standard deviations in the least significant figure are given in parentheses.

Table 6.3. Selected intramolecular angles and bond distances for **6.2**[a]

Atom	Atom	Distance(Å)	Atom	Atom	Atom	Angle(°)
Re(1)	Hg(1)	2.8382(4)	Re(1)	Hg(1)	Re(2)	64.816(11)
Re(2)	Hg(1)	2.9574(5)	Re(1)	C(1)	Re(2)	88.4(3)
Re(3)	Hg(1)	2.8420(4)				
Re(4)	Hg(1)	2.9530(4)				
Re(1)	Re(2)	3.1077(5)				
Re(3)	Re(4)	3.1132(5)				
Re(1)	C(1)	2.129(9)				
Re(2)	C(1)	2.324(9)				
Re(2)	C(2)	2.481(9)				
Re(3)	C(7)	2.151(11)				
Re(4)	C(7)	2.411(11)				
Re(4)	C(8)	2.505(15)				
C(1)	C(2)	1.382(13)				
C(7)	C(8)	1.417(17)				

[a] Estimated standard deviations in the least significant figure are given in parentheses.

REFERENCES

1) Adams, R. D.; Chen, M. *Organometallics*, **2012,** *31***,** 6457−6465.

2) Adams, R. D.; Rassolov, V.; Zhang, Q. *Organometallics*, **2013**, *32*, 6368−6378.

3) Adams, R. D.; Rassolov, V.; Wong, Y. O. *Angew. Chem.* **2014**, *53,* 11006-11009.

4) Adams, R. D.; Rassolov, V.; Zhang, Q. *Organometallics* **2013**, *32*, 1587-1590.

5) Adams, R. D.; Luo, Z.; Wong, Y. O. *J. Organomet. Chem.*, **2014** http://dx.doi.org/10.1016/

6) Nubel, P. O.; Brown, T. L. *J. Am. Chem. Soc.,* **1984***,106*, 644-652.

7) Westland, A. D. *Canad. J. Chem.*, **1969**, *47*, 4135-4140.

8) SAINT+, version 6.2a, Bruker Analytical X-ray Systems, Inc., Madison, WI, 2001.

9) Sheldrick, G. M. SHELXTL, version 6.1, Bruker Analytical X-ray Systems, Inc., Madison, WI, 1997.

10) Ma, M.; Sidiropoulos, A.; Ralte, L.; Stasch, A.; Jones, C. *Chem. Commun.* **2013**, *49*, 48-50.

11) Fahmy, R.; King, K.; Rosenberg, E.; Tiripicchio, A.; Tiripicchio Camellini, M. *J. Am. Chem. Soc.* **1980**, *102*, 3626-3628.

12) Johnson, B. F. G.; Kwik, W.-L.; Lewis, J.; Raithby, P. R.; Saharan, V. P. *J. Chem. Soc. Dalton Trans.* ,**1991**, 1037-1042.

13) Churchill, M. R.; Amoh, K. N.; Wasserman, H. J. *Inorg. Chem.*, **1981**, *20*, 1609–1611.

14) (a) Ermer, S.; King, K.; Hardcastle, K. I.; Rosenberg, E.; Lanfredi, A. M. M.; Tiripicchio, A.; Tiripicchio Camellini, M. *Inorg.Chem*. **1983**, *22, 1339*-1344. (b) Farrugia, L. J. *Chem. Commun*., **1987,** 147-149. (c) Bianchini, A.; Farrugia, L. J. *Organometallics*, **1992**, *11*, 540-548. (d) Miu, C.-Y.; Chi, H.-H.;

15) Chen, S.-W.; Cherng, J.-J.; Hsu, M.-H.; Huang, Y.-X.; Shieh, M. *New J. Chem*. **2011**, *35*, 2442. (e) Reina, R.; Riba, O.; Rossell, O.; Seco, M.; Gomez-Sal, P.; Martin, A.; de Montauzon, D.; Mari, A. *Organometallics* **1998**, *17*, 4127-4135. (f) Kong, F.-S.; Wong, W.-T. *J. Chem. Soc., Dalton Trans.*, **1999**, 2497-2510. (g) Johnson, B. F. G.; Kwik, W. L.; Lewis, J.; Raithby, P. R.; Saharan, V. P. *J. Chem. Soc., Dalton Trans.*,**1991**,1037-1042. (h) Andreu, P. L.; Cabeza, J. A.; Llamazares, A.; Riera, V.; Bois, C.; Jeannin, Y. *J. Organomet. Chem.* **1991**, *420*, 431-442. (i) Egold, H.; Schraa, M.; Florke, U.; Partyka, J. *Organometallics* **2002**, *21, 1925*-1932. (j) Seyferth, D.; Ruschke, D. P.; Davis, W. M.; Cowie, M.; Hunter, A. D. *Organometallics* **1994**, *13, 3834*-3848. (k) Au, Y.-K.; Wong, W.-T. *Inorg. Chem*. **1997**, *36*, 2092-2096. (l) Gade, L. H.; Johnson, B. F. G.; Lewis, J.; McPartlin, M.; Powell, H. R. *J. Chem. Soc., Chem. Commun*. **1990**, 110. (m) Gade, L. H.; Johnson, B. F. G.; Lewis, J.; McPartlin, M.; Powell, H. R. *J. Chem. Soc., Dalton Trans*. **1992**, 921-931. (n) Rosenberg, E.; Hardcastle, K. I.; Day, M. W.; Gobetto, R.; Hajela, S.; Muftikian, R. *Organometallics* **1991**,*10*, 203-210. (o) Shieh, M.; Tsai, Yi-Chou *Inorg. Chem*. **1994**, *33*, 2303-2305. (p) Au, Y.-K.; Wong, W.-T. *J. Chem. Soc., Dalton Trans.* **1996**, 899-911.

16) (a) Aitchison, A. A.; Farrugia, L. J. *Organometallics* **1986**, *5*, 1103. (b) Farrugia, L. J. *J. Organomet. Chem.* **1986**,*310*, 67.

APPENDIX A – COPYRIGHT RELEASE